



Innovation Fund Denmark HALDOR TOPSØE   
RESEARCH, TECHNOLOGY & GROWTH

# Design, synthesis and characterization of small-pore zeolites for industrial environmental applications

PhD thesis submitted by

Cristian-Renato Boruntea

Supervisors:

Dr. Peter N. R. Vennestrøm

Prof. Dr. Avelino Corma

November 2019



UNIVERSITAT  
POLITÈCNICA  
DE VALÈNCIA



INSTITUTO DE  
TECNOLOGÍA  
QUÍMICA



CONSEJO SUPERIOR DE INVESTIGACIONES CIENTÍFICAS

**CSIC**



“Add prayers in the equation of effort and you will find wider solutions to problems.”

Anonymous

“Stop trying to fill your head with science – for to fill your heart with love is enough.”

Richard P. Feynman

*To my grandmother*

# Acknowledgments

This PhD thesis would not have been possible without the support of many people. I would like to present my sincere gratitude to:

My supervisors, Dr. Peter N. R. Vennestrøm and Prof. Dr. Avelino Corma, for their guidance, intelligent discussions and fruitful advices. I was always impressed by the rapidity of proposing solutions to problems that usually require a long and sometimes superfluous mechanism of thinking.

Dr. Lars F. Lundegaard, for his help with complicated diffraction patterns and especially for his availability, with the mention that I have rarely seen such a deep passion for science.

Dr. German Sastre, for his unbelievable help and support, in a moment when these were most needed. I still remember the computational mindset in playing chess.

Dr. Ramchandra Tirumvalan for our discussions on philosophy of religion.

Brian Jensen and Peter Hammershøi for their friendship, help and pleasant atmosphere in the lab, lunch breaks or around a coffee.

My girlfriend Brigitte Devocht for her love, support and understanding.

# Contents

List of abbreviations .....	iv
Abstract (English) .....	v
Resumen (Español).....	vii
Resum (Valencià).....	ix
Hypotheses and objectives .....	xi
Introduction .....	1
Part 1.....	3
Chapter 1 .....	3
Zeolites .....	3
Zeolite synthesis.....	8
Chapter 2 .....	15
Computational studies for novel zeolites .....	15
References: .....	36
Part 2.....	42
Paper 1 .....	42
Paper 2 .....	64
Paper 3 .....	77
General overview and conclusions.....	96
A future perspective .....	105
Annexes .....	109

# List of abbreviations

AFM	Atomic force microscopy
CPA	Crystallization by particle attachment
D6R	Double six ring
D8R	Double eight ring
DABCO	1,4-diazabicyclo[2.2.2]octane
$E_{(\text{ORG-ZEO})}$	Energy difference between organic template – zeolite framework
$E_{\text{ORG}}$	Energy of the organic template
$E_{\text{ZEO}}$	Energy of the zeolite framework
I.E.	Interaction energy
IZA-SC	Structure Commission of the International Zeolite Association
MTO	Methanol-to-olefins
NO <sub>x</sub>	Nitrogen oxides
OS	Original synthesis
OSDA	Organic structure directing agent
PXRD	Powder X-ray diffraction
SAR	Silicon to aluminum ratio
SCIBS	Symmetry-Constrained Intersite Bonding Search
SCR	Selective catalytic reduction
SEM	Scanning electron microscope
SNCR	Selective non-catalytic reduction
u.c.	Unit cell
ZTZ	Zeolite-to-zeolite transformation

## Abstract (English)

The research project described herein is structured in two parts. The first part is focused on the fundamental research with the aim of creating a toolbox for zeolite preparation. The second part deal with the design, synthesis and characterization of novel zeolites particular useful for DeNO<sub>x</sub> applications, but could be also useful for MTO applications.

The fundamental research is addressing a novel approach of preparing zeolites by using other zeolites as raw materials. This process is known as zeolite-to-zeolite transformation or interzeolite conversion. The high yield obtained, fast crystallization time and the better utilization of the raw materials (e.g. parent zeolite, organic structure directing agent (OSDA)), are important benefits of interzeolite conversion technic, which answer the objectives formulated for an industrial PhD project. The method has been exemplified by using various raw materials as parent zeolites, such as FAU and CHA for the preparation of two target small pore zeolites AEI and AFX.

In the second part the focus has been on the design of novel small pore zeolites. Three hypothetical frameworks have been selected by narrowing down a database containing 933611 structures. The selection has been performed by using the general descriptors for the state-of-the-art DeNO<sub>x</sub> zeolites (e.g. CHA). This was followed by finding suitable OSDAs for the selected frameworks, by using computational methods. The usage of the theoretically predicted OSDAs in synthesis gels made possible the synthesis of a novel high-silica zeolite. PXRD analysis, revealed that the zeolite has the ERI framework topology. The obtained material has a distinct particle morphology and smaller crystallites, which are key parameters for various catalytic processes.

The synthesis work revealed also a novel dense zeolite, named K-paracelsian. The new material has been obtained while exploring the phase space using 1-methyl-DABCO as OSDA. The synthesis of this zeolite is especially interesting in the sense that the OSDA is not being incorporated into the zeolite channels, but rather influencing the nucleation and crystallization. Further characterization revealed

a material compositionally closely related to the mineral microcline and structurally closely related to the mineral paracelsian, both of which are feldspars. In contrast to the feldspars, K-paracelsian contains intrazeolitic water corresponding to one molecule per cage and can be described as the simplest endmember of a family of dense double-crankshaft zeolite topologies. By applying the identified building principle, a number of known zeolite frameworks (e.g. GIS, APC, MER, PHI, SIV) and hypothetical zeolite topologies can be constructed.



# Resumen (Español)

El Proyecto de investigación aquí descrito se estructura en dos partes. La primera parte se centra en la investigación fundamental con el objetivo de crear un protocolo para la síntesis de zeolitas. La segunda parte se refiere al diseño, síntesis y caracterización de nuevas zeolitas, particularmente útiles para aplicaciones DeNO<sub>x</sub>, pero también podría ser útil para aplicaciones MTO.

La investigación fundamental sugiere un Nuevo modelo de preparación de zeolitas utilizando otras zeolitas como simiente. Este proceso se llama transformación zeolita-zeolita o también conversión interzeolita. El alto rendimiento obtenido, la rápida cristalización y la mejor utilización y rendimiento de los materiales de partida se han tenido en cuenta para mejorar el proceso en base a un proyecto de doctorado financiado por una empresa. Este método se ha ilustrado utilizando varias zeolitas como semilla, entre otras FAU y CHA, para la preparación de las dos zeolitas objetivo: AEI y AFX.

En la segunda parte, la investigación se centra en el diseño de nuevas zeolitas de poro medio. Se han seleccionado tres zeolitas hipotéticas de una base de datos de 933611 estructuras. Esta selección se ha realizado utilizando descriptores específicamente diseñados en base a la aplicabilidad de estas zeolitas en procesos DeNO<sub>x</sub> zeolitas. A continuación se han buscado los agentes directores de estructura (ADE) más apropiados, con la ayuda de métodos computacionales, algunos de los cuales se han sintetizado posteriormente. El uso de dichos ADE en el gel de síntesis ha permitido la obtención de una zeolita cuya topología (ERI) ha sido identificada mediante análisis por PXRD, y cuya morfología y tamaño de cristal (particularmente pequeño) la hacen muy adecuada para su uso como catalizador en algunos procesos.

El trabajo de síntesis también reveló la aparición de una nueva zeolita de alta densidad, llamada 'paracelsio-K'. Este nuevo material se ha obtenido al explorar el espacio de fases que cristalizan al utilizar 1-methyl-DABCO como ADE. La síntesis de esta zeolita tiene un especial interés porque el ADE no se incorpora en los canales de la zeolita, pero más bien influyendo en la nucleación y cristalización. La caracterización reveló que la composición del material es próxima al mineral

microcline, estructuralmente cercano al paracelsio, ambos feldespatos. A diferencia de los feldespatos el paracelsio-K contiene moléculas de agua en su interior (1 molécula por cavidad) y puede describirse como el material más simple de la familia de las zeolitas que contiene cadenas del tipo 'doble-cigüeñal'. Utilizando los elementos topológicos correspondientes a esta estructura es posible generar estructuras zeolíticas ya conocidas, como GIS, APC, MER, PHI, SIV y algunas otras zeolitas hipotéticas.

# Resum (Valencià)

El Projecte d'investigació aquí descrit s'estructura en dos parts. La primera part se centra en la investigació fonamental amb l'objectiu de crear un protocol per a la síntesis de zeolites. La segona part es refereix al disseny, síntesis i caracterització de noves zeolites, particularment útils per a aplicacions DeNOx , però també podria ser útil per a aplicacions MTO.

La investigació fonamental suggereix un nou model de preparació de zeolites utilitzant altres zeolites com a llavor. Aquest procés s'anomena transformació zeolita-zeolita o també conversió interzeolita. L'alt rendiment obtingut, la ràpida cristallització i la millor utilització i rendiment dels materials de partida s'han tingut en compte per millorar el procés en base a un projecte de doctorat finançat per una empresa. Aquest mètode s'ha il·lustrat utilitzant diverses zeolites com a llavor, entre altres FAU i CHA, per a la preparació de les dues zeolites objectiu: AEI i AFX.

A la segona part, la investigació se centra en el disseny de noves zeolites de porus mitjà. S'han seleccionat tres zeolites hipotètiques d'una base de dades de 933.611 estructures. Aquesta selecció s'ha realitzat utilitzant descriptors específicament dissenyats sobre la base de l'aplicabilitat d'aquestes zeolites en processos DeNOx zeolites. A continuació s'han buscat els agents directors d'estructura (ADE) més apropiats, amb l'ajuda de mètodes computacionals, alguns dels quals s'han sintetitzat posteriorment.

L'ús d'aquests ADE al gel de síntesi ha permès l'obtenció d'una zeolita la topologia (ERI) ha estat identificada mitjançant anàlisi per PXRD, i la morfologia i mida de vidre (particularment petit) la fan molt adequada per al seu ús com a catalitzador en alguns processos. El treball de síntesi també va revelar l'aparició d'una nova zeolita d'alta densitat, anomenada 'paracelsio-K'. Aquest nou material s'ha obtingut a explorar l'espai de fases que cristal·litzen en utilitzar 1-methyl-DABCO com ADE. La síntesi d'aquesta zeolita té un especial interès perquè el ADE no s'incorpora en els canals de la zeolita, però més aviat influent en la nucleació i cristallització. La caracterització va revelar que la composició del material és propera al mineral microcline, estructuralment proper al paracelsio, tots dos feldspats. A diferència dels feldspats el

paracelsio-K conté molècules d'aigua al seu interior (1 molècula per cavitat) i pot descriure com el material més simple de la família de les zeolites que conté cadenes del tipus 'doble-cigonyal'. Utilitzant els elements topològics corresponents a aquesta estructura és possible generar estructures zeolítiques ja conegudes, com GIS, APC, MER, PHI, SIV i algunes altres zeolites hipotètiques.

# Hypotheses and objectives

## Hypotheses:

1. By applying the interzeolite conversion method of preparing zeolites the synthesis features (e.g. crystallization time, yields and morphology properties) are affected.
2. Hypothetical frameworks to meet the descriptors of state-of-the art small pore zeolites, thermodynamic stability and general feasibility criteria.
3. Hypothetical zeolites can be realized by applying in silico predicted OSDA molecules and potentially through the use of zeolite-to-zeolite transformations.

## Objectives:

1. Preparation of a toolbox for the synthesis of novel zeolites by exemplifying this method on already known small-pore zeolites.
2. Selecting 3 hypothetical zeolites from a database of theoretical structures.
3. Finding by computational methods 15 OSDAs that could help to synthesize the hypothetical frameworks.
4. High-throughput synthesis of zeolites, followed by their characterization and testing.

# Introduction

The industrial PhD project “Synthesis of novel zeolites for industrial environmental applications” has been performed between Haldor Topsøe A/S, Denmark and Institute of Chemical Technology, Polytechnic University of Valencia (ITQ-UPV), Spain.

One of the major problems in our world today is the air pollution and its irreversible impact on the environment, as a direct consequence of heavy industrialization, exploration and processing of fossil fuels for energy demands and their usage in combustion engines.

The removal of NO<sub>x</sub>, particles and other pollutants like CO from the exhaust systems of stationary and mobile sources become an important challenge as the EU, USA and many other countries continuously introduced tight legislation that regulate emissions to the air, trend that is foreseen to increase in the near time future. This challenge is reflected in the need of a better in depth understanding of catalytic processes leading to the improvement of currently existing catalyst for DeNO<sub>x</sub> applications among others, and the most important, discovery of new catalyst materials.

In this thesis, a potential method for the synthesis of novel zeolites is addressed from two different viewpoints. First, a preparation method is extensively studied with the aim of preparing a toolbox for the zeolite preparation. The obtained results from this fundamental research made possible two publications. The first one addresses the synthesis aspects and the testing results of the prepared catalyst (Chem. Commun., 2015, 51, 11030-11033). The paper entitled “Crystallization of AFX and AEI zeolites through zeolite-to-zeolite transformations” has been recently published in Microporous and Mesoporous Materials journal and is offering a detailed insight of zeolite-to-zeolite transformations. The second part is applying the results from the fundamental research in an attempt to synthesize selected hypothetical frameworks, by using *in silico* predicted OSDAs. The results from the novel zeolites preparation work have been summarized in an article, recently accepted for publication in Chemistry of Materials journal. The industrial relevance of the obtained results made possible the submission of 3 patents. The synthesis work also revealed

a novel dense zeolite. This work has been recently published in International Union of Crystallography Journal.

# Part 1

## Chapter 1

### Zeolites

Zeolites represents a class of crystalline aluminosilicates, part of the tectosilicates minerals, characterized by well-defined pores of various size (approx. 0.3 – 1.5 nm in diameter) and channel systems that open in cavities of different dimensions and shapes [1], [2], [3], [4]. They are part of a much larger category of so called “molecular sieves”, along with carbon, glasses and oxides that show a certain degree of porosity. Although zeolites are found in nature as both natural minerals and synthetic materials; the most important category is represented by the zeolites that are synthetically produced, covering applications that range from ion-exchange materials to the petrochemical industry [2]. Their crystalline tridimensional network resemble that of an inorganic polymer, where the repetitive crystallographic unit cell, as the smallest structural unit can be expressed by the formula:  $xM_{2/n}O \cdot xAl_2O_3 \cdot ySiO_2 \cdot WnH_2O$ ; where M is an organic or inorganic cation that belongs to the group IA or IIA, n is the cation valence and W is molecular water, that is present in the zeolite void space [5], [6].

Their specificity is arising from the unique structure, such as the channel systems, pores aperture and cavities of molecular dimensions. This particular characteristics, make zeolites to be materials with very high surface area and pore volume which are parameters of paramount importance in catalysis.

From a structurally point of view zeolites are made by corner sharing  $[SiO_4]$  tetrahedra. When  $Si^{4+}$  is substituted by  $Al^{3+}$  a negative charge is introduced in the lattice, that is balanced by a cation. When this cation is a proton, a Brönsted acid site is created, which is known to be connected to the oxygen atom neighboring the silicon, thus creating a bridged hydroxyl group [7], [8].

The first zeolite was discovered by the Swedish mineralogist Axel Fredrik Cronstedt in 1756 [9]. Based on his observations that the stilbite mineral is producing large amounts of steam due to water removal upon heating with a blowpipe flame, he introduced the concept of *zeolite*. The word is derived from Greek  $\zeta\acute{\epsilon}\omega$  (*zéō*) which means “to boil” and  $\lambda\acute{\iota}\theta\omicron\varsigma$  (*lithos*), which translates for “stone”. Another early scientific



reference for zeolites was made in 1840 by the French mineralogist Augustin-Alexis Damour who discovered that dehydration of zeolites is a reversible process that takes place without any modification on their morphology. [10] He also discovered the natural zeolite faujasite (framework code FAU, see figure 1), with late important catalytic applications in petrochemistry, named after the French geologist Barthélemy Faujas de Saint-Fond [11], [12]. The ion exchange reversibility of zeolite materials was described in 1858 [13], and in 1862, the first zeolite synthetic preparation (levynite, LEV) was reported, by hydrothermal synthesis [14]. Although their absorption property was known since 1896 [15] and 1909 [16], followed by experimental observation that various liquids (with a preference for the more polar ones) are getting trapped in dehydrated zeolites, it was only in 1932 [17] that the term of “molecular sieves” was introduced. A consistent review on the earliest state and evolution on zeolites and silicates preparation by the hydrothermal synthesis is presented in various reviews [18], [19], [20], [21].

The specific molecular sieving ability is highly explored in separation processes such as ion exchange or sorption. On the other hand their characteristic as solid acids make them, one of the most important heterogeneous catalysts for industrial applications. Gasoline production relies almost entirely on the catalytic cracking of petroleum over zeolite catalysts [4]. The zeolites general applications in catalysis are dependent on the type of acid sites.

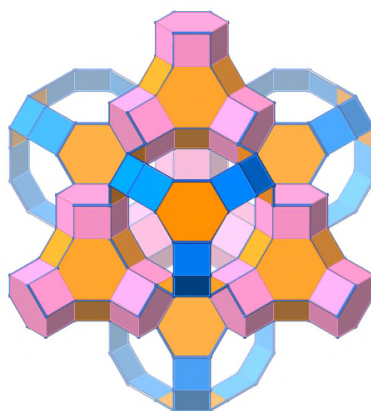


Figure 1. 3D structure of faujasite (framework code FAU), seen along  $[1\ 1\ 1]$  direction. Colors have been used to emphasize the composite building units: sod (t-toc) – yellow; d6r (t-hpr) – pink; big cage – partially blue is unfilled for porosity visualization.

Besides aluminosilicates, zeolites can also be made from other types of atoms and in this situation the materials are named generally as *zeotypes*. For example the aluminophosphate molecular sieves, ALPO were developed in 1982 and were followed by various compositions such as SAPO [22], [23]. Different metals have been incorporated in the framework of silica, aluminosilicate or aluminophosphate e.g. germanium, iron, gallium, titanium, lithium, magnesium, etc. [23], [24]. Some of these type of materials include SAPO-11 [25], (framework code AEL) but also other varieties are well known, such as ALPO-11 and MeAPO (Me = Ge and Mn) [26], [27], [28]. SAPO-18 (framework code: AEI) [29], has recently been extensively studied for NH<sub>3</sub>-SCR [30], [31] as well as for methanol-to-olefins (MTO) reaction [32] and as a catalyst for propylene production [33].

When it comes to comparison with zeolites, the literature presents the aluminophosphate materials being described by a “univariant framework composition” with the ratio Al/P = 1 and pore sizes that easily reach dimensions bigger than those observed for aluminosilicates [5]. This includes a wide range of dimensions starting for instance from 8-rings (e.g. ALPO-17, framework code ERI), medium rings, such as 10 and 12 rings (e.g. ALPO-11 (AEL), ALPO-41 (AFO) and ALPO-5 (AFI)) to extra-large 18-ring materials (VIP-5). Their frameworks are described to be neutral, which makes this type of materials to show no ion-exchange properties, a slightly hydrophilic surface selectivity and very good hydrothermal stability. On the other hand the silicoaluminophosphates (SAPO) materials, which include among others: Si-VPI-5, SAPO-37 (FAU) or SAPO-34, show weak to mild acidic cation exchange properties. This is due to the introduction of Si in the phosphorus network which produces a negative charge in the framework.

A different type of materials resulted from the substitution of the aluminum in the ALPO's framework with various divalent and trivalent metals such as: Co, Zn, Fe<sup>2+</sup>, Mg, etc. or Fe<sup>3+</sup>. These new materials are known as MeAPO and represent a breakthrough for the introduction of divalent metals in the frameworks. Although their properties (e.g. adsorption and hydrophilic surface selectivity) resemble those showed for SAPO materials, their hydrothermal stability is less than that of other zeotype molecular sieves. Also, the catalytic properties are dependent on the metal and the framework structure, showing weak to strong acidic behavior [5].

The properties of the zeolites are in many ways directly correlated with the Si/Al ratio. Table 1 presents the variation of the zeolite properties when the Si/Al ratio is changing from 1 to  $\infty$ .

Table 1. Properties of zeolites related to the changes of the Si/Al ratio, adapted from [5].

Property	Transition
Stability	From $\leq 700$ °C to approx. 1300 °C
Surface selectivity	From hydrophilic to hydrophobic
Acidity	Increasing strength, decreasing number
Cation concentration	Decreasing
Structure	From 4, 6 and 8 – rings to 5 – rings

One of the most important property of the zeolites is based on the tetrahedral building blocks that are connected through oxygen bridges producing in this way a three-dimensional network with channels and cages of various dimensions. This specific property is highly explored in catalysis and separation applications. A classification based on the size of the rings it is presented in the literature. For example channel sizes bigger than 12 are defined as ultra large, large with a 12 – ring and medium by 10 – rings and finally small pore zeolites characterized by 8 – rings. This channels system is responsible of the very high surface area and pore volume. When it is combined with the possibility of introducing active sites inside the internal surface of the zeolite, it is produced in this way a special type of catalyst with superior properties to other types of materials.

A brief description will be given in the next paragraph on how a catalytic reaction or process is taking place when the catalyst implied it is a zeolite. A catalytic reaction is taking place in a series of events in order to obtain the product. For example the process is starting with the diffusion of the reactant through the zeolite channels and pores with the aim of reaching the active site, the adsorption of the reactant on the active site followed by the chemical reaction that will make the adsorbed product; the desorption of the product and the diffusion of the product outside the zeolite micropore system. The diffusion effects play a major role in the reactions that involve molecules with the dimensions that are close to those of the zeolite channels and thus

have an important role in the overall rate of the reaction. The literature describes the diffusion in the zeolites based on Weisz [34] studies on configurational diffusion which describes the intracrystalline migration as a strongly dependent diffusion mechanism on the type of the zeolite, the nature of the reactant, the site and the temperature. An important aspect is that the pore diameter in zeolites is larger than the crystallographic one. This is explained based on the lattice vibration effects that take place during an ordinary catalytic process and it is exemplified by the behavior of Y zeolite, where the difference can be as much as 0.6 Å [35] when the zeolite is heated at elevated temperature. Another important aspect where the temperature is playing a crucial role is in the situation where the size of the reactants molecules are able to penetrate the zeolite pores. In this situation the temperature plays an important role and it is influencing the rate, due to the fact that the molecular diffusion is an activated process. It is understandable that in order to use the zeolite at its full extend the diffusion rate of the raw materials, has to be larger than the intrinsic chemical conversion rate. The rate of a reaction can be further increased, in the situation where the diffusion of the reactant is slower than the chemical reaction, by decreasing the diffusion path, e.g. by shortening the crystallite size. The diffusion of the reactants into the zeolites is also dependent on the geometry of the zeolite framework. A powerful example in this case are the zeolite structures that are characterized by a 1-dimensional channel system. The diffusivities in this situation are well-known to strongly decrease due to the small amounts of impurities generated during the synthesis, that block the pores. This effect is less seen in the zeolite frameworks with 2-dimensional or 3-dimensional pore system. Another important aspect regarding the diffusivities in the zeolite catalyst is the tortuosity. The literature contains a direct example on ZSM-5 [36], where it is shown that the diffusion in the zeolites with straight channels are 5 times higher compared with the zeolites where the channel system is more sinusoidal.

Another important step for a reaction performed over a zeolite catalyst is represented by the adsorption effects. These effects represents energy terms that takes place when the raw materials are passing through the zeolite channels [37]: dispersion energy ( $\Phi_D$ ), close-range repulsion energy ( $\Phi_R$ ), polarization energy ( $\Phi_P$ ), field-dipole energy ( $\Phi_{FN}$ ), field gradient quadrupole energy ( $\Phi_{FQ}$ ), dipole-dipole energy ( $\Phi_{NN}$ ), quadrupole-dipole energy ( $\Phi_{NQ}$ ), quadrupole-quadrupole energy ( $\Phi_{QQ}$ ). This shows that zeolites are materials that their adsorption properties are easily changeable, by changing the composition of the zeolite or by changing its framework

structure. Preference for certain reactants or products can be given in this way, by changing the adsorption characteristics of a molecule. For example, for the zeolites with a low framework Si/Al ratio, there is a large number of compensating cations and as a consequence very high electrostatic fields ( $\Phi_{FN}$ ) or fields gradients ( $\Phi_{FQ}$ ) will be produced inside the channels and cages. Zeolites with a high framework Si/Al ratio contains mainly dispersion forces ( $\Phi_D$ ) and the presence of electrostatic fields or polarization forces is very low or there is no influence. This is an important prove that zeolites are able to be prepared with either hydrophilic or hydrophobic properties, by just changing the Si/Al ratio, either by synthesis procedures or by post synthesis treatments, controlling in this way the sorption properties and also the relative adsorption contributing to the discrimination between polar or nonpolar molecules. It is well established that the modification of the adsorption properties of the zeolites have a decisive impact on their reactivity. This can be done by changing the number of active sites and changing the total adsorption capacity or the adsorption of a specific reactant or product. The concentration of the reactant is possible to be varied when the zeolite is modified from the hydrophilic to the hydrophobic form. In general this specific feature of the zeolites can have a direct impact on the reactions that are known to compete, being well-known that decreasing the adsorption capacity it is affecting the bimolecular rather than unimolecular reactions. The presence or absence of water, depending on the adsorption properties, in the zeolite pores is also affecting the reaction. The selectivity it is also influenced by the sorption properties of the zeolites as results of inhibiting as mentioned above bimolecular or unimolecular transfer reactions, that are responsible of creating undesired byproducts.

## Zeolite synthesis

As it was described above, the specific features of zeolites and their applications especially in the chemical industry, has attracted a huge interest. This is reflected in the development of intensive research studies for the synthesis of zeolite materials in general and novel zeolite frameworks in particular, for targeted applications, in order to improve chemical processes for the petrochemical industry.

Although there are over 40 different natural zeolites known today, the number of synthetic zeolites or zeotypes is more than 190, thus there are 239 distinct zeolite frameworks as to the fall of 2018 [38], [39].

The need for zeolite materials to satisfy various limitations imposed by the stringent reaction conditions lead to the development of the zeolite synthesis, especially after 1950. For a rigorous and detailed overview on the historical development of zeolite synthesis to the present day, the reader is directed to various papers [4], [40], [41], [42], [43]. A general overview on zeolite synthesis is presented below. For an insight on the interzeolite conversion method (zeolite-to-zeolite transformation) the reader is directed to Part 2, Paper 1 presented in this thesis.

The synthesis of medium to high silica zeolite materials is usually taking place as follows:

1. The amorphous raw materials containing Si or Al compounds are mixed together with an inorganic hydroxide (most common NaOH or KOH) in order to make a high pH environment. (An organic cation is often added in the synthesis gel at this stage.)
2. The mixture is afterwards transferred to an autoclave and heated to temperatures above 100 °C (typically between 100 – 200 °C) for several days.
3. At this stage, immediately after the introduction of the autoclave in the oven the raw materials are still found amorphous and only after a period of time, known as the “induction time”, the first traces of the zeolite appear.
4. In a process that takes place gradually, all the Si and Al atoms from the amorphous raw materials are transferred to crystalline network of the zeolite.

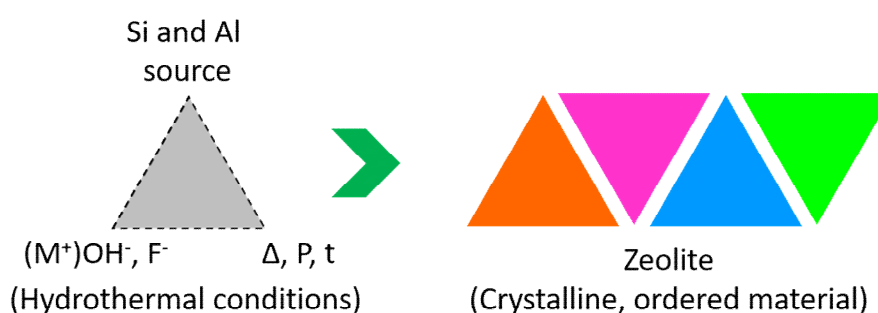


Figure 2. Artistic representation of zeolite synthesis.

A special mention for the contribution to the zeolite synthesis, has to be given to Richard Barrer, whom (besides many other achievements in the field of zeolite synthesis) was one of the first to introduce organic cations (quaternary ammonium compounds) in the synthesis gels [44]. Usually the raw materials introduced in the reaction are amorphous in nature with different reactivities. A mineralizing agent is

generally introduced in order to dissolve the SiO<sub>2</sub> bonds and to mobilize the T atoms. As seen in the Figure 2, the synthesis of zeolites is highly influenced by all the parameters involved in the reaction.

Although during the last decades various possible mechanisms have been proposed for the nucleation and crystal growth of zeolites (page 7 in [41]), this field is still not fully understood. From a classical point of view, a possible route, in order to understand the mechanism of zeolite synthesis, can be described as follows: the induction period, the nucleation part and the crystal growth of the zeolite. The induction period is regarded as the time that takes the reaction to reach the first crystalline material, from when the raw materials are mixed together to the moment the product is seen on the PXRD. Usually the induction period ( $\tau$ ) is described as:

$$\tau = t_r + t_n + t_g$$

Where  $t_r$  is the time that takes the raw materials to undergo equilibration reactions and a distribution of solution species, when all the reaction parameters are starting to interconnect together and act on the reacting gel.  $t_n$  – stands for the time that is necessary to form a stable nucleus. This is especially important as it might be possible that a big number of nuclei appear and disappear in the mother solution, until the nucleus is reaching a certain dimension.  $t_g$  – represents the time that takes for nucleus to grow and to form small crystals. From a different point of view the stage when the materials are bring into contact is considered as the primary amorphous phase. This stage is characterized by a gel or even a colloidal phase and the products of the first interaction between the raw materials. It is described as being the non-equilibrium stage, being less homogeneous in nature, containing individual species and unreacted (or only partially reacted) raw materials. After heating the solution mixture various equilibrium reaction are believed to take place, with the formation of a nutrient – rich, mother liquor, namely the secondary amorphous phase. This leads to a better distribution and repartition of the reaction components and a transfer solid – liquid as the equilibrium is being established. Cations are playing an important role at this stage, by imposing a structuring effect on the random species, leading to a local periodic organization of this nutrients. When all the reaction parameters are acting on this stage and for a satisfactory period of time, the secondary amorphous phase is converted into the zeolite product.

From a classic perspective, the zeolite nucleation is a highly complex sequence of events, starting with the pseudo-nuclei that are formed in the secondary

amorphous phase, which are created by the mother solution, some of them are becoming larger, or other are re-digested by dissolution. This is regarded as the first order transition and corresponds in the same time to the formation of nucleus with a critical radius which energetically favors the growth of the crystal network. At this stage the kinetics responsible for the nuclei growth are overcoming the kinetics for their dissolution and the  $t_g$  term is almost replacing the  $t_r$  component in the induction period expression. This means that in order for the crystal lattice to propagate, a nucleus of a critical volume must be formed. The radius of this sphere it is believed to not be of a certain value, but more a variable that depends on the reaction conditions e.g. supersaturation and temperature. As being said the necessity for the creation of stable and sufficient numbers of nuclei is extremely important in order for the structure to propagate and the crystal growth to take place on the named nuclei. This is basically done by reversible condensation reactions T – O – T bonds, which brake and form continuously in the synthesis gel. The cations organize the newly formed T – units in compounds having the form  $(T(OH)_3O^-)$ , which further reacts with similar or different fragments giving rise to the periodic zeolite lattice. The zeolite crystals are growing based on small monomeric species that are taken from solution, generally anions of silicate and aluminate species in the form of  $Si(OH)_3O^-$  and  $Al(OH)_4^-$ . In the literature [41] the process of the zeolite crystal growth is presented to be slower than the crystallization of ionic and molecular crystals, such as inorganic salts and sugar. Although there are presented various pathways for the zeolite crystal growth the objective of this introduction is to present a general overview on this subject. In this regard, the most generally applied model for the crystal growth of the zeolite systems is based on the transfer of predominantly simple, monomeric species from solution to the growing site. After the nucleation is taking place, either in the proximity or on the surface of an amorphous particle, the crystalline part is starting to grow on the expense of the nutrient species from the solution. The small monomeric units are than replaced by the re-adjustment of the solution equilibria through the dissolution of the amorphous material or short – range order particles, which supply new species for the growing site. Such species are highly dependable on the chemical units that are present in the synthesis gel, for example  $OH^-$  or  $F^-$  as the type of mineralizing agent will influence their nature. The crystal growth of the zeolites is generally considered to be based on solution – mediated mechanism or from the aggregation, followed by the ordering of the species and it is solely relying on the reversible T – O – T equilibration reactions



of continuously making and breaking the bonds. The reversibility of the crystal growth at the hydrothermal conditions was extensively exploited in recent studies. For example Maldonado *et al.* [45] established ternary (kinetic) phase diagrams for the system  $\text{SiO}_2 - \text{Al}_2\text{O}_3 - \text{Na}_2\text{O}$  for the zeolite syntheses, in the absence of organic structure directing agents (OSDAs). They have been able to establish limits for the safe modification of the synthesis parameters without the risk of obtaining unwanted crystalline phases. This is also allowing a fine tuning of various properties of the zeolite product inside the boundaries delimited by the synthesis parameters. An important aspect of the work was the experimental observation of the Ostwald rule of stages. As such, it was observed that for the Na syntheses system, first crystallizes structures with a low framework density (e.g. EMT, LTA, FAU) and then, by increasing the temperature and the reaction time zeolites with a high framework density crystallizes such as GIS, SOD, CAN, JBW, ANA.

Recent studies performed on the mechanism of crystallization of silicalite-1 (framework code: MFI) suggest that a combination of classical and non-classical approach for the zeolite crystal growth is possible [46]. By using in situ atomic force microscopy (AFM), the growth of the (010) facet of the silicalite-1 crystals was monitored under realistic hydrothermal conditions. It was found that crystallization mechanism appear as a 2D nucleation and step by step formation of crystal layers and their spreading as they grow. At high temperature (160 °C), well faceted silicalite-1 crystals are observed, whereas at lower temperature (80 °C) surfaces with well-defined layers are not present anymore, suggesting that crystallization at low temperature is taking place by a 3D mechanism. This is indeed pointing to the fact that in this case the crystal growth occurs by the addition of the silica molecules, part of the classic mechanism, as well as by involving the direct attachment of the nanoparticles, which represents the nonclassical mechanism approach. Similar results for the crystallization mechanism of SSZ-13 (framework code: CHA), have been recently published by Kumar *et al.* [47]. They have been able to show that the growing mechanism of SSZ-13 is taking place by the attachment of the amorphous silicate species to the crystal surfaces that assembly the nonclassical mechanism approach and also the incorporation of molecules layer-by-layer, which is regarded as the classical mechanism of zeolite crystal growth. This shows that the crystal growth of the zeolites is a highly complex mechanism. Further results published from the same group shows that for zeolite L (framework code: LTL) the growth mechanism involves

crystallization by particle attachment, describing a nonclassical crystal growth pathway [48]. Other studies, performed on FAU and LTA – type zeolites have shown that the heterogeneous nucleation of this materials involves a nonclassical crystallization pathway and the nucleation possible occurs on the exterior surface of the amorphous species [49]. The induction period and the crystal formation is believed to be dependent on the heterogeneity of the synthesis gels, or the rate of the Si extraction and release in Al-rich gels. Recently two potential mechanism pathways has attracted considerable attention from the zeolite community: the classical addition of monomer-by-monomer that involves organic molecules, metal ions and mineralizing agents, but also the possibility of formation of various precursors during the induction period such as clusters and oligomers, may play an important role in the nucleation. This comes alongside with the crystallization by particle attachment (CPA) which represents the nonclassical crystallization approach of zeolite materials [50]. Water is usually the preferred medium for hydrothermal reactions and this is because of economic reasons but also due to the water properties that change when it is sealed at high temperature and pressure. The vapor pressure and the ionic product will increase and on the other hand the values of the surface tension, the viscosity and the density will decrease.

The zeolite synthesis is highly dependent on the reaction parameters such as: reactants, time and temperature of the crystallization, aging, pH and the presence of inorganic and/or organic cations, in the synthesis gel. The Si/Al ratio of the synthesis gel is an important player in determining the structure and the composition of the product. It must be mentioned that there is no mathematic correlation between the Si/Al ratio of the synthesis gel and that of the obtained product, except that the Si/Al ratio is never higher than that in the gel. Usually from gels with a low Si/Al ratio, zeolites with a low SAR (Si/Al ratio) are obtained, whereas from high SAR gels, siliceous materials are resulting. The Si/Al ratio in the product is lower than the one of the synthesis gel. This points to the poor utilization of the T-atoms, which is influencing the yield of the synthesis. The Si and Al source used in the reaction gel is also important due to various aspects such as: dissolution of the reactants and the relative configuration of the T-atoms. The zeolite synthesis is highly dependent on the alkalinity of the reaction system. This can be defined as  $\text{OH}^-/\text{Si}$  and is represented by the amount of hydroxide introduced in the reaction (e.g. NaOH), the amount of hydroxide introduced with the template (in the  $\text{OH}^-$  form) and with the hydroxide introduced with the raw materials (e.g.  $\text{Na}_2\text{SiO}_3$ ). High ratio of  $\text{OH}^-/\text{Si}$  is leading to a high solubility of

the T-atoms. It is also believed that a high amount of  $\text{OH}^-$  will be detrimental for the polymerization of the silicate anions, but will favor the polymerization of the polysilicate and aluminate anions [51]. This also means that an increase in the alkalinity will make the induction and nucleation time shorter and will make the zeolites crystallization faster. Zeolite synthesis gels with a high pH are usually generating aluminum-rich zeolites and FAU zeolite is a powerful example in this regard. Another aspect of the alkalinity is that it is responsible of speeding up the crystallization rate and it is also responsible of decreasing the particle size, as well as narrowing the particle size distribution. Aging – is defined as the period between the formation of a homogeneous gel and the formation of the first crystals and it is dependent on the time and temperature. It is usually applied to increase the nucleation speed. The inorganic cations play an extremely important role, by influencing the polymerization state of polysilicate and aluminate species, as well as supporting the framework structure of the zeolite materials. The templating effect of the inorganic cations has been described by R. Barrer [44]. On the other hand the organic cations have a more pronounced templating effect and are responsible of increasing the diversity of the zeolite frameworks. It is generally accepted that the silicate and aluminate species condensate on the organic template, generating in this way a crystalline network, where the organic molecules are found to be trapped in the zeolite pores. Although it is complicated to express the exact role of the organic molecules and their interactions with the inorganic zeolite framework, several ideas have been proposed such as, e.g. from lowering the surface tension to the various interactions that may take place. These interactions are assumed to take place with the precursors and are Coulombic, van der Waals or H-bonds [51]. An extensive insight on the OSDAs is given in the third paper attached in this thesis.

## Chapter 2

### Computational studies for novel zeolites

To define structural descriptors for a zeolite framework in the light of the SCR reaction, one may ask the question: How the best zeolite for SCR of NO<sub>x</sub> should look like? When one tries to imagine how a hypothetical new zeolite have to be structurally for a specific application, it is without a doubt the application who dictates the zeolite specificity. It is already well known that the structure of zeolites highly influences the catalyst behavior. The pore system dimension, the size of cavities and rings in the zeolite framework have a decisive impact on the catalyst. In this consideration we tried to answer at the question how a perfect zeolite for SCR of NO<sub>x</sub> should look like? What special structural features it needs? and the most important what makes a zeolite the best catalysts and what additional structural features it requires in order to exhibit an even better performance than the existing state-of-the-art catalyst materials. A structural definition, matrix-like would be tried out, in which we identified the fundamental characteristics with elements that are considered to be the most important and then, showing how these elements form a system that describes the zeolite catalyst for DeNO<sub>x</sub> applications.

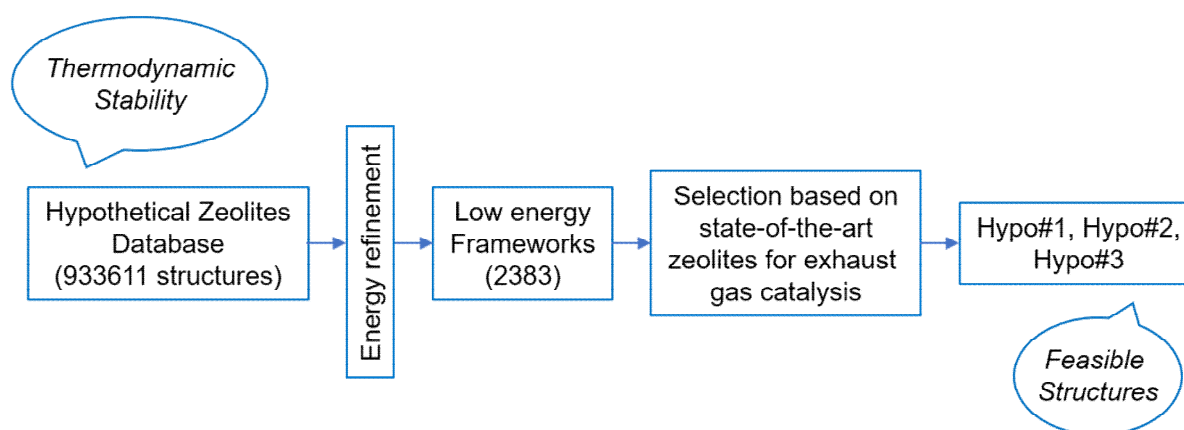


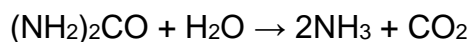
Figure 3. Rational selection of hypothetical zeolites for NH<sub>4</sub>-SCR reaction.

What do we know?

The Selective Catalytic Reduction of nitrogen oxides (SCR of NO<sub>x</sub>) is the most researched method and the leading process for cleaning the exhaust gas emitted by the diesel engines and related combustion activities. It is equally used for the stationary premises, e.g. plants and factories with high polluting activities and also for the automotive industry. Although combustion controls procedures have been developed and applied for reducing the impact of the exhaust gas on the environment, the amount of NO<sub>x</sub> gases is considerable high compared to the tight legislation for emissions control.

For NO<sub>x</sub> abatement, various techniques have been developed and based on the literature information have been ordered in three main groups [52]. The first group refers to the pre-combustion methods and involve the purification of the fuel, by lowering its nitrogen content before being used for the engines. The second group are comprised from methods that prevent the formation of NO<sub>x</sub>. This suppose the conditions optimization to avoid the formation of NO<sub>x</sub>, e.g. by reducing the amount of oxygen that is present in the process and also by lowering the peak temperature and the residence time at the peak residence. The third group involves installation of tail-end control equipment after the combustion and is divided into two parts: the selective non-catalytic reduction (SNCR), the selective catalytic reduction (SCR) and also NO<sub>x</sub> storage / reduction and cleaning the flue gas with an electron beam radiation. The reduction techniques mentioned above make use of both anhydrous and aqueous solution of ammonia (NH<sub>3</sub>) and urea (CO(NH<sub>2</sub>)<sub>2</sub>), used to reduce the NO<sub>x</sub> to N<sub>2</sub> and H<sub>2</sub>O. The SCR process is made up from the following steps [52]:

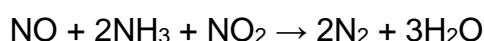
1. The formation of ammonia:

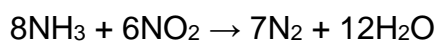


2. The standard SCR reaction:



3. The fast SCR reaction:





The fast SCR reaction takes place if the  $\text{NO}_2/\text{NO}_x$  ratio is high enough. The literature also mention for this type of reactions, that the lowest activation barrier associated with the highest reaction rate is below 200 °C. Besides this reactions described above, there are also possible other reactions that are responsible for the generation of  $(\text{NH}_4)_2\text{SO}_4$ ,  $(\text{NH}_4)_2\text{HSO}_4$  and  $\text{H}_2\text{SO}_4$ , due to the oxidation of  $\text{SO}_2$  to  $\text{SO}_3$ . Another unwanted product that can take place as a consequence of a side reaction is the  $\text{N}_2\text{O}$ , which is a greenhouse gas with more powerful global warming effect than  $\text{CO}_2$  [52].

The traditional SCR catalysts make use of transition or noble metal oxides or mixed metal oxides. One such example is the V-SCR catalyst ( $\text{V}_2\text{O}_5/\text{TiO}_2$  promoted with  $\text{WO}_3$  and  $\text{MoO}_3$ ), supported by  $\text{TiO}_2$ . Although Vanadium-based catalysts are known to have various advantages such as: low cost, high tolerance to Sulphur compounds and high de $\text{NO}_x$  activity it has also some important drawbacks. For example they are working at high temperatures and also a narrow temperature window (300 – 400 °C). Another problem is that the vanadia, which is the active site for the de $\text{NO}_x$  reaction it is also oxidizing the  $\text{SO}_2$  to  $\text{SO}_3$ . Maybe the most important issue is that  $\text{V}_2\text{O}_5$  it is highly toxic and carcinogenic and can be a direct threat to the human health and to the environment. It must be mentioned that the commercially available V-SCR catalysts release V and W at temperatures starting from 550 °C and even higher, but such system can be used if the temperature never exceeds the mentioned temperature limit [52].

The range of zeolites studied so far for the selective catalytic reduction of nitrogen oxides ( $\text{NO}_x$ ) is not very large relative to the number of existing frameworks. The reasons for this is that sometimes only commercially available or so called “easy-to-make” zeolites have been catalytically tested and in other situations zeolites with a specific framework structure and pore sizes were introduced as catalysts in this field. Some of these microporous materials tested for SCR of  $\text{NO}_x$  are presented in table 2 along with their structural characteristics.

Table 2. Selected zeolite frameworks loaded with transition metal ions (Fe<sup>2+</sup>, Cu<sup>2+</sup>) tested as DeNO<sub>x</sub> catalysts for NH<sub>3</sub>-SCR reaction.

Zeolite framework	Pore system (D)	Rings size (R)	Limiting rings dimension	Framework density T/1000 Å <sup>3</sup>	Special CBU
*BEA [53-55]	3D	12 6 5 4	[100] <b>12</b> 6.6 x 6.7 [001] <b>12</b> 5.6 x 5.6	15.3	-
MFI [54, 56, 57]	3D	10 6 5 4	[100] <b>10</b> 5.1 x 5.5 [010] <b>10</b> 5.3 x 5.6	18.4	-
MOR [54]	2D	12 8 5 4	[001] <b>12</b> 6.5 x 7.0 [001] <b>8</b> 2.6 x 5.7	17.0	-
FER [58]	2D	10 8 6 5	[001] <b>10</b> 4.2 x 5.4 [010] <b>8</b> 3.5 x 4.8	17.6	-
CHA [59]	3D	8 6 4	[001] <b>8</b> 3.8 x 3.8	15.1	d6r
AFX [60]	3D	8 6 4	[001] <b>8</b> 3.4 x 3.6	15.1	d6r
AEI [61]	3D	8 6 4	[001] <b>8</b> 3.8 x 3.8	15.1	d6r

The presented table above shows that both large, medium and small pore zeolites have been tested for SCR reaction. However, it is well known that the gas flow needs to have a good and continuous access to the active sites for a high conversion of nitrogen oxides (NO<sub>x</sub>). As a consequence, any forms of diffusion limitation should be avoided. In this way, the first important parameter that arises from this observation is in direct correlation with the zeolite pore system. A *three dimensional* channel system for the zeolite seems to be relevant and represents the first element that our selected zeolites should contain. The open literature contains clear indications that large pore zeolites (\*BEA, MOR, FER, MFI) create also large amounts of laughing gas (N<sub>2</sub>O) [62, 63]. This is one of the reasons why the second criterion considered is that the zeolite should contain *rings no bigger than 8 T-atoms*. These 2 elements made us focus on small-pore zeolites. The last 3 zeolites presented in table 2 are part of such a class of molecular sieves. The CHA framework is considered to be the state-of-the-art of zeolites for NH<sub>3</sub>-SCR, due to its high hydrothermal stability. The other 2 zeolites AEI and AFX have also shown exceptionally high performance. All 3 of them show unprecedented hydrothermal stability and catalytic activity compared with zeolites with larger pores, making them by far the best reference for any attempt of designing new zeolites. A more detailed analysis of the presented small-pore zeolites shows that their

characteristics superimpose on other features also, besides the 3D pore system and the presence of only 8, 6 and 4 rings. The circularity of the 8-MR with equal or almost equal diameters is one such example. Table 2 is showing the dimensions of the limiting rings. For the AEI and CHA, the 8-MR is circular with the diameter length of 3.8 Å in difference from AFX, where the 8-MR is a slightly deformed circle, close to an ellipsoid form. This is a very important criterion as it is believed that Al-species are more easily escaping from the framework positions, when the rings have a different form than circular, affecting the hydrothermal stability of such material. Another important structural feature for all small-pore zeolites presented in table 2 is the *double 6-ring (d6r)*. Previous studies made by Lobo *et. al.* showed that the d6r is the preferred coordination for the Cu<sup>2+</sup> cations. [60] While all state-of-the-art zeolites for DeNOx applications (CHA, AEI, AFX) have this feature, it is unclear if it is necessary. It definitely affects the Cu mobility and the d6r is a particularly stable coordination site for Cu<sup>2+</sup>. As such, we are interested in looking at zeolites even without this feature.

#### Hypothetical zeolites

It is beyond the scope of this thesis to present in a detailed manner some of the most important chapters regarding hypothetical zeolites such as the graph theory, systematic enumeration of molecular sieves and mathematical tiling theory applied on zeolites. However, a brief description of some of these concepts is definitely necessary in order to familiarize the reader with the vast domain of hypothetical zeolites and with some of the most important achievements that have been done in this field.

At the intersection between abstract mathematics and computational chemistry, a large set of hypothetical zeolites have been defined with the help of graph theory. For zeolites as crystalline materials their structure is not changing with any existing 230 crystallographic space groups. Even if it is easier to imagine the unit cell of the zeolites as a crystallographic tile that fills the space, graph theory makes use of a fix fundamental domain, smaller in size than the unit cell and specific for each space group. The fundamental domain represents the smallest entity that cannot be further subdivided without breaking the space group symmetry. Tiling of the “puzzle” copies of the fundamental domain made by translation, rotation, mirroring or glide reflection movements helps building the zeolite unit cell. In this way the zeolites are seen as



combinatorial models of different structures and are considered to be what is known as “four-regular periodic graphs”, where vertices (in graph theory a vertex is a node or point) are represented by the T-atoms (Si and Al for aluminosilicates) and the edges (term used in graph theory as the line that connects the vertices) are represented by the oxygen bridges. Due to the geometric constraints imposed by the way in which the tetrahedral atoms connect to each other, and the chemistry of such atoms for a fixed number of vertices the four-regular periodic graphs possibilities is small [64], [65], [66].

## Zeolites Databases

The International Zeolite Association online database was the first database created for zeolite frameworks. It started in 1996, when on a server of the ETH university in Zurich and under the guidance of Christian Berlocher an online version of two books appeared. The books published on behalf of the Structure-Commission of the International Zeolite Association named “Atlas of zeolite structure type” [67] and “Collection of simulated XRD powder patterns for zeolites” [68] represents the fundamental stone and path the way for the IZA-SC database as we know it today. The database is able to show all the necessary characteristics for a good understanding of zeolites chemistry such as, crystallographic parameters, pore system, rings sizes and cavities of different zeolite structures.

The total number of distinct zeolite frameworks characterized so far, (counting both synthetic and natural zeolites) is 239 structures by fall 2018 [40]. All of these structures are believed to represent approximately 0.01 % from the hypothetical zeolites predicted to be possible [69]. However, this number may be even lower due to the increasing interest in theoretic zeolites predicted by advanced computational methods. When it comes to hypothetical zeolites databases, there are several research groups, whom by applying different computational methods, they have been able to generate a considerable high number of zeolite frameworks. It is expected that hypothetical frameworks may assist the research scientists involved in the synthesis and structure solving of novel zeolite materials.

In this way the database hosted by the <http://www.hypotheticalzeolites.net> website have been created and is freely available since April 2004. The structures have been generated by using the Symmetry-Constrained Intersite Bonding Search (SCIBS). The body of the database is divided into 3 sections: Bronze, Silver and Gold.

These 3 groups contain frameworks stored as CIF files with a different level of refinement, making possible to search for the space group number, energies relative to quartz, cell parameters, framework density and the number of unique crystallographic atoms. The database has also three different tools for framework topological analysis, TOTOPOL; a program for simulated PXRD patterns, CIF-2-POWD; and a program that generates spheres that can fill the void volume of a framework structure, Sphere Viewer [52].

A number of 97 zeolite frameworks, which count for around 42 % from the well-defined IZA zeolites are found in the Bronze database made by M. D. Foster and M. M. J. Treacy at Arizona State University, part of the database hosted by the <http://www.hypotheticalzeolites.net> website [70]. The Bronze database is made up from 5389407 frameworks with an energy value below 1.0 eV / SiO<sub>2</sub>.

#### Selection of 3 zeolite frameworks

In order to select 3 zeolite frameworks that have the characteristics and structural features established above a database referred herein as “hypothetical zeolites database” with 933611 structures has been used. The structures are part of the silver database from [www.hypotheticalzeolites.com](http://www.hypotheticalzeolites.com) (Martin D. Foster and Michael M. J. Treacy) containing maximum 6 different T-atoms. The sections have been performed by using the ZeoTsites Code developed at ITQ [71]. Figure 3 shows schematically the selections that were performed and applied to the hypothetical zeolites database.

The thermodynamic stability of the theoretic zeolites is one of the most important parameter. As mentioned above it represents the first clue that the selected zeolite is feasible. As a consequence, the first selection step was done by imposing an energy requirement criterion that would refine only the zeolite structures with energies lower than (or equal with) 0.15 eV (3.459 Kcal mol<sup>-1</sup>, or 14.473 KJ mol<sup>-1</sup>), as it is shown in equation 1. However, even if this energy cut-off rules out some of the importantly well-defined zeolite frameworks such as zeolite Y (framework code: FAU), the ability of such criterion for the selection of new zeolites, should be efficient when applied to hypothetical, unrefined framework structures.

$$(1) E \leq 0.15 \text{ eV/SiO}_2$$

When this energy limiting factor is applied to the hypothetical zeolites database the output of this selection step was a number of 2383 frameworks. This set of thermodynamically accessible structures was used as a custom build database for further selections. In order to increase the probability of finding good potential zeolites for NH<sub>3</sub>-SCR of NO<sub>x</sub>, 6 different selection criteria have been applied to the set of 2383 structures refined above.

Table 3. Overview on the different selections performed, their descriptors and the output structures.

<b>Selection</b>	<b>1</b>	<b>2</b>	<b>3</b>	<b>4</b>	<b>5</b>	<b>6</b>
<b>Descriptors</b>	Rings(R): 4, 6, 8	✓	R: 4, 6	R: 4, 5, 6, 8	R: 5, 6, 8	R: 6, 8
	D6R	-	-	-	-	-
	8-MR: D <sub>1</sub> ≈D <sub>2</sub>	✓	-	✓	✓	✓
	∠(T-T-T)=119-121°	-	-	-	-	-
<b>Total: 823</b>	<b>211</b>	<b>457</b>	<b>18</b>	<b>121</b>	<b>14</b>	<b>2</b>

#### Selection 1:

For the first selection the input criteria were: the presence of only 4, 6 and 8 rings, minimum 80 % of the 8-MR to be circular, the frameworks should have double 6-rings (d6r) and the T-T-T angle should be between 119-121 degrees. The output for this selection process was a number of 211 structures.

#### Selection 2:

In a similar manner with the first selection, for the second refinement only 2 criteria were used: the presence of only 4, 6 and 8 rings and minimum 80 % of the 8-MR to be circular. The output for this selection step was a number of 457 structures.

#### Selection 3:

For this set of frameworks many requirements used in the previous selections were ruled out. The selection criteria were the same as for selection 2, with the change that all the structures to have only 4 and 6 rings, without the use of the 8-MR to be circular. The output of this search was 18 structures.

#### Selection 4

The selection criteria were the same as for selection 2, with the change that all the structures to have only 4, 5, 6 and 8 rings were considered and the. The result of this search was 121 structures.

### Selection 5

The selection criteria were the same as for selection 2, with the change that all the structures to have only 5, 6, 8 rings. The output of this search was 14 structures.

### Selection 6

The selection criteria were the same as for selection 2, with the change that all the structures to have only 6, 8 rings. The result of this search was 2 structures.

As a consequence, a total number of **823** frameworks had been selected from which only 3 theoretically possible zeolites were selected by carefully visual inspection of each structure individually. In order to make a more feasible zeolite from synthesis point of view (only 1 type of cage), the zeolites have been manually modified, resulting new frameworks called: Hypo#11, Hypo#1, Hypo#22, Hypo#21, Hypo#2, Hypo#31, Hypo#3. The final 3 zeolites that were selected in order to be synthesized are: **Hypo#1**, **Hypo#2** and **Hypo#3** (named Hypo#1 in the Paper 3 *Synthesis of high-silica ERI driven by computational screening of hypothetical zeolites*).

All the selected frameworks are presented below with their given names and also with the database names in the brackets. For each structure a table with the structural properties of the zeolite is presented and also the zeolite framework is presented for a better clarity and understanding of the chosen structures as synthesis target.

Table 4. The main framework properties for the selected Hypo#11 structure.

<b>Zeolite features</b>	
<b>Name</b>	Hypo#11 (139_4_82028)
<b>Number of cavities</b>	2 (sas and sav)
<b>Number of T-atoms</b>	4
<b>Channel system</b>	3-dimensional
<b>Composite Building Units (CBU)</b>	sas, sav, D8R
<b>Rings</b>	4, 6, 8

The principal characteristics of the selected framework are shown in Table 4. The 3-dimensional channel system is perfectly answering the issues with the diffusion limitations, that may arise in harsh working conditions. Structurally, as seen in Figure 4, the Hypo#11 is made from columns of sas and sav cages linked together. Interestingly, arranged columns can easily be distinguished. The framework is composed by columns made up of 2 sas cavities assembled in a mirror configuration. This group of structural units are connected along the z-axis through double 8-rings (D8Rs) and sas cages.

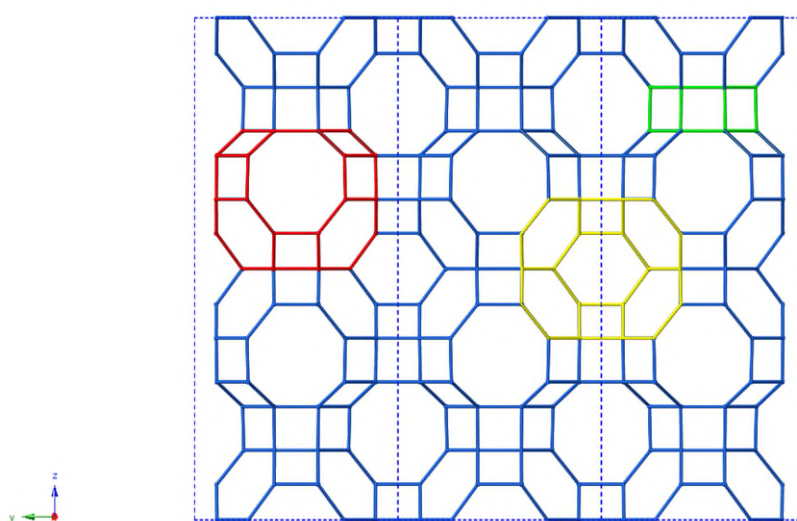


Figure 4. Hypo#11 zeolite framework viewed along the x-axis. The sas (red) and the sav (blue) cavities and D8R (yellow) unit are highlighted.

Structural modification of the Hypo#11 zeolite framework.

As it was presented above the selected Hypo#11 framework, shows good structural features for a possible DeNOx catalysts. However, the presence of *two* different cavities sas and sav, is raising a series of difficulties when it comes to the preparation of this zeolite. From the synthesis point of view such frameworks are difficult to be made.

In the light of this consideration the selected framework, Hypo#11 has been manually modified by eliminating the sas cavity (highlighted in red) and structurally rearranging the atoms network to a novel framework structure. The framework geometry was optimized using the well-known slc force field.

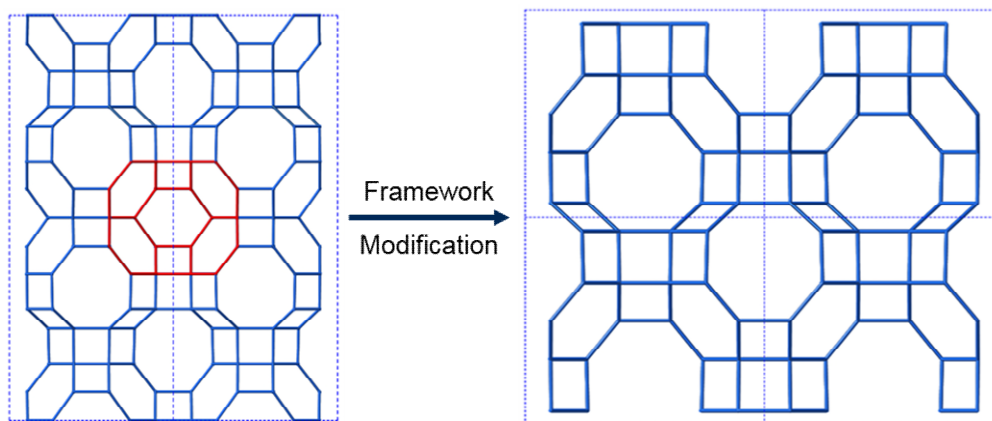


Figure 5. Images of Hypo#11 (left) and Hypo#1 (right) framework structures.

Table 5. The main framework properties for the Hypo#1 structure.

<b>Zeolite features</b>	
<b>Name</b>	Hypo#1 (139_4_82028_modif)
<b>Number of cavities</b>	1 ( <i>sav</i> )
<b>Number of T-atoms</b>	3
<b>Channel system</b>	3-dimensional
<b>Composite Building Units (CBU)</b>	<i>sav</i> , D8R
<b>Unit cell</b>	2 cavities and 40 T atoms per u. c.
<b>Rings</b>	4 [4.3 x 4.3]; 6 [5.7 x 6.2]; 8 [7.5 x 7.9]; [8.1 x 8.1]

The rearrangement process modified the Hypo#11 framework in such a way that *sas* cages were eliminated from the structure. The newly created framework, named herein Hypo#1 contains only 1 type of cavity (e.g. *sav*) and is respecting the feasibility criteria (see Annexes, The geometry and connectivity parameters for hypo#1 (thesis)). From the structural point of view, the framework is constructed from columns of *sav* cages linked together through double 8-rings (D8Rs). The *sav* cages are then rotated to 180° in the next column and still united by similar D8R. This pattern makes the hypo#1 a simple framework that is a very good candidate as a synthesis target zeolite. Figure 6 is showing the structure of hypo#1 and Figure 7 is presenting the 3D image of the framework, for a better visualization of the cages and their particular orientation.

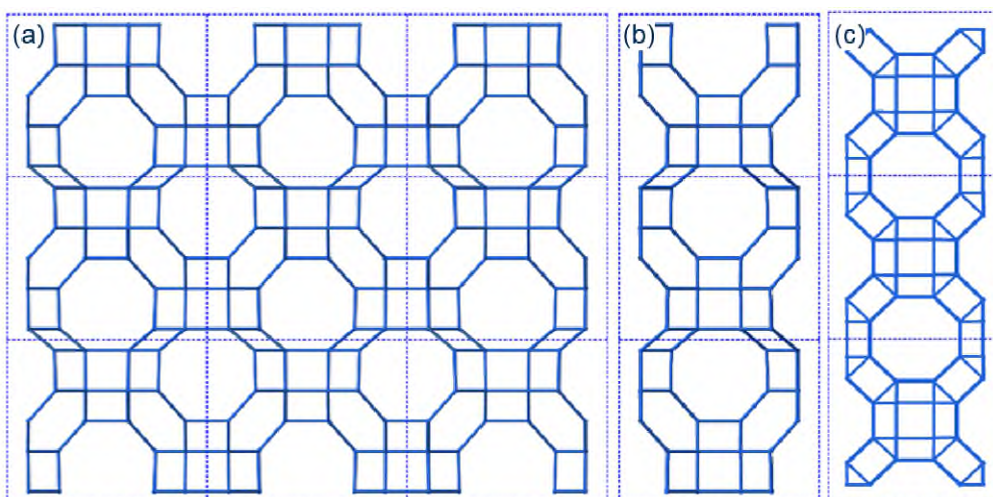


Figure 6. Hypo#1 zeolite framework seen along N(100) direction (a), N(010) direction (b) and N(001) direction (c).

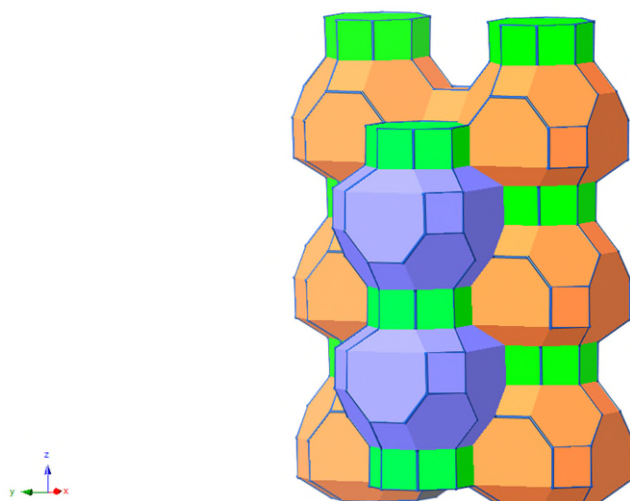


Figure 7. 3D image of Hypo#1 zeolite structure.

Table 6. contains the main framework properties of the second hypothetical zeolite selected from the database and named herein, Hypo#22. The structure contains three types of cavities, which makes it very difficult to be synthesized, due to the need to fill at least two cages. Figure 8 presents the image of hypo#22, seen along the x-direction, with the *atn* (green), *pau* (yellow), *hypo#2* (red) cages highlighted for a better visualization.

Table 6. The main framework properties for the Hypo#22 structure.

<b>Zeolite features</b>	
<b>Name</b>	Hypo#22 (139_5_3770809)
<b>Number of cavities</b>	3 ( <i>atn</i> , <i>pau</i> , <i>hypo#2</i> )
<b>Number of T-atoms</b>	5
<b>Channel system</b>	3-dimensional
<b>Composite Building Units (CBU)</b>	<i>pau</i> , <i>hypo#2</i> , D8R, <i>atn</i>
<b>Rings</b>	4 6 8

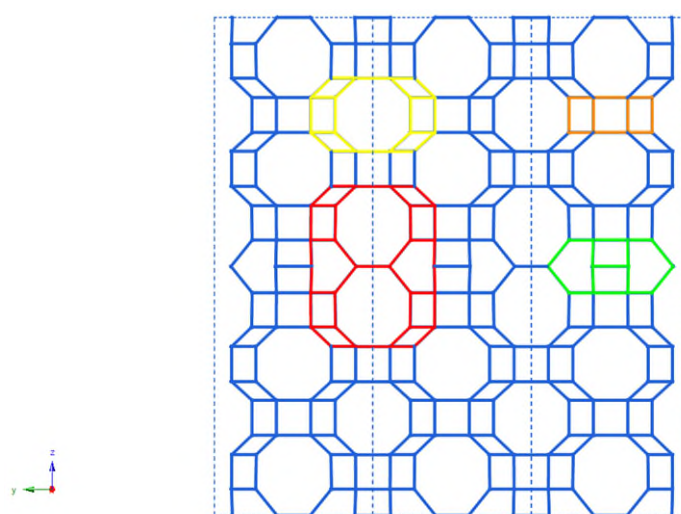


Figure 8. Framework structure of Hypo#22.

The zeolite Hypo#22 was manually modified and other zeolites named Hypo#21 and Hypo#2 have result from this modification. The first structure that have result from this modification (Figure 9), *hypo#21* (see Table 7 and Figure 10) still contains three different types of cages which impose several issues when it comes to the synthesis part. However, the second structure that have been made by rearranging the atom positions (Figure 11), *hypo#2* (Table 8 and Figure 12), contains only two cages from a structural point of view, but only 1 cavity should be considered in terms of stabilization by the OSDAs.



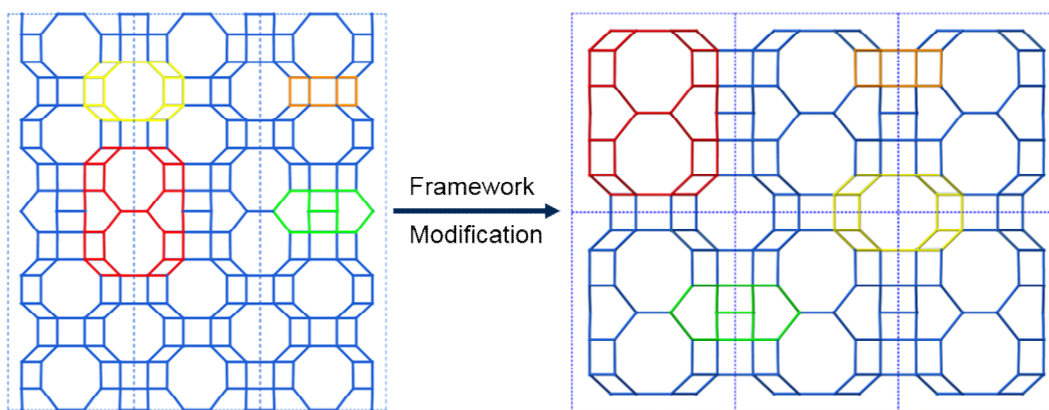


Figure 9. Images of Hypo#22 (left) and Hypo#21 (right).

Table 7. The main framework properties for the Hypo#21 structure.

<b>Zeolite features</b>	
<b>Name</b>	Hypo#21 (139_5_3770809_modif1)
<b>Number of cavities</b>	3 ( <i>atn</i> , <i>pau</i> , <i>hypo#2</i> )
<b>Number of T-atoms</b>	4
<b>Channel system</b>	3-dimensional
<b>Composite Building Units (CBU)</b>	<i>pau</i> , <i>hypo#2</i> , D8R, <i>atn</i>
<b>Rings</b>	4 6 8

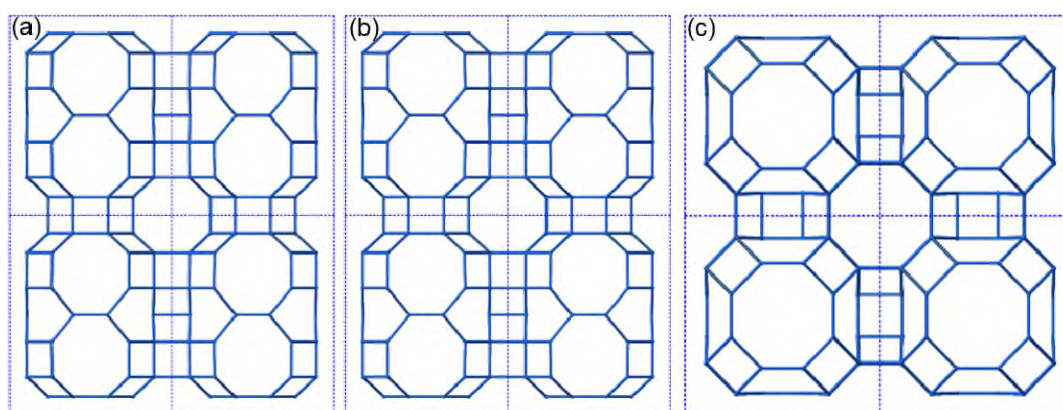


Figure 10. Hypo#21 zeolite framework seen along N(100) direction (a), N(010) direction (b) and N(001) direction (c).

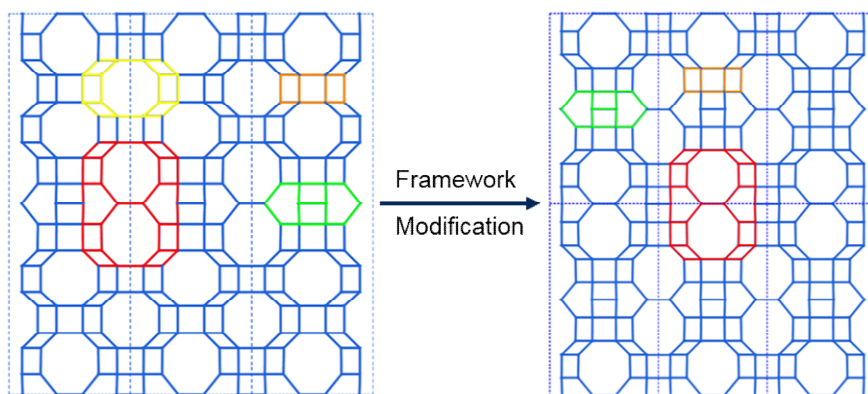


Figure 11. Images of Hypo#22 (left) and Hypo#2 (right).

Table 8. The main framework properties for the Hypo#2 structure.

<b>Zeolite features</b>	
<b>Name</b>	Hypo#2 (139_5_3770809_modif2)
<b>Number of cavities</b>	2 ( <i>atn</i> , <i>hypo#2</i> )
<b>Number of T-atoms</b>	3
<b>Channel system</b>	3-dimensional
<b>Composite Building Units (CBU)</b>	Hypo#2, D8R, <i>atn</i>
<b>Unit cell</b>	2 cavities and 80 SiO <sub>2</sub> per u.c.
<b>Rings</b>	4 6 8

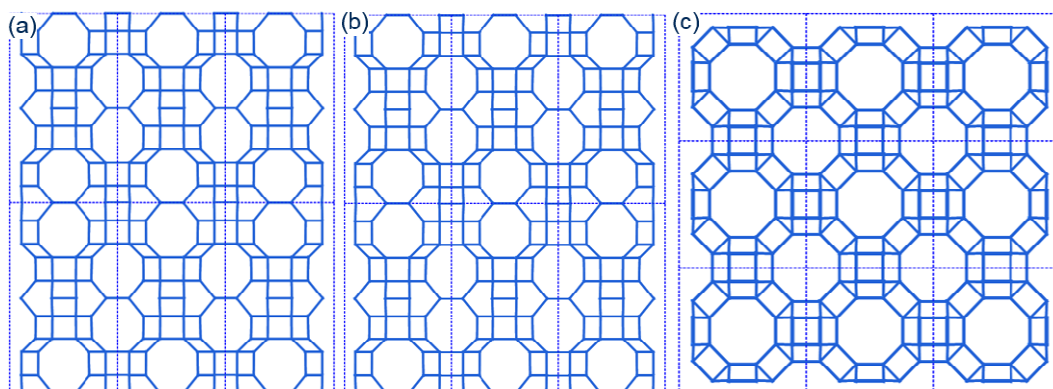


Figure 12. Hypo#2 zeolite framework seen along N(100) direction (a), N(010) direction (b) and N(001) direction (c).

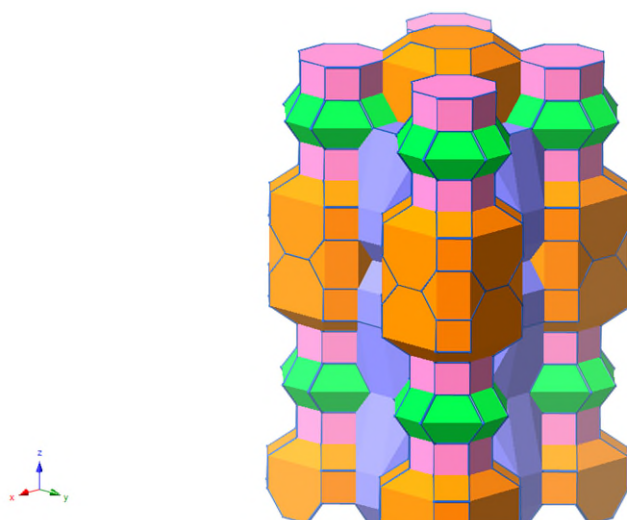


Figure 13. 3D image of Hypo#2 zeolite structure.

The framework of the third zeolite is presented below (see Table 9 and Figure 14). A modification (Figure 15) has been performed in order to make a more feasible structure. The resulting framework, Hypo#3 (see Table 9 and Figure 16) it is extensively studied in Part 2, the third paper, attached to this thesis, named “Synthesis of high-silica ERI driven by computational screening of hypothetical zeolites” under the name of “hypo#1”. The geometry and connectivity parameters of Hypo#3 can be found in the supporting information of the above mentioned article, page 112.

Table 9. The main framework properties for the Hypo#31 structure.

<b>Zeolite features</b>	
<b>Name</b>	Hypo#31 (139_4_48475)
<b>Number of cavities</b>	4 ( <i>atn</i> , <i>pau</i> , <i>hypo#3</i> , ...)
<b>Number of T-atoms</b>	4
<b>Channel system</b>	3-dimensional
<b>Composite Building Units (CBU)</b>	<i>hypo#3</i> , D8R, <i>atn</i> , <i>pau</i> , ...
<b>Rings</b>	4 5 8

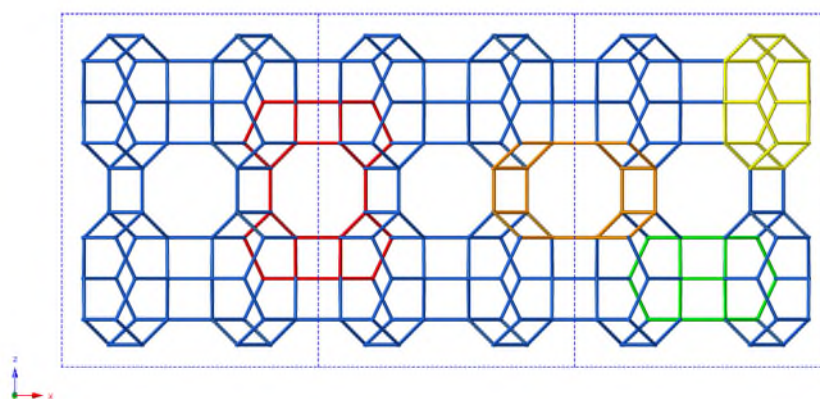


Figure 14. Hypo#31 seen along y-direction.

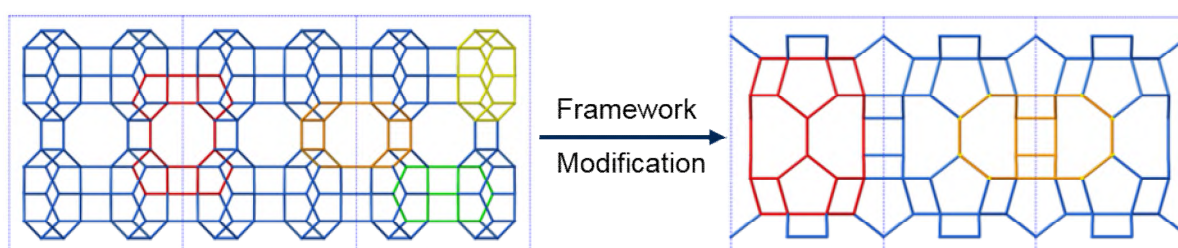


Figure 15. Images of Hypo#31 (left) and Hypo#3 (presented as Hypo#1 in paper 3) (right).

Table 9. The main framework properties for the Hypo#3 structure.

<b>Zeolite features</b>	
<b>Name</b>	Hypo#3 (139_4_48475_modif)
<b>Number of cavities</b>	2 ( <i>pau</i> , <i>hypo#3</i> )
<b>Number of T-atoms</b>	2
<b>Channel system</b>	3-dimensional
<b>Composite Building Units (CBU)</b>	Hypo#3, <i>pau</i>
<b>Unit cell</b>	2 x <i>hypo#3</i> + 2 x <i>pau</i> and 48 SiO <sub>2</sub> per u.c.
<b>Rings</b>	4 5 8

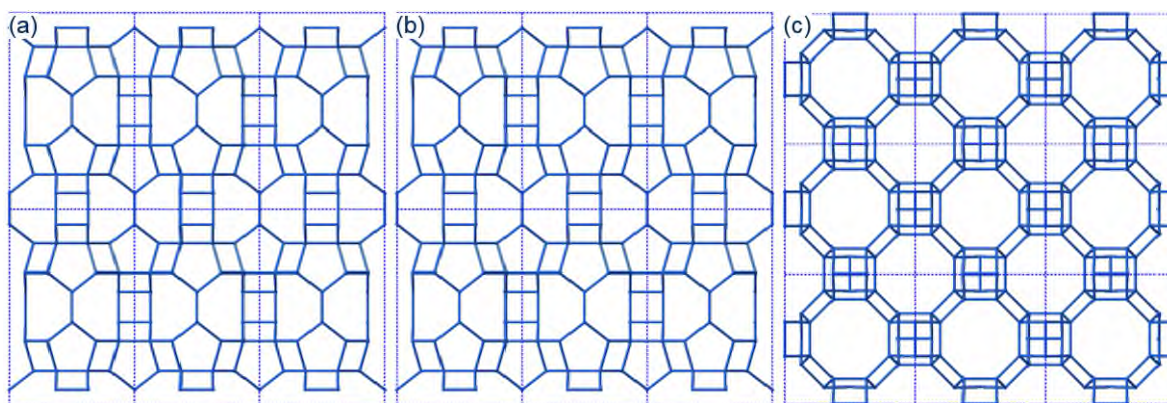


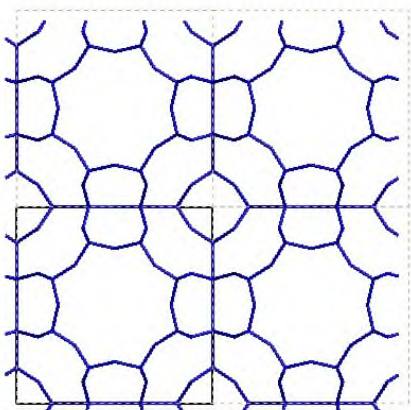
Figure 16. Hypo#3 zeolite framework seen along N(100) direction (a), N(010) direction (b) and N(001) direction (c).

During an extensive analysis of the IZA database in order to identify frameworks or zeolite cavities with similar building approach, several structures have been identified to correspond in some ways with the selected hypothetical zeolites. One such example is illustrated below. The *sav* cage that make up the Hypo#1 framework is not only already known from the SAV framework, but also it can be constructed relatively easy from the *lta* cage. If one of the 4-rings of the *lta* cavity (48 T atoms) is removed, then the *sav* cavity (40 T atoms) can be constructed. This special arrangement of a well-known cage is rising the question whether the synthesis procedure and the role of OSDAs have been used at their full potential and weather a wide range of conditions have been applied or something is missing. By simple observation it was also noticed that the *eri* cage (42 T atoms) could be taken as being a smaller *hypo#2* cage (56 T atoms). The general structural configuration of both cages is at a large extend similar. If for example the 8-ring from the top and bottom of the *hypo#2* cavity is replaced by a 6-ring, followed by the elimination of the 4-4-6-4-4 rings chain from the side, then the *hypo#2* cage is transformed into an *eri* cavity.

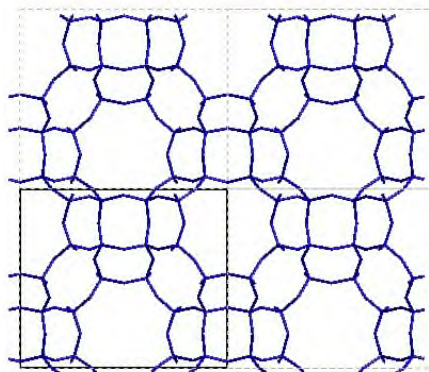
A similar building principal can easily be distinguished for well-known zeolites. The series LEV-CHA-AFX is an example in this sense. LEV cavity can easily be constructed from the CHA, by replacing the upper 8-ring windows with 6-rings. In the same way the AFX cavity can be considered as a CHA cage extended on the longest dimension with half of a cavity. This shows that this principle is already common for the already made zeolite and could be used for increasing the knowledge of hypothetical framework, where the information is limited.



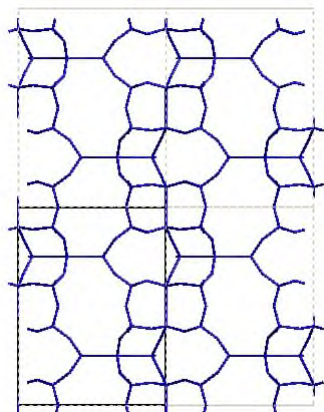
Similarities between the selected new zeolites and IZA frameworks



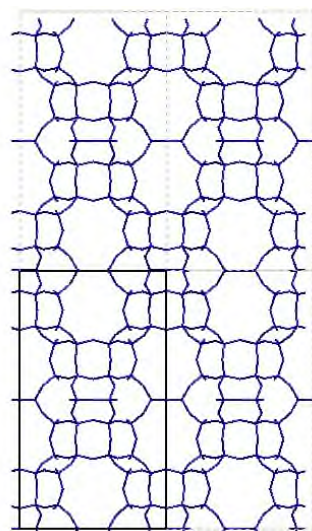
**LTA** framework seen along x direction, *lta* cage 48 T atoms, 6 x 8-R Windows.



**Hypo#1** framework seen along x direction, *sav* cage 40 T atoms, 6 x 8-R Windows.

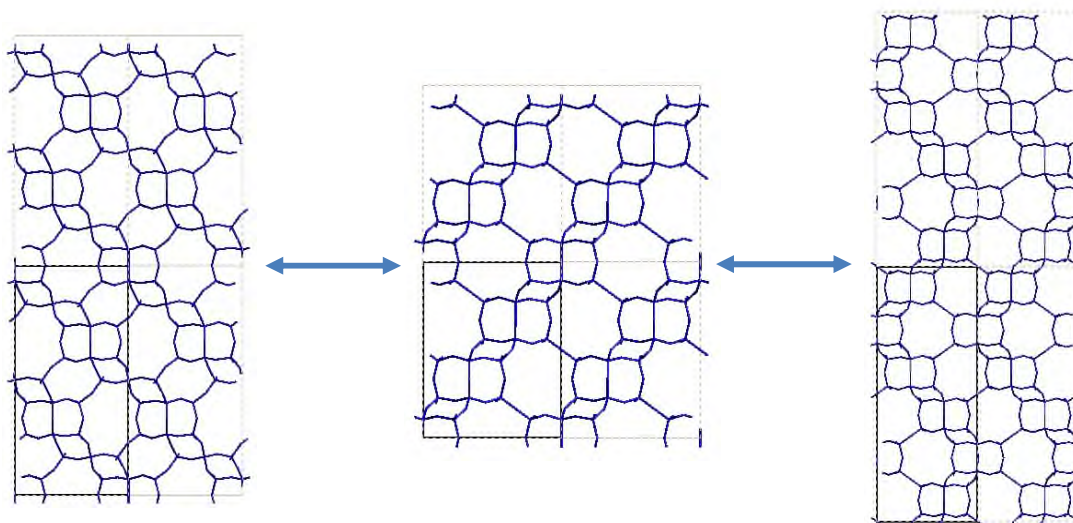


**ERI** framework seen along x Direction, *eri* cage 42 T atoms, 6 x 8-R Windows.



**Hypo#2** framework seen along x direction, *hypo#2* cage 56 T atoms, 10 x 8-R Windows.

Same building principles for IZA zeolites



**LEV** framework seen along x direction, *lev*  
cage 30 T atoms,  
3 x 8-R windows.

**CHA** framework seen along x direction, *cha*  
cage 36 T atoms,  
6 x 8-R windows.

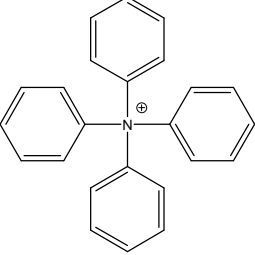
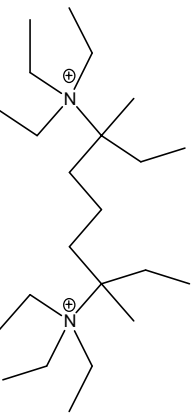
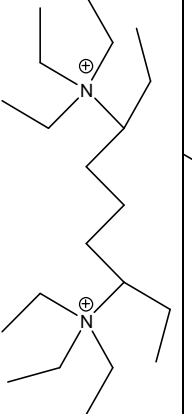
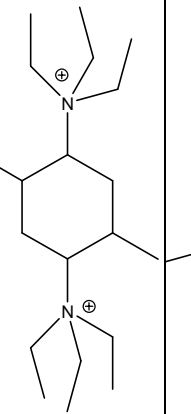
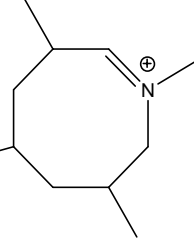
**AFT** framework seen along x direction, *aft*  
cage 48 T atoms,  
8 x 8-R windows.

The OSDAs found for each of the hypothetical zeolite frameworks are presented below. The A values correspond to the energies calculated with Universal force field and the B values corresponds to energies calculated with COMPASS2 force field and are expressed in Kcal/mol per SiO<sub>2</sub>. The formula used to calculate the interaction energy was: I.E. = E<sub>(ORG-ZEO)</sub> - E<sub>ORG</sub> - E<sub>ZEO</sub>; and for the interaction energy per SiO<sub>2</sub>: I.E.<sub>SiO<sub>2</sub></sub> = I.E.\*No. of occupied cages/No. of SiO<sub>2</sub> units.


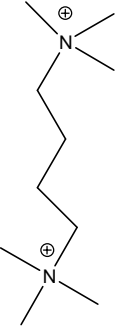
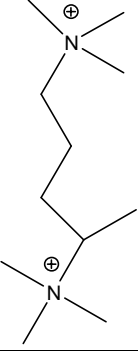
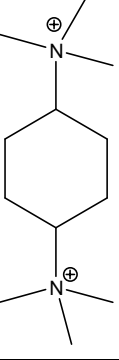
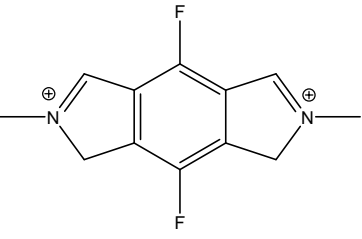
Organic structure directing agents (OSDAs) candidates for Hypo#1

OSDA					
A	-3.14	-2.73	-3.22	-2.86	-3.15
B	-4.3	-4.1	-4.07	-4.04	-4.44

Organic structure directing agents (OSDAs) candidates for Hypo#2

OSDA					
A	-2.02	-2.34	-2.34	-2.25	-2.33
B	-1.28	-1.79	-1.82	-1.63	-1.28

Organic structure directing agents (OSDAs) candidates for Hypo#3 (presented as Hypo#1 in paper 3)

OSDA					
A	-2.43	-2.67	-2.36	-2.33	-2.33
B	-4.64	-4.70	-4.31	-3.81	-2.02



## References:

- [1] Barrer, R. M. *Hydrothermal Chemistry of Zeolites*; Academic Press: London, 1982.
- [2] Breck, D. W. *Zeolite Molecular Sieves*; Wiley, New York, 1974.
- [3] Jacobs, P.A.; Flannigan, E.M.; Jansen, J.C. Herman van Bekkum, *Introduction to Zeolite Science and Practice*, Elsevier, 2001.
- [4] Cundy, C. S.; Cox, P. A. *The Hydrothermal Synthesis of Zeolites: History and Development from the Earliest Days to the Present Time*, *Chem. Rev.*, 103, 663–702, 2003.
- [5] Flannigan, E. M. Chapter 2 *Zeolites and Molecular Sieves an Historical Perspective*, *Studies in Surface Science and Catalysis*, 58, 13-34, 1991.
- [6] Davis, M. E. *Zeolites and molecular sieves: not just ordinary catalysts*, *Ind. Eng. Chem. Res.* 30, 8, 1675-1683, 1991.
- [7] Uytterhoeven, J. B.; Christner, L. G.; Hall, W. K. *Studies of the Hydrogen Held by Solids. VIII. The Decationated Zeolites*, *J. Phys. Chem.*, 69, 6, 2117-2126, 1965.
- [8] Mortier, W. J.; Sauer, J.; Lercher, J. A.; Noller, H. *Bridging and terminal hydroxyls. A structural chemical and quantum chemical discussion*, *J. Phys. Chem.*, 88, 5, 905–912, 1984.
- [9] Cronstedt, A. F. *Akad. Handl. Stockholm*, 18, 120-130, 1756.
- [10] Damour, A. *Ann. Mines*, 17, 191, 1840.
- [11] Chester, A. H. *A dictionary of the names of minerals including their history and etymology*, J. Wiley & Sons, 1896.
- [12] <http://www.iza-online.org/natural/Datasheets/Faujasite/faujasite.htm> (accessed June 12, 2017 )
- [13] Eichhorn, H. *Poggendorf Ann. Phys. Chem.*, 105, 126, 1858.
- [14] de St. Claire-Deville, H. *Compt. Rend.*, 54, 324, 1862.
- [15] G. Friedel, *Bull. Soc. Franc. Mineral. Cristallogr.*, 19, 94-118, 1896.

- [16] F. Grandjean, *Compt. Rend.*, 149, 866-868, 1909.
- [17] J. W. McBain, *The Sorption of Gases and Vapors by Solids*, Rutledge and Sons, London, Chap. 5, 1932.
- [18] Niggli P.; Morey, G. W. *Z. Anorg. Allg. Chem.*, 83, 369, 1913.
- [19] Morey, G. W.; Ingerson, E. *Econ. Geol.*, 32, 607, 1937.
- [20] George W. Morey, *Z. Anorg. Allg. Chem.*, 86, 1, 305-324, 1914.
- [21] Rabenau, A. *Angew. Chem., Int. Ed. Engl.*, 24, 1026, 1985.
- [22] Wilson, S. T.; Lok, B. M.; Messina, C. A.; Cannan, T. R.; Flanigen, E. M.; *J. Am. Chem. Soc.*, 104, 1146-1147, 1982.
- [23] Flanigen, E. M.; Lok, B. M.; Patton, R. L.; Wilson, S. T. in Y. Murakami, A. Ijima and J.W. Ward (Eds.), *New Developments in Zeolite Science and Technology*, Proc. 7<sup>th</sup> Intl. Zeolite Conf., Tokyo, Aug. 17-22, 1986, Kodansha Ltd., Tokyo and Elsevier, Amsterdam, 103-112, 1986.
- [24] Szostak, R.; *Molecular Sieves, Principles of Synthesis and Identification*, 2<sup>nd</sup> Ed., Blacklie Academic & Professional, London, 208-244, 1998.
- [25] Flanigen, E. M.; Lok, B. M.; Patton, R. L.; Wilson, S. T. *Pure Appl. Chem.*, 58, 1351-1358, 1986.
- [26] Bennett, J. M.; Richardson Jr., J. W.; Pluth, J. J.; Smith, J. V. *Zeolites*, 7, 160-162, 1987.
- [27] Pluth, J. J.; Smith, J. V.; Richardson Jr., J. W. *J. Phys. Chem.*, 92, 2734-2738, 1988.
- [28] Meriaudeau, P.; Tuan, V. A.; Hung, L. N.; Szabo, G. *Zeolites*, 19, 449-451, 1997.
- [29] Chen, J. S.; Thomas, J. M.; Wright, P. A.; Townsend, R. P. *Catalysis Letters*, 28, 241-248, 1994.
- [30] Yongheng, L.; Jianlin, D.; Weiyu, S.; Jian, L.; Zhen, Z.; Manglai, G.; Yuechang, W.; Liang, Z. *J. Phys. Chem. C*, 120, 27, 14669–14680, 2016.

- [31] Martinez-Franco, R.; Moliner, M.; Corma, A. *Journal of Catalysis* Volume 319, 36-43, 2014.
- [32] Martinez-Franco, R.; Li, Z.; Martinez-Triguero, J.; Moliner, M.; Corma, A. *Catal. Sci. Technol.*, 6, 2796-2806, 2016.
- [33] Epelde, E.; Ibáñez, M.; Valecillos, J.; Aguayo, A. T.; Gayubo, A. G.; Bilbao, J., Castaño, P. *Applied Catalysis A: General*, 547, 176-182, 2017.
- [34] Weisz, P. B. *Chemtech*, 3, 498, 1973.
- [35] Corma, A. *Inorganic Solid Acids and Their Use in Acid-Catalyzed Hydrocarbon Reactions*, *Chemical Reviews*, 95, 3, 559-614, 1995.
- [36] Karger, J.; Pfeifer, H. *Int. Zeolite Conf.*, 9, B.22, 1992.
- [37] Barrer, R. M. J. *Colloid Sci.*, 21, 416, 1966.
- [38] [http://webmineral.com/dana/dana.php?class=77#.W8xrD\\_ZuJPY](http://webmineral.com/dana/dana.php?class=77#.W8xrD_ZuJPY) (accessed June 12, 2017)
- [39] Baerlocher, C.; McCusker, L. B. *Database of Zeolite Structures*, [http://europe.iza-structure.org/IZA-SC/ftc\\_table.php](http://europe.iza-structure.org/IZA-SC/ftc_table.php), 2018
- [40] Lok, B. M.; Cannan, T. R.; Messina, C. A. The role of organic molecules in molecular sieve synthesis, *Zeolites*, 3, 4, 282-29, 1983.
- [41] Cundy, C.S.; Cox, P.A. The Hydrothermal Synthesis of Zeolites: Precursors, Intermediates and Reaction Mechanism. *Microporous and Mesoporous Materials*, 82, 1-78, 2005.
- [42] Moliner, M.; Martínez, C.; Corma, A. Synthesis Strategies for Preparing Useful Small Pore Zeolites and Zeotypes for Gas Separations and Catalysis, *Chem. Mater.*, 26, 246–258, 2014.
- [43] Dusselier, M.; Davis, M. E. Small-Pore Zeolites: Synthesis and Catalysis. *Chem. Rev.*, 118, 5265–5329, 2018.
- [44] Barrer, R. M.; Denny, P. J. 201. Hydrothermal chemistry of the silicates. Part IX. Nitrogenous aluminosilicates. *J. Chem. Soc.*, 0, 971-982, 1961.

- [45] Maldonado, M.; Oleksiak, M. D.; Chinta, S.; Rimer, J. D. Controlling Crystal Polymorphism in Organic-Free Synthesis of Na-Zeolites. *J. Am. Chem. Soc.*, 135, 2641–2652, 2013.
- [46] Lupulescu A. I.; Rimer, J. D. In Situ Imaging of Silicalite-1 Surface Growth Reveals the Mechanism of Crystallization. *Science*, 344, 6185, 729-732, 2014.
- [47] Kumar, M.; Luo, H.; Román-Leshkov, Y.; Rimer, J. D. SSZ-13 Crystallization by Particle Attachment and Deterministic Pathways to Crystal Size Control. *J. Am. Chem. Soc.*, 137, 40, 13007–13017, 2015.
- [48] Kumar, M.; Li, R.; Rimer, J. D. Assembly and Evolution of Amorphous Precursors in Zeolite L Crystallization. *Chem. Mater.*, 28, 6, 1714–1727, 2016.
- [49] Oleksiak, M. D.; Soltis, J. A.; Conato, M. T.; Penn, R. L.; Rimer, J. D. Nucleation of FAU and LTA Zeolites from Heterogeneous Aluminosilicate Precursor. *Chem. Mater.*, 28, 14, 4906–4916, 2016.
- [50] Rimer, J.; Tsapatsis, M. Nucleation of open framework materials: Navigating the voids. *MRS Bulletin*, 4, 15, 393-398, 2016.
- [51] Xu, R.; Pang, W.; Yu, J.; Huo, Q.; Chen, J. *Chemistry of Zeolites and Related Porous Materials: Synthesis and Structure*, John Wiley & Sons (Asia) Pte Ltd. 2007.
- [52] Yu, L.; Jun, Z.; Jong-Min, L. Conventional and New Materials for Selective Catalytic Reduction (SCR) of NO<sub>x</sub>. *ChemCatChem*, 10, 1499 –1511, 2018.
- [53] Auvray, X.; Partridge, W. P.; Choi, J. S.; Pihl, J. A.; Yezerets, A.; Kamasamudram, K.; Olsson, L. Local ammonia storage and ammonia inhibition in a monolithic copper-beta zeolite SCR catalyst. *Applied Catalysis B: Environmental*, 126, 144-152, 2012.
- [54] Ma, L.; Li, J.; Cheng, Y.; Lambert, C. K.; Fu, L. Propene Poisoning on Three Typical Fe-zeolites for SCR of NO<sub>x</sub> with NH<sub>3</sub>: From Mechanism Study to Coating Modified Architecture. *Environmental science & technology*, 46, 3, 1747-1754, 2012.
- [55] Coq, B.; Mauvezin, M.; Delahay, G.; Butet, J. B.; Kieger, S. The simultaneous catalytic reduction of NO and N<sub>2</sub>O by NH<sub>3</sub> using an Fe-zeolite-beta catalyst. *Applied Catalysis B: Environmental*, 27, 3, 193-198, 2000.

- [56] Sullivan, J. A.; Cunningham, J.; Morris, M. A.; Keneavey, K. Conditions in which Cu-ZSM-5 outperforms supported vanadia catalysts in SCR of NO<sub>x</sub> by NH<sub>3</sub>. *Applied Catalysis B: Environmental*, 7, 1, 137-151, 1995.
- [57] Sjövall, H.; Fridell, E.; Blint, R. J.; Olsson, L. Identification of adsorbed species on Cu-ZSM-5 under NH<sub>3</sub> SCR conditions. *Topics in Catalysis*, 42, 1-4, 113-117, 2007.
- [58] Malpartida, I.; Ivanova, E.; Mihaylov, M.; Hadjiivanov, K.; Blasin-Aubé, V.; Marie, O.; Daturi, M. CO and NO adsorption for the IR characterization of Fe<sup>2+</sup> cations in ferrierite: An efficient catalyst for NO<sub>x</sub> SCR with NH<sub>3</sub> as studied by operando IR spectroscopy. *Catalysis Today*, 149, 3, 295-303, 2010.
- [59] Kwak, J. H.; Tonkyn, R. G.; Kim, D. H.; Szanyi, J.; Peden, C. H. Excellent activity and selectivity of Cu-SSZ-13 in the selective catalytic reduction of NO<sub>x</sub> with NH<sub>3</sub>. *Journal of Catalysis*, 275, 2, 187-190, 2010.
- [60] Fickel, D. W.; Lobo, R. F. Copper Coordination in Cu-SSZ-13 and Cu-SSZ-16 Investigated by Variable-Temperature XRD, *J. Phys. Chem. C*, 114, 1633–1640, 2010.
- [61] Martín, N.; Boruntea, C.-R.; Moliner, M.; Corma, A. Efficient synthesis of the Cu-SSZ-39 catalyst for DeNO<sub>x</sub> applications. *Chemical Communications*, 51, 55, 11030–11033, (2015).
- [62] Beale, A. M.; Gao, F.; Lezcano-Gonzalez, I.; Peden, C. H. F.; Szanyi, J. Recent advances in automotive catalysis for NO<sub>x</sub> emission control by small-pore microporous *Chem. Soc. Rev.* 44, 7371-7405, 2015.
- [63] Gao, F.; Kwak, J. H.; Szanyi, J.; Peden, C. H. F. Current Understanding of Cu-Exchanged Chabazite Molecular Sieves for Use as Commercial Diesel Engine DeNO<sub>x</sub> Catalysts *Top. Catal.* 56, 1441–1459, 2013.
- [64] [https://en.wikipedia.org/wiki/Hypothetical\\_zeolite](https://en.wikipedia.org/wiki/Hypothetical_zeolite) (accessed June 12, 2017)
- [65] Treacy, M. M. J.; Foster, M. D.; Rivin, I. Chapter 12, Towards a Catalogue of Designer Zeolites, in *Turning Points in Solid-state, Materials and Surface State*, Kenneth D. M. Harris, Peter P. Edwards, Royal Society of Chemistry (Great Britain) Royal Society of Chemistry, 2008.

- [66] Foster, M. D.; Treacy, M. M. J. Progress towards an atlas of designer zeolites in From Zeolites to Porous MOF Materials, Ruren Xu, Jiesheng Chen, Zi Gao, Wenfu Yan, Elsevier, 2007.
- [67] Meier, W. M.; Olson, D. H.; Baerlocher, Ch. Atlas of Zeolite Structure Types, 1996.
- [68] Treacy, M. M. J.; Higgins, J. B. Collection of Simulated XRD Powder Patterns for Zeolites, 1996.
- [69] Hennesy, J. Zeolites: A synthetic solution, Nature Materials, 15, 6, 2016.
- [70] Foster, M. D.; Treacy, M. M. J. A Database of Hypothetical Zeolite Structures: <http://www.hypotheticalzeolites.net> (accessed July 10, 2014)
- [71] Sastre, G.; Gale, J. D. ZeoTsites: a code for topological and crystallographic tetrahedral sites analysis in zeolites and zeotypes. Microporous Mesoporous Mater., 43, 27–40, 2001.

## Part 2

### Paper 1

The manuscript attached below represents the author's version of the article:

Cristian-R. Boruntea, Lars F. Lundegaard, Avelino Corma, Peter N. R. Vennestrøm, Crystallization of AEI and AFX zeolites through zeolite-to-zeolite transformations. *Microporous and Mesoporous Materials* 2019, 278, 105-114.

The research presented in this paper is offering a detailed insight of zeolite-to-zeolite transformations, exemplified on two small-pore zeolites: SSZ-39 (AEI) and SSZ-16 (AFX). When FAU is used as raw material, the transformation proceed without any solid intermediates. It has been found that the lattice parameter of FAU, which is proportional with the Al content, is converging until a certain value before the onset of product crystallization. The synchronization of the Si/Al ratio of the reactant-product leads to high yields. The target zeolites have also been synthesized from CHA zeolites, which have a similar structural features, but higher framework density than FAU. A scheme is introduced, where the dissolution rate of the starting zeolite must be lower than the crystallization of the zeolite product.

The work presented herein serves as a toolbox for understanding and applying the zeolite-to-zeolite transformation for preparation of other and potentially novel zeolites as well.

# Crystallization of AEI and AFX zeolites through zeolite-to-zeolite transformations

Cristian-R. Boruntea<sup>a,b</sup>, Lars F. Lundegaard<sup>a</sup>, Avelino Corma<sup>b\*</sup>, Peter N. R. Vennestrøm<sup>c\*</sup>

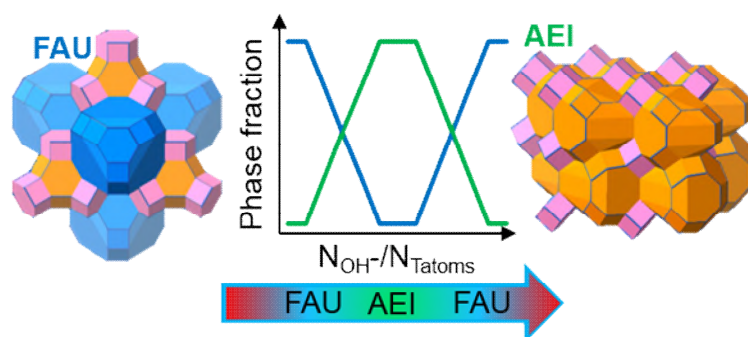
<sup>a</sup> Haldor Topsøe A/S, Haldor Topsøes Alle 1, DK-2800 Kgs. Lyngby, Denmark

<sup>b</sup> Instituto de Tecnología Química, Universitat Politècnica de València-Consejo Superior de Investigaciones Científicas, Avenida de los Naranjos s/n, 46022 Valencia, España

<sup>c</sup> Umicore Denmark ApS, Nøjsomhedsvej 20, DK-2800 Kgs. Lyngby, Denmark

\*Corresponding Author, Email: [acorma@itq.upv.es](mailto:acorma@itq.upv.es); [peter.vennestrom@eu.unicore.com](mailto:peter.vennestrom@eu.unicore.com)

## Abstract



The OH/T-atom ratio and the Al-source are identified as critical parameters for the successful crystallization of AEI and AFX type zeolites when sufficient organic structure directing agent (OSDA) molecules are present. Especially the use of a zeolite as the Al-source is essential. When a complete zeolite-to-zeolite transformation of FAU is explored it is found to proceed without any solid crystalline intermediates. The optimal OH/T-atom ratio can also be decreased when the Al-content in the reactant zeolite is increased to resemble the product composition better. This makes higher yields and better utilization of the OSDA possible compared to gels with less Al. During successful zeolite transformations the lattice parameter of FAU, which is proportional to the Al-content, seems to converge at a certain range before the onset of product crystallization. This indicates that successful nucleation and/or formation of the target zeolite is dependent on this type of intermediate and dependent on the dissolution of the starting zeolite. Based on the findings of optimal OH/T-atom ratios and synchronization of Si/Al ratio in the reactant zeolite with the product zeolite we also show that AEI and AFX can be obtained from CHA, which has similar structural features, but a higher framework density (FD) than e.g. FAU. This indicates that zeolite-to-zeolite transformations does not have to proceed from zeolites with low FDs (i.e. high stabilization energies) to higher FDs (i.e. lower stabilization energies), but is mainly driven by favorable OSDA-zeolite interactions. Overall results are rationalized in a scheme where especially the dissolution rate of a starting zeolite with key structural features must be lower than the crystallization of the zeolite product in order to obtain a successful zeolite-to-zeolite transformation.

**Keywords:** zeolite-to-zeolite transformations, zeolite crystallization, small-pore zeolite, AEI and AFX



## 1. Introduction

Zeolites are crystalline microporous tectosilicates that are widely applied in industry and studied in academia, due to their properties provided by their porous three-dimensional structure and the possibility to ion exchange cations into extra framework positions. Most zeolites applied in industry are made up from tetrahedrally coordinated Si and Al atoms (T-atoms), linked together through oxygen bridges that gives rise to channels and cavities of different sizes and shapes [1], [2]. In catalysis the size and shape of the uniform microporous structure is exploited as well as the ability of the zeolite to host active cations such as protons or transition metal ions. Each specific zeolite framework topology and chemical composition provides a unique microporous environment that leads to specific properties such as activity, selectivity and stability.

Especially the application of small-pore zeolites (defined by pore-openings that contains eight oxygen atoms) have attracted considerable attention lately. For the conversion of methanol to olefins the small-pore windows in the structure provides required selectivity towards small olefins instead of larger branched hydrocarbons as well as aromatics that are excessively produced by medium- and large-pore zeolites [3], [4], [5], [6], [7]. Similar features can also be exploited in gas separation applications, where small-pore zeolites show high selectivity, and permeability for small light molecules such as CO<sub>2</sub>, H<sub>2</sub>, N<sub>2</sub> in different mixtures [8], [9], [10] and even for ethane/ethene separations [11]. For NO<sub>x</sub> abatement applications the small-pore nature of the zeolite provides sufficient stability to withstand hydrothermal conditions (typically >700 °C) [12], [13], [14]. More than this, small-pore zeolites show high tolerance towards hydrocarbon poisoning and produce less unwanted N<sub>2</sub>O than zeolite catalysts with larger pores [15], [16].

A useful description on synthesis strategies of small-pore zeolites is presented in [17]. However, the synthesis of specific framework topologies is not always straightforward and typically depends on the selection of starting materials, nucleation, crystallization kinetics and stabilization by specific organic structure directing agents (OSDAs). The use of zeolites as an aluminum source has been known since the studies on zeolites synthesis made by Richard Barrer in the late 70s and early 80s [1] and it has since then been used by other research groups for synthesizing various zeolite frameworks, such as CHA, AEI, PHI, HEU, BRE, GME, BEA\*, RUT, MFI, LEV under alkaline conditions and in some instances together with OSDAs [18], [19], [20], [21], [22], [23].

In specific cases zeolites have also been used as the sole source of T-atoms in complete zeolite-to-zeolite transformations. One of the first examples from 1979 is the conversion of a FAU zeolite into ZSM-4 using the tetramethylammonium cation (TMA<sup>+</sup>) as an OSDA [24]. Another example is the conversion of P-zeolite (GIS) into CHA investigated by researchers at Chevron in the late 80s, motivated by the observation that P-zeolite was observed as an intermediate during CHA crystallization. By this transformation the product was obtained with changes in morphology and chemical composition [25]. The use of zeolites as an Al source in fluoride media has also recently been demonstrated as an effective method to incorporate higher amounts of Al in the framework compared to conventional Al-sources [26].

The use of zeolite seeds with common composite building units have also been used to obtain other zeolites with similar building units without the requirement of OSDAs [27], [28]. It is hypothesized

that a zeolite containing composite building units also present in the target zeolite can direct the formation of said zeolite through a solution-mediated transfer of the building unit to the growth site.

When Zones *et al.* studied the introduction of boron in the framework of pure-silica SSZ-24 (AFI) the use of boron-containing Beta-zeolite (\*BEA) was required. Zones *et al.* described the process of using another zeolite as not just being a rearrangement, but also speculated that the use of a zeolite as raw material provides a high surface area that generates nucleation sites, making the zeolite product crystallize faster [29]. This could indicate that the role of the zeolite is not necessarily only to provide composite building units, but also to influence nucleation.

Furthermore, it can be speculated that by using zeolites that are already meta-stable phases with well-defined thermodynamic stabilization energies (e.g. relative to  $\alpha$ -quartz) the crystallization of related structures with similar or lower stabilization energies become more easily accessible. This may especially be the case for complete zeolite-to-zeolite transformations. It was indeed reported that for interconversions that proceed without the presence of OSDAs a parent zeolite with a lower FD than the target zeolite is necessary [30].

Interestingly, certain zeolites have only been obtained through the use of other zeolites as starting materials. AEI (SSZ-39) is an example of such. AFX (SSZ-16) was also first synthesized through the use of another zeolite, but has recently been achieved from a non-crystalline starting point [31], [32]. Both SSZ-16 and SSZ-39 were first synthesized by Zones *et al.* [33], [34], [35] and later by others [36], [37], [38], [39]. Common for all these cases has been the use of a FAU zeolite in the synthesis gel combined with high alkalinity. The FAU zeolite contains, among others, a double-six-ring (d6R) building unit in the structure similar to both AEI and AFX. Recently it was even shown that SSZ-39 can be synthesized with high solid yields obtained by synchronization of the FAU Si/Al ratio with the AEI product and by applying a complete zeolite-to-zeolite transformation approach [40]. This approach is particularly appealing for studying the zeolite crystallization because all T-atoms comes from the same source and the starting point is completely well-defined, which is usually not the case in zeolite crystallization.

In this contribution we investigate the synthesis of AEI and AFX aluminosilicate zeolites by identifying critical factors for their successful synthesis. In particular, the special role of zeolites as a source of Al (and Si), its structural features, together with the amount of mineralizing agent and organic structure directing agent is addressed. Results are rationalized by considering the rate of dissolution of the starting crystalline aluminosilicate must be lower than the crystallization of the zeolite product.

## 2. Experimental

### 2.1. Materials and methods

For the synthesis of AEI zeolites (SSZ-39) two approaches were followed, namely using a combination of FAU and sodium silicate as Al- and Si-sources as well as the use of FAU as the sole source of Al and Si. The critical amount of mineralizing agent ( $\text{OH}^-$ ) was first deduced from the synthesis approach using sodium silicate, which is based on the original report of SSZ-39 preparation using 1,1,3,5-tetramethylpiperidinium hydroxide as the OSDA. [33] For a typical synthesis with sodium silicate

1.5 mmol OSDA (1,1,3,5-tetramethylpiperidinium hydroxide) was mixed with 2.215 mmol NaOH and 178.9 mmol H<sub>2</sub>O, then 4.26 mmol Na<sub>2</sub>SiO<sub>3</sub> and 6.957 mmol H-FAU-zeolite (Si/Al=15) were added. In a second set of experiments AEI zeolites were synthesized by complete zeolite-to-zeolite transformations. Typically, 2.04 mmol OSDA was mixed with 6.03 mmol NaOH, then 52.78 mmol of H<sub>2</sub>O and 12.359 mmol H-FAU (Si/Al=30) was added. In all cases the gel was mixed for 1 h at room temperature and then transferred into a Teflon lined autoclave and crystallization was carried out at 135 °C for seven days unless otherwise stated.

For the synthesis of AFX (SSZ-16), only the zeolite-to-zeolite transformation approach was undertaken. In a typical synthesis 2.17 mmol OSDA 1,4-bis(1,4-diazabicyclo[2.2.2]octane)butyl dihydroxide was mixed with 4.5 mmol NaOH, then 51.11 mmol of H<sub>2</sub>O and 17.077 mmol H-FAU (Si/Al=15) was added. The resulting gel was mixed for 1 h at room temperature and then transferred into a Teflon lined autoclave. The crystallization was carried out at 150 °C for 6 days unless otherwise stated. Solid yields are calculated based on Si/Al ratio in the reactant compared to the product assuming that all Al ends up in the product. The raw materials used were: 1,1,3,5-tetramethylpiperidinium hydroxide, 1,4-bis(1,4-diazabicyclo[2.2.2]octane)butyl dihydroxide (synthesis procedure for both OSDAs can be found in the Supporting Information), sodium hydroxide (NaOH, reagent grade ≥ 98 %, Sigma Aldrich), sodium silicate (reagent grade 10.6 % Na<sub>2</sub>O, 26.5 % SiO<sub>2</sub> Sigma-Aldrich), tetraethyl orthosilicate (reagent grade, 98 %, Sigma Aldrich) and aluminum isopropoxide (98 %, Sigma Aldrich), FAU type-zeolites (Si/Al = 6, 15 and 30), CHA-type zeolites (Si/Al = 7 and 15), \*BEA-type zeolites (Si/Al = 5, 12.5 and 30) and ASA (amorphous-silica-alumina) were either obtained from commercial suppliers or prepared in-house.

## 2.2. Characterization

The zeolite materials were analyzed in the as-synthesized form by X-ray diffraction using a Phillips PW1800 instrument system in  $\theta$ - $2\theta$  geometry working in reflectance mode using CuK $\alpha$  radiation ( $\lambda = 1.541 \text{ \AA}$ ). SEM images were recorded using an XL30-SEM instrument operated at 10 kV. The samples were sprinkled over carbon tape and attached on Al-stubs and then coated with a ca. 30 nm layer of carbon to prevent charging. Product composition was determined using inductively coupled plasma optical emission spectroscopy (ICPOES) on acid digested samples using a Perkin Elmer Optima 7300 DV instrument. The <sup>27</sup>Al MAS NMR spectra were recorded using a Bruker Avance II HD 400 Mhz instrument at spinning rate of 20Khz in a Bruker 3.2 mm probe, using a flip angle of  $\pi/12$  and a recycle delay of 1s. The <sup>29</sup>Si MAS NMR spectra were recorded at spinning rate of 5kHz in Bruker 4 mm probe, using a flip angle of 60° and a recycle delay of 60s.

## 3. Results

### 3.1. Identification of critical parameters in the preparation of AEI

In the original reported synthesis of aluminosilicate AEI, cyclic ammonium cations were used as OSDA and various FAU zeolites as the Al-source in combination with sodium silicate and sodium hydroxide [34], [41]. Later reports have showed that the successful achievement of AEI is highly

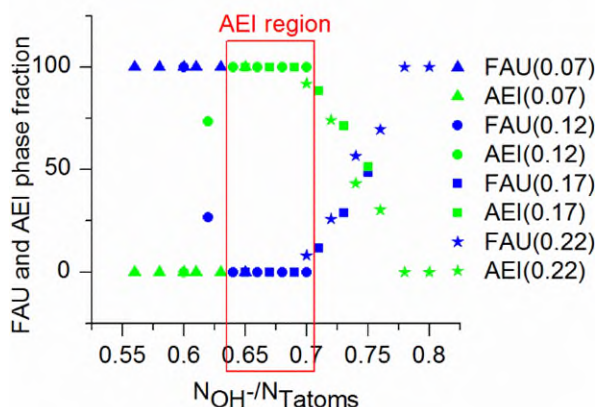
dependent on the specific composition and choice of raw materials [42]. In order to identify critical parameters for the successful achievement of AEI we initially studied a broad range of synthesis compositions using the combination of FAU (Si/Al=15) and sodium silicate as aluminum and silicon sources, respectively, similar to the originally reported synthesis. Especially the amount of sodium hydroxide and OSDA (1,1,3,5-tetramethylpiperidinium hydroxide) was found to dictate the overall product phase.

**Table 1 Phase diagram of products in the 1 Si : 0.033 Al : x NaOH : y OSDA : 40 H<sub>2</sub>O synthesis system, with the use of sodium silicate and FAU (Si/Al=15). Crystallization conditions were seven days at 135 °C. Lattice parameters (Å) for FAU are presented below the identified phase.**

		NaOH/Si					
		0.11	0.13	0.15	0.17	0.19	0.21
OSDA/Si	0.07	FAU $a_{\text{FAU}}=24.372$	FAU $a_{\text{FAU}}=24.429$	FAU $a_{\text{FAU}}=24.487$	FAU $a_{\text{FAU}}=24.488$	FAU $a_{\text{FAU}}=24.491$	AEI
	0.12	FAU $a_{\text{FAU}}=24.465$	AEI+FAU $a_{\text{FAU}}=24.479$	AEI	AEI	AEI	AEI
	0.17	AEI	AEI	AEI	AEI+FAU $a_{\text{FAU}}=24.511$	AEI+FAU $a_{\text{FAU}}=24.517$	AEI+FAU $a_{\text{FAU}}=24.523$
	0.22	AEI+FAU $a_{\text{FAU}}=24.493$	AEI+FAU $a_{\text{FAU}}=24.493$	AEI+FAU $a_{\text{FAU}}=24.499$	AEI+FAU $a_{\text{FAU}}=24.525$	FAU $a_{\text{FAU}}=24.541$	FAU $a_{\text{FAU}}=24.545$

As can be seen from Table 1, the appearance of AEI is seen across a broad range of synthesis compositions. Phase-pure AEI appears as a diagonal area of phase space when sodium hydroxide and OSDA amounts are varied. On each side of the diagonal, a mixture of FAU and AEI is seen, and further away only unconverted FAU is observed. This diagonal shape indicate that AEI only crystallizes in a specific range of OH<sup>-</sup> concentrations. Interestingly, FAU is seen as the only competing crystalline phase at both low and high amounts of OH<sup>-</sup>. Looking at the phase diagram an increase in the lattice parameter of FAU zeolite is also seen going from low OH<sup>-</sup> amounts to higher OH<sup>-</sup> amounts on both sides of the AEI diagonal.

In Figure 1, the phase fractions of FAU and AEI determined by refinement of the PXRD data recorded on the products are shown. Pure AEI is obtained only in a narrow region where the OH<sup>-</sup>/T-atoms ratio (T-atoms = Al and Si) is between ca. 0.63 - 0.70 independent of the amount of OSDA. At least this is the case when sufficient amounts of OSDA is present. The high OH<sup>-</sup> amount required is typical for zeolites belonging to the ABC-6 family such as SSZ-13, -16 and -52 containing 4-, 6- and double-6-rings in the structure [43]. Although AEI does not belong to the ABC-6 family, it is composed of similar structural features, so it is not unexpected that AEI appear at such high OH<sup>-</sup>/T-atom ratios.



**Figure 1** Phase fractions of FAU and AEI of the products also reported in Table 1 depending on the total OH/T-atoms in the synthesis mixture. Numbers in parenthesis indicates the amount of OSDA/Si. OH/T-atoms is calculated based on both the added sodium hydroxide and the amount introduced from sodium silicate.

### 3.2. Attempts to synthesize AEI from various Si- and Al-sources.

Based on the observation that a critical amount of OH<sup>-</sup> is key in obtaining AEI, several attempts were made to prepare AEI using various Si- and Al-sources. Table 2 summarizes the observed product phases. In general, reactive Si-sources (Si(OEt)<sub>4</sub> and fumed SiO<sub>2</sub>) in combination with a reactive Al-source only leads to amorphous products. Perhaps counterintuitively, but when a less reactive Al-source is used (co-precipitated amorphous silica-alumina) GME and GIS are observed. These are typical phases obtained from sodium-rich synthesis mixtures and without OSDAs. This observation points towards the inefficient use of the OSDA and that this is most likely not included in the crystallized zeolite. AEI is only obtained when FAU is used as the Al-source and both when Si is introduced as sodium silicate or by the FAU zeolite.

**Table 2** Summarized product phases from syntheses using various Si- and Al-sources in combination with 1,1,3,5-tetramethylpiperidinium hydroxide as OSDA and NaOH as mineralizing agent.

<i>Si-source</i>	<i>Al-source</i>	<i>Synthesis composition</i>	<i>Product phase(s)</i>
<i>Si(OEt)<sub>4</sub></i>	<i>Al(<i>i</i>-PrO)<sub>3</sub></i>	<i>1Si:0.033Al:0.12OSDA:0.58NaOH:40H<sub>2</sub>O:0.68N<sub>OH<sup>-</sup>}/N<sub>Tatoms</sub></sub></i>	<i>Amorphous</i>
<i>ASA</i>	<i>ASA</i>	<i>1Si:0.033Al:0.12OSDA:0.58NaOH:40H<sub>2</sub>O:0.68N<sub>OH<sup>-</sup>}/N<sub>Tatoms</sub></sub></i>	<i>GME+GIS</i>
<i>Fumed SiO<sub>2</sub></i>	<i>Al(<i>i</i>-PrO)<sub>3</sub></i>	<i>1Si:0.033Al:0.12OSDA:0.58NaOH:40H<sub>2</sub>O:0.68N<sub>OH<sup>-</sup>}/N<sub>Tatoms</sub></sub></i>	<i>Amorphous</i>
<i>Na<sub>2</sub>SiO<sub>3</sub></i>	<i>FAU zeolite</i>	<i>1Si:0.033Al:0.12OSDA:0.19NaOH:40H<sub>2</sub>O:0.68N<sub>OH<sup>-</sup>}/N<sub>Tatoms</sub></sub></i>	<i>AEI</i>
<i>FAU zeolite</i>	<i>FAU zeolite</i>	<i>1Si:0.033Al:0.12OSDA:0.58NaOH:40H<sub>2</sub>O:0.68N<sub>OH<sup>-</sup>}/N<sub>Tatoms</sub></sub></i>	<i>AEI</i>

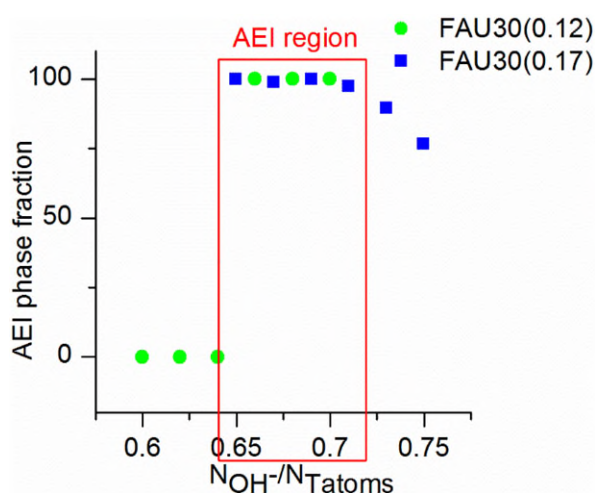
The general observation that the outcome is highly dependent on the Al-source indicate that the reactivity of the Al-source is critical in the synthesis system investigated herein. It would seem that only when a source of intermediate reactivity, such as FAU is chosen, AEI is successfully achieved. This indeed points to the special role of a zeolite as the Al-source in this type of zeolite crystallization.

### 3.3. AEI obtained from complete zeolite-to-zeolite transformations

In the case where FAU is used both as the Si- and the Al-source AEI is achieved as a complete zeolite-to-zeolite transformation and have recently been reported to provide additional advantages in terms of yield [40], but it also offers other advantages such as the possibility of studying zeolite crystallization from a completely well-defined crystalline starting point.

**Table 3 Phase diagram of products in the 1 Si : 0.033 Al : x NaOH : y OSDA : 40 H<sub>2</sub>O synthesis system using only FAU (Si/Al=30) as the source of Si and Al. Crystallization conditions were seven days at 135 °C. Lattice parameters (Å) for FAU are presented below the identified phase.**

		NaOH/Si					
		0.50	0.52	0.54	0.56	0.58	0.60
OSDA/Si	0.12	FAU $a_{FAU}=24.414$	FAU $a_{FAU}=24.430$	FAU $a_{FAU}=24.448$	AEI	AEI	AEI
	0.17	AEI	AEI	AEI	AEI+FAU $a_{FAU}=24.509$	AEI+FAU $a_{FAU}=24.514$	AEI+FAU $a_{FAU}=24.522$

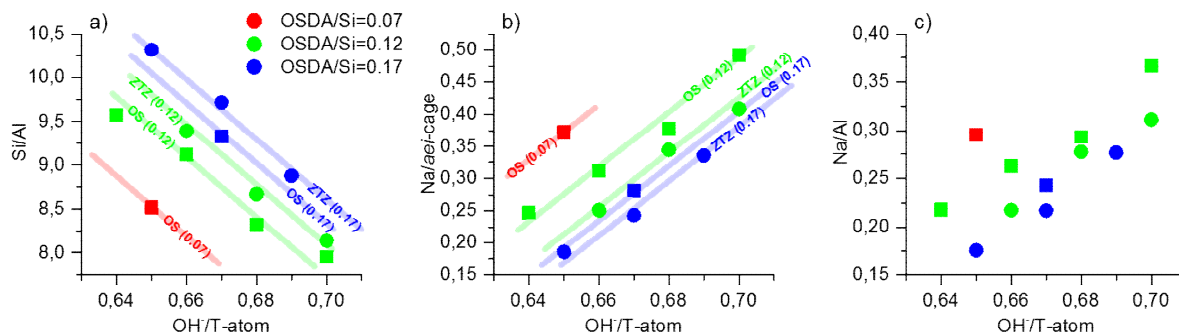


**Figure 2 Phase fraction AEI in the products also reported in Table 3 depending on the OH-/T-atoms in the synthesis mixture. Numbers in parenthesis indicates the amount of OSDA/Si.**

Exploration of phase space for the FAU (Si/Al=30) transformation into AEI (Table 3 and Figure 2) leads to the same behavior as for the synthesis using a combination of sodium silicate and FAU (Si/Al=15) (see Table 1 and Figure 1).

In particular, the optimal OH-/T-atom ratio is the same, or shifted to slightly higher numbers, even though the solubility rate of the FAU zeolite is expected to be higher due to the lower Al content. Figure 3 summarizes compositional variations in the obtained AEI-type zeolite materials (see also Table S1) from the original synthesis (OS) using sodium silicate and from the complete zeolite-to-zeolite transformation (ZTZ). In general a trend is observed where product Si/Al ratio is decreasing and sodium content is increasing when higher OH-/T-atom ratios are applied in the crystallization gel. In a similar

manner product Si/Al ratio is increasing and sodium content is decreasing when the OSDA content is increased.

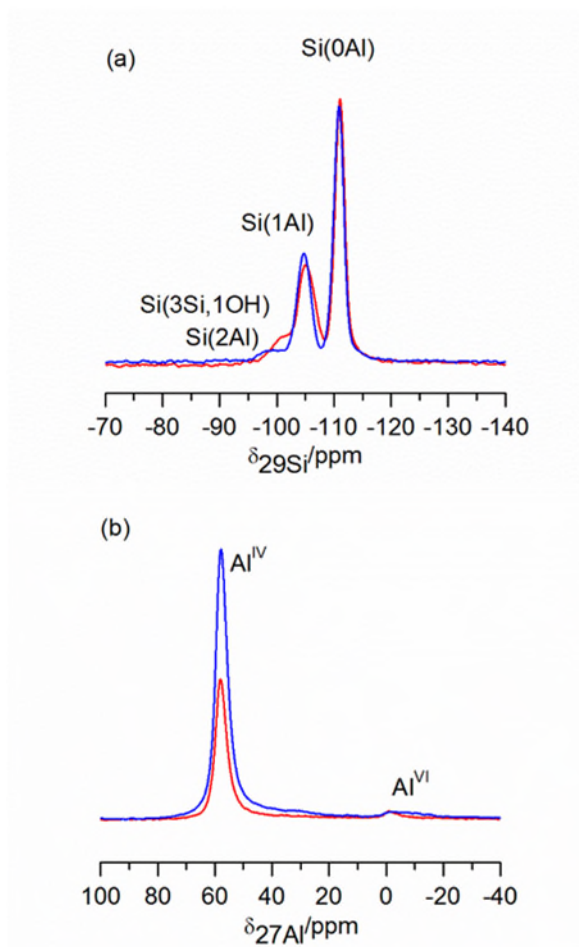


**Figure 3 Comparison of (a) Si/Al ratio, (b) Na/aei-cage and (c) Na/Al relative to the  $N_{OH^-}/N_{Tatoms}$  for the AEI-type zeolites prepared by the original synthesis (OS, squares) using sodium silicate and FAU and from the complete zeolite-to-zeolite transformation (ZTZ, circles).**

Interestingly, it would also seem that for similar amounts of OSDA and  $OH^-$  in the gel, higher Si/Al as well as lower sodium content (both Na/Al and Na/aei-cage) are achieved in the AEI product from the complete zeolite-to-zeolite transformation compared to the synthesis with sodium silicate. This is the same features seen when more OSDA is applied in general and suggests an improved inclusion of the OSDA into the product during the zeolite-to-zeolite transformation compared to syntheses where sodium silicate is used.

Comparison of  $^{13}C$  CP-MAS NMR of the solid product with  $^{13}C$ -NMR of the OSDA in solution before use (see Figure S5) also reveal that the OSDA remain intact during synthesis. For this reason, the different behavior of the zeolite-to-zeolite transformation is not ascribed to degradation of the OSDA.

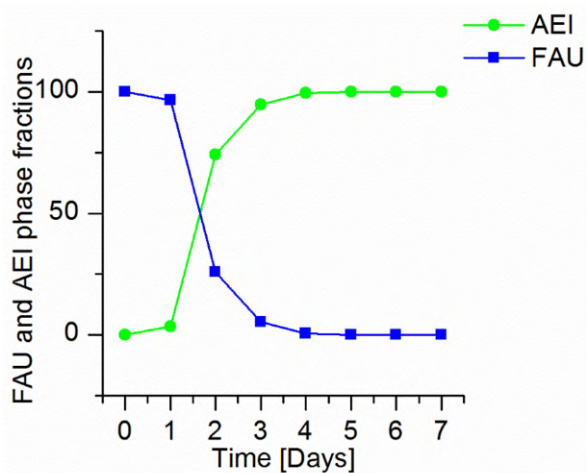
Recorded  $^{29}Si$  and  $^{27}Al$  MAS NMR spectra for the AEI zeolites is presented in Figure 4. From the Al-NMR, both synthesis approaches leads to spectra where the vast majority (95+%) of aluminum is tetrahedrally coordinated as evidenced by the main peak at approx. 60 ppm. For both materials the Si-NMR spectrum contains one well-defined intense peaks located at -111 ppm corresponding to Si without any neighboring Al atoms. The second peak located at -105 ppm corresponds to Si environments with one neighboring Al. Here, the peak from the synthesis with sodium silicate is less well-defined than from the zeolite-to-zeolite transformation. At -100 to -103 ppm a small peak most likely associated with Si with two neighboring Al atoms is seen, but for the sample synthesized with sodium silicate the signal is broader and again less well-defined. Si environments associated with defects also appear in the same range. The above observations, showing less well-defined NMR peaks in the samples synthesized with sodium silicate indeed points towards an obtained material with more structural defects. Also this observation seems to suggest an improved occlusion of the OSDA during the complete zeolite-to-zeolite transformation approach.



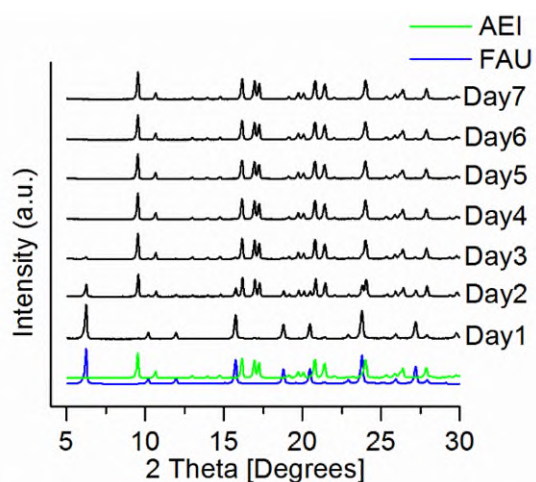
**Figure 4**  $^{29}\text{Si}$  (a) and  $^{27}\text{Al}$  MAS NMR (b) spectra of AEI-type zeolites prepared by OS (red curve) and ZTZ transformation (blue curve).

To study the intermediate stages during the zeolite-to-zeolite transformation, samples were prepared with different crystallization times. As seen from Figure 5 and Figure 6 FAU is converted directly into AEI. Full conversion is achieved within five days and no intermediates nor amorphous phases could be observed during the transformation seen from both PXRD (Figure 6) and SEM (Figure 7), which indicates that no other solid phases are involved in the formation of AEI. The SEM images clearly reveal the initial presence of agglomerates of randomly orientated octahedral crystallites of FAU (day 1) into orthorhombic box shaped ( $\{100\}$ ,  $\{010\}$  and  $\{001\}$  pinacoids) crystallites of AEI. SEM images from the product crystallized for one day furthermore show the presence of the AEI crystals located on the surface of FAU, suggesting that nucleation could occur on the available FAU surface. Typical Si/Al ratios for all achieved AEI zeolites fall in the range between 8 and 11 (see Figure 3), which is similar to earlier reported results [42]. When FAU with Si/Al=30 is used as a reactant and the AEI product appears with approximately one third of the Si-content, the remaining two thirds of Si does not become incorporated in the AEI product i.e. low yields are seen.

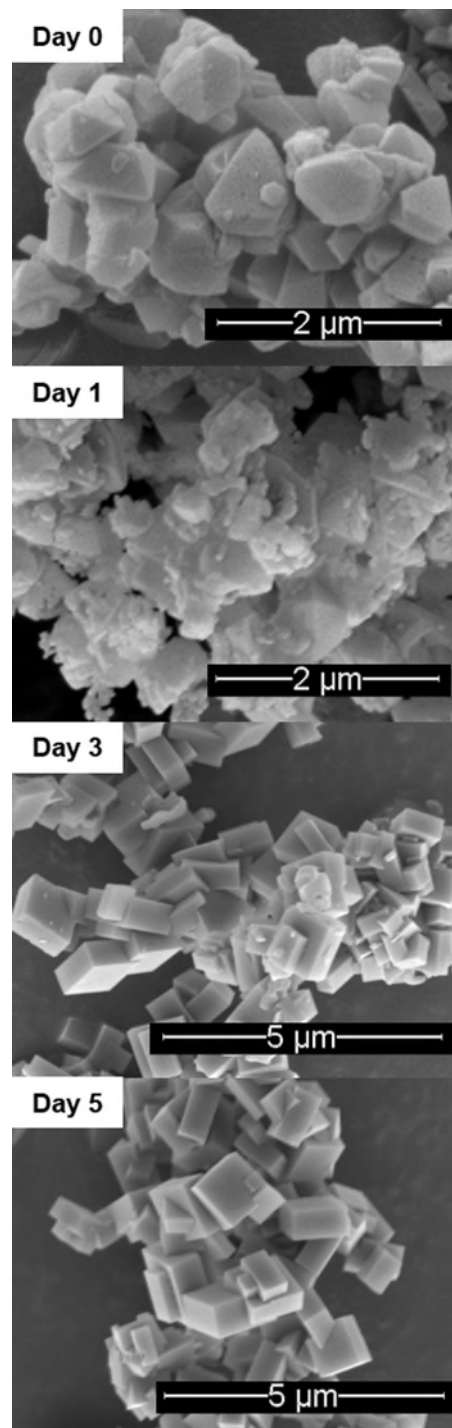




**Figure 5** Quantification of the phase composition of the products obtained with increasing crystallization time in the synthesis of AEI with FAU as the sole Si- and Al-source.

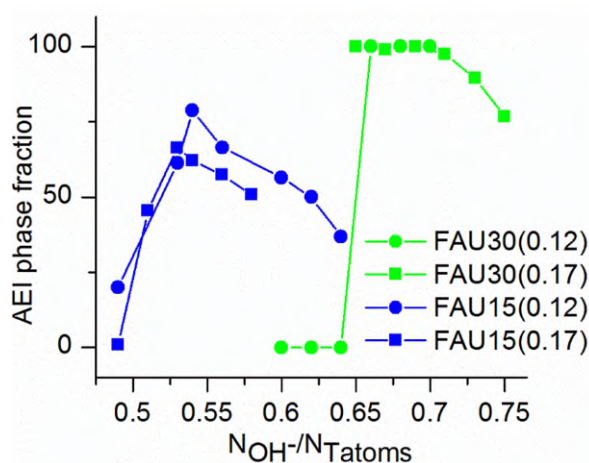


**Figure 7** XRD patterns of obtained products with increasing crystallization time in the synthesis of AEI with FAU as the sole Si- and Al-source.



**Figure 6** SEM images of selected products obtained with increasing crystallization time in the synthesis of AEI with FAU as the sole Si- and Al-source. Scale bars in the images corresponds to 5  $\mu\text{m}$ .

Efficient use of the FAU source giving high solid yields can be achieved by synchronization of the reactant-product Si/Al ratio (i.e. matching the preferred Si/Al ratio of the product in the reaction mixture) as recently shown [40]. In Figure 8 we report the AEI phase fraction of the complete zeolite-to-zeolite transformation of a FAU with Si/Al=15 as well as the results obtained earlier using FAU with Si/Al=30. Herein, we observe that when the Si/Al ratio of the FAU is decreased, the optimal OH<sup>-</sup>/T-atom ratio for achieving AEI also shifts to lower values (see Figure 8), despite the slower solubility of FAU expected. Indeed, the possibility of shifting to lower OH<sup>-</sup> amounts improves the solid yield because less Si will end up in the filtrate due to the lower solubility Si at lower pH values, but it also allows for a more efficient use of the OSDA. We furthermore note that the product from FAU with Si/Al=15 still contains some unconverted FAU. This is ascribed to the slower dissolution rate of the FAU zeolite as well as the slower crystallization of AEI due to the lower alkalinity, but can be improved in several ways, such as by temperature increase, lower water amounts in the gel or increased crystallization time.



**Figure 8** Phase fractions of AEI in the products obtained from zeolite-to-zeolite transformations with FAU (Si/Al=30) and FAU (Si/Al=15) depending on the OH<sup>-</sup>/T-atoms in the synthesis mixture. Numbers in parenthesis indicates the amount of OSDA/Si.

### 3.4. Preparation of AEI from other zeolites than FAU

So far AEI has only been obtained when Al is introduced into the synthesis as FAU. This raises the question if FAU is unique with its similar structural features (d6R units) and low framework density (13.3 T/1000 Å<sup>3</sup>), or if other zeolites can also be used. In this regard two other zeolites were applied: one with similar structural features and framework density as the target zeolite i.e. CHA (15.1 T/1000 Å<sup>3</sup>), and a second one with different structural building units as well as a similar framework density i.e. BEA\* (15.3 T/1000 Å<sup>3</sup>). Table 4 summarize the products obtained with the use of these zeolites as the sole source of Si and Al.

In general, a correlation between the thermodynamic stabilization energy of a given framework and the framework density can be expected [41]. Conversion of FAU into AEI (15.1 T/1000 Å<sup>3</sup>) should therefore be energetically “down-hill” and suggests that FAU is a good starting material. The results reported in Table 4 show that CHA can also be converted into AEI once the optimal OH<sup>-</sup>/T-atom

ratio has been identified, whereas we were not able to identify any conditions for the conversion of \*BEA into AEI although they have a similar overall composition. In this sense the successful achievement of AEI is most likely related to the similar structural features of the reactant zeolite with the target zeolite as well as the energetically favorable OSDA interaction with AEI.

**Table 4 Products from synthesis using various starting materials and 1,1,3,5-tetramethylpiperidinium hydroxide as OSDA.**

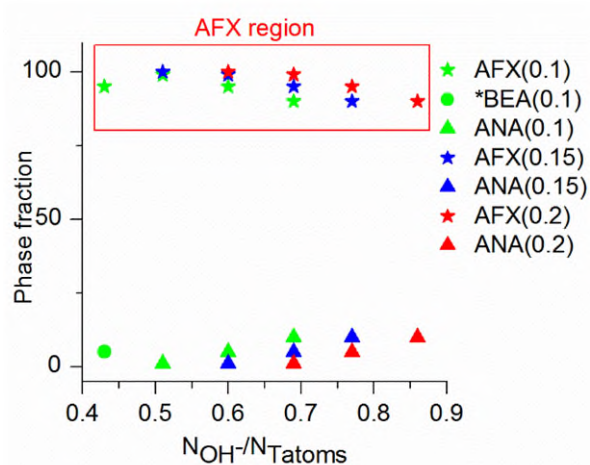
Si- and Al-source	Synthesis composition	OH <sup>-</sup> / N <sub>Tatoms</sub>	Product	Solid yield <sup>a</sup>
FAU (Si/Al=11) <sup>b</sup>	1.0 Si : 0.091 Al : 0.2 OSDA : 0.2 NaOH :: 15 H <sub>2</sub> O	0.37	AEI	~80%
FAU (Si/Al=15)	1.0 Si : 0.067 Al : 0.12 OSDA : 0.47 NaOH :: 40 H <sub>2</sub> O	0.55	AEI + FAU	-
FAU (Si/Al=30)	1.0 Si : 0.033 Al : 0.12 OSDA : 0.58 NaOH : 40 H <sub>2</sub> O	0.68	AEI	~35%
*BEA (Si/Al=12.5)	1.0 Si : 0.08 Al : 0.12 OSDA : 0.3 NaOH : 40 H <sub>2</sub> O	0.39	*BEA	-
*BEA (Si/Al=12.5)	1.0 Si : 0.08 Al : 0.12 OSDA : 0.45 NaOH : 40 H <sub>2</sub> O	0.53	*BEA	-
*BEA (Si/Al=12.5)	1.0 Si : 0.08 Al : 0.12 OSDA : 0.56 NaOH : 40 H <sub>2</sub> O	0.63	*BEA	-
*BEA (Si/Al=12.5)	1.0 Si : 0.08 Al : 0.12 OSDA : 0.6 NaOH : 40 H <sub>2</sub> O	0.67	*BEA	-
*BEA (Si/Al=30)	1.0 Si : 0.033 Al : 0.12 OSDA : 0.58 NaOH : 40 H <sub>2</sub> O	0.68	ANA+SOD	-
CHA (Si/Al=15)	1.0 Si : 0.067 Al : 0.12 OSDA : 0.6 NaOH : 40 H <sub>2</sub> O	0.68	AEI <sup>c</sup>	-

### 3.5. Preparation of AFX

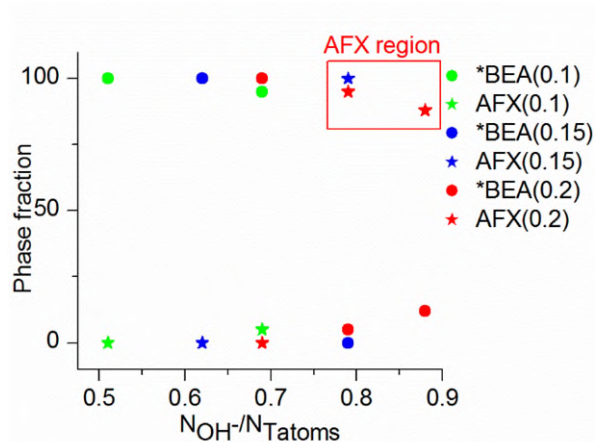
AFX (SSZ-16) is typically prepared using 1,4-bis(1,4-diazabicyclo[2.2.2]octane)butyl dihydroxide as the OSDA, but otherwise the preparation have many identical features with that of AEI, i.e. NaOH is used as a mineralizing agent and typically FAU is used as the Al-source. We therefore followed a similar approach as that shown above for AEI, applying a complete zeolite-to-zeolite transformation of FAU having Si/Al ratios of 6 and 15. As seen in Figure 9 and Figure 10 AFX is successfully obtained from both Si/Al ratios. For a starting Si/Al ratio of 15 AFX is obtained only at OH<sup>-</sup>/T-atom ratios above 0.8, whereas for Si/Al=6 AFX is obtained in the entire tested interval (0.4-0.9 OH<sup>-</sup>/T-atoms), and with an optimum around 0.50 OH<sup>-</sup>/T-atoms. Typically, AFX crystallizes with a Si/Al ~ 5. Hence, the FAU transformation to AFX follow the same trend as the AEI, namely when the reactant-product Si/Al ratio is synchronized, the required OH<sup>-</sup> amount to obtain AFX is decreased. This also leads to higher yields in the case of AFX, where solid yields above 90% could be achieved.

In general, \*BEA is a competing phase, which is not unexpected since the OSDA have also been reported to stabilize the \*BEA structure. [44] Typically, \*BEA crystallizes from gels with low amounts of OH<sup>-</sup> and is also observed here at the low OH<sup>-</sup>/T-atom ratios for both Si/Al=15 and 6. Interestingly, for the high silica-system \*BEA also appear at high OH<sup>-</sup>/T-atom ratios. It is therefore concluded that there is a narrow set of conditions that provides the necessary features to crystallize

AFX. In the low-silica system ANA appears at higher OH<sup>-</sup>/T-atom ratios, and it is the product of non-OSDA directed crystallization of this more thermodynamically stable structure.



**Figure 9** Phases obtained in the zeolite-to-zeolite transformation using FAU as the sole Si and Al source (Si/Al=6) and 1,4-bis(1,4-diazabicyclo[2.2.2]octane)butyl dihydroxide as OSDA.

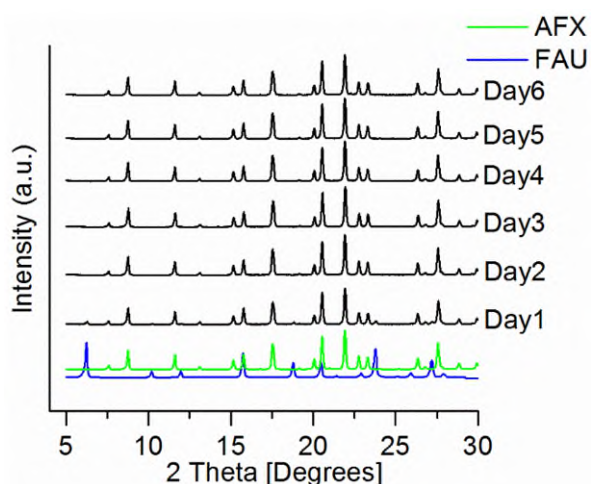


**Figure 10** Phases obtained in the zeolite-to-zeolite transformation using FAU as the sole Si and Al source (Si/Al=15) and 1,4-bis(1,4-diazabicyclo[2.2.2]octane)butyl dihydroxide as OSDA.

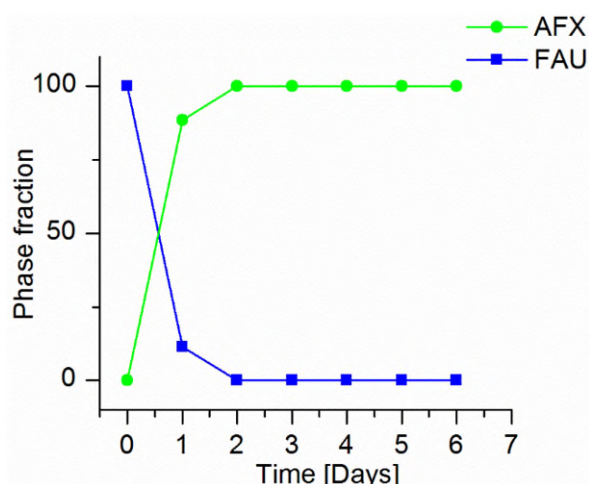
Also similar to the case of AEI the OSDA remains intact during the zeolite-to-zeolite transformation as seen from the <sup>13</sup>C CP-MAS NMR of the occluded OSDA in the as-prepared AFX zeolite and the <sup>13</sup>C-NMR on the OSDA in solution (see Figure S6).

When the zeolite transformation into AFX is followed over time no amorphous intermediates are observed in the solid phase (see Figure 11 and Figure 12). Again, this is similar to what was observed for AEI and seems to suggest that the species formed from the FAU is quickly consumed in the crystallization of the target zeolite and that the AFX crystallization follow a similar mechanism as that of AEI. Table 5 summarize the obtained phases and the synthesis composition, when the Si- and Al- sources are introduced by using 3 different zeolites. Following the same approach as for AEI, we found that AFX-type zeolites are easily synthesized from both FAU and CHA zeolites as raw materials. The successful achievement of AFX with a similar framework density (15.1/1000 Å<sup>3</sup>) from CHA-type zeolites once again emphasize the need of the parent zeolite to possess similar structural features with the target zeolite, which is in line with observations made for the CHA-OSDA-AEI system presented earlier. SEM images (see figure S4) of AFX-type zeolites reveal that the majority of the particles have hexagonal bipyramidal crystal morphology of different size. Although zeolites with a similar composition were used, we have not been able to identify any conditions for the transformation of \*BEA zeolite into AFX.

Similar to the case of the zeolite-to-zeolite transformation to obtain AEI, the AFX zeolite obtained by this approach contains predominantly Al in tetrahedral framework positions and only little amounts of structural defects inferred from the <sup>29</sup>Al MAS NMR and well-defined peaks in the <sup>27</sup>Si MAS NMR spectra, respectively (see Figure S7).



**Figure 11** PXRD patterns of obtained products with increasing crystallization time in the synthesis of AFX with FAU as the sole Si- and Al-source.



**Figure 12** Quantification of the phase composition of the products obtained with increasing crystallization time in the synthesis of AFX with FAU as the sole Si- and Al-source.

**Table 5.** Products from synthesis using various starting materials and 1,4-bis(1,4-diazabicyclo[2.2.2]octane)butyl dihydroxide as OSDA.

Si- and Al- source	Synthesis composition	$\frac{N_{OH^-}}{N_{Tatoms}}$	Product	Yield
FAU (Si/Al=6)	1.0 Si : 0.167 Al : 0.15 OSDA : 0.3 NaOH : 30 H <sub>2</sub> O	0.51	AFX	>90%
FAU (Si/Al=15)	1.0 Si : 0.067 Al : 0.15 OSDA : 0.55 NaOH : 30 H <sub>2</sub> O	0.79	AFX	~35%
*BEA (Si/Al=12,5)	1.0 Si : 0.08 Al : 0.15 OSDA : 0.35 NaOH : 30 H <sub>2</sub> O	0.6	*BEA	-
*BEA (Si/Al=12,5)	1.0 Si : 0.08 Al : 0.15 OSDA : 0.45 NaOH : 30 H <sub>2</sub> O	0.69	*BEA	-
*BEA (Si/Al=12,5)	1.0 Si : 0.08 Al : 0.15 OSDA : 0.55 NaOH : 30 H <sub>2</sub> O	0.79	*BEA	-
*BEA (Si/Al=5)	1.0 Si : 0.2 Al : 0.10 OSDA : 0.3 NaOH : 30 H <sub>2</sub> O	0.42	*BEA	-
*BEA (Si/Al=5)	1.0 Si : 0.2 Al : 0.10 OSDA : 0.4 NaOH : 30 H <sub>2</sub> O	0.5	*BEA	-
CHA (Si/Al=15)	1.0 Si : 0.067 Al : 0.15 OSDA : 0.35 NaOH : 30 H <sub>2</sub> O	0.6	*BEA	-
CHA (Si/Al=15)	1.0 Si : 0.067 Al : 0.15 OSDA : 0.45 NaOH : 30 H <sub>2</sub> O	0.69	*BEA	-
CHA (Si/Al=15)	1.0 Si : 0.067 Al : 0.15 OSDA : 0.55 NaOH : 30 H <sub>2</sub> O	0.79	*BEA	-
CHA (Si/Al=7)	1.0 Si : 0.143 Al : 0.10 OSDA : 0.3 NaOH : 30 H <sub>2</sub> O	0.44	*BEA + AFX	-
CHA (Si/Al=7)	1.0 Si : 0.143 Al : 0.10 OSDA : 0.4 NaOH : 30 H <sub>2</sub> O	0.53	AFX <sup>a</sup>	-

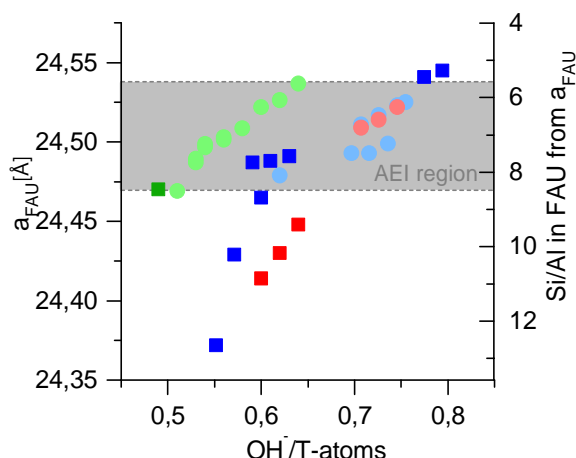
<sup>a</sup>Traces of unknown phase (see Figure S3)

## 4. Discussion

For the synthesis of AEI and AFX, we observe in all cases that when the OH<sup>-</sup> amount is increased the lattice parameter of unconverted FAU is increasing (see e.g. reported  $a_{FAU}$  values for synthesis using FAU in Table 1 and Table 3). The increase in lattice parameter is related to the selective dissolution of Si from the FAU material. This means that the initially extracted species are more siliceous in nature than the starting FAU zeolite. Only when a certain amount of Si is extracted from the FAU-material the target zeolite is observed in phase space. For the reported synthesis on AEI we observe



that at higher OH<sup>-</sup>/T atom ratios AEI is no longer formed and FAU remains with even higher amounts of Si extracted (see that the  $a_0$  is always above 24.52 Å when AEI is no longer appearing in Table 1). Fichtner-Schmittler et al. [45] reported a general correlation between the Si/Al ratio and FAU lattice parameters. Using this correlation, we have summarized the lattice parameters of the remaining FAU material and the corresponding Si/Al ratio (Figure 13).



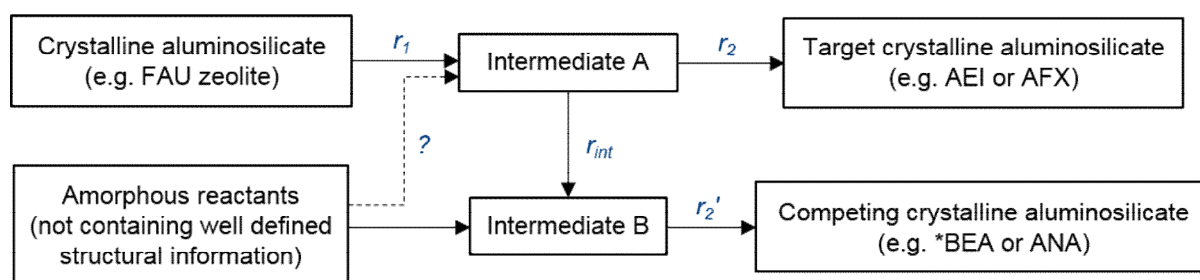
**Figure 13** Lattice parameters and related Si/Al in FAU in syntheses where FAU is still present in the product. The region where AEI appear in the product phase is marked as a grey box. Circles show products where a mixture of FAU + AEI is obtained and squares indicate that only FAU were present after synthesis. The colors corresponds to blue = synthesis with FAU and sodium silicate (overall Si/Al=30 in the gel), red = complete zeolite-to-zeolite transformation (overall Si/Al =30 in the gel) and green = complete zeolite-to-zeolite transformation (overall Si/Al =15 in the gel). All lattice parameters and corresponding Si/Al ratios in the FAU phase are reported relative to the OH<sup>-</sup>/T-atoms in the gel.

We observe that AEI is no longer formed at higher OH<sup>-</sup> amounts when the Si/Al drops < 6. Furthermore, we see that the FAU observed using low OH<sup>-</sup> amounts, just before AEI appears, typically show Si/Al ratios of approximately > 8. A similar treatment of the FAU lattice parameters when we follow the AEI crystallization with time (see crystallization curve in Figure 5) reveals that FAU has an approximate Si/Al ratio around 6 at the onset of the crystallization. This indeed indicates that the AEI is preferably achieved from an intermediate zeolite with a Si/Al ratio close to these numbers, although the correlation between the lattice parameters and Si/Al may not be exact. More generally we see that when the starting FAU zeolite has a Si/Al ratio close to that of the preferred Si/Al ratio in the target zeolite, crystallization proceeds at even lower OH<sup>-</sup> amounts, perhaps because Si extraction is not necessary. This specific feature also allows the target zeolite to be obtained with higher yields.

For AEI with 4 *aei* cages per unit cell presumably occupied by one monocationic OSDA per cage the optimal Si/Al is expected to be 11. Whereas the AFX unit cell has 3 *aft* and 2 *gme* cages occupied by a dicationic OSDA and a sodium ion, respectively, which gives an optimal expected Si/Al ratio of 5. These numbers are in good line with reported values for AEI and AFX type zeolites as well as the ones achieved in this study.

From the correlation between Si/Al ratio and FAU lattice parameter it is interesting that the onset of crystallization observed for AEI does not occur at the optimal Si/Al ratio, but at slightly lower numbers, which seems to suggest nucleation of the target zeolite requires a somewhat more Al-rich starting point than the composition of final zeolite. We also observe that when the OSDA is not present, FAU is completely amorphized (not shown above), which indicates that the remaining more Al-rich part of the FAU is stabilized by the OSDA and in this way also influences the Si-leaching rate of the FAU zeolite.

In general, we can introduce a scheme as shown in Figure 14, where the reactant zeolite is dissolved by the  $\text{OH}^-$  with a certain rate ( $r_1$ ). This rate is mainly influenced by the  $\text{OH}^-$  amount in the system, the Al-content in the reactant zeolite (materials with high Si/Al ratios are more quickly dissolved), and the OSDA, as this will protect the zeolite from  $\text{OH}^-$  attack as well as the general structural features of the zeolite (i.e. more strained rings in the structure may be more prone to  $\text{OH}^-$  attack). An intermediate set of species (Intermediate A) are most likely formed, that still contain some structural information leading to the target zeolite at a rate ( $r_2$ ). If  $r_1$  and  $r_2$  are not matched such that  $r_1 \leq r_2$ , the intermediate species can lose the structural information leading to a competing zeolite phases through another intermediate B. From our results, we observe that target zeolites are only formed inside specific  $[\text{OH}^-]$  windows (see Figure 1, Figure 2, Figure 8, Figure 9 and Figure 10) that are especially dependent on the Si/Al ratio in the reactant zeolites indicating that  $r_1$  is critical.



**Figure 14 Overall scheme for the formation of a target zeolite dependent on an unstable intermediate.**

In the case of AEI synthesized using 1,1,3,5-tetramethylpiperidinium hydroxide as OSDA no competing phases exists (at the compositions applied) and FAU remains as the only phase observed outside the optimal  $\text{OH}^-$  window. When other materials (than e.g. FAU or CHA) than crystalline aluminosilicate materials with similar structural features are applied, the AEI target is no longer obtained; most likely because the required intermediate(s) are not created.

In the case where 1,4-bis(1,4-diazabicyclo[2.2.2]octane)butyl dihydroxide is used as the OSDA to synthesize AFX, \*BEA is a known competing phase, and ANA also appear for lower Si/Al ratios. These two competing phases are not strongly dependent on the type of raw materials used and can, in general be synthesized under a broad range of conditions from many different raw materials. Therefore, the competing phases most likely do not require a specific intermediate to form.

The identity of the intermediate(s) in this type of transformation is unknown, but as stated above, it most likely contains some structural information from the parent zeolite and the specific Al-

configuration. This statement is consistent with the observation that AFX and AEI can be crystallized from FAU and CHA, but not from \*BEA that does not contain similar structural features with the target zeolite. This statement is also in line with the working hypothesis earlier proposed by Okubo et al. [27]

On the other hand, the inability of a zeolite with different structural features (e.g. \*BEA) relative to the target zeolite (e.g. AEI or AFX) to direct the synthesis towards the desired product, can also be explained by the fact that the \*BEA zeolite is not able to undergo dissolution at a rate that would satisfy  $r_1 \leq r_2$ . This does not exclude the formation of necessary intermediate(s) from \*BEA, just that it is not sufficient to match the crystallization of the target system under the conditions investigated herein.

Additionally, we note, that if  $r_2$  is not sufficiently large, the structural information is lost by transformation of the intermediate, making the crystallization of target zeolites with structural features that are difficult to manufacture less likely. One can imagine the dissolution of small oligomeric structures from the reactant that are digested into more monomeric structures if they are not quickly consumed in the formation of the target zeolite as a possible scenario.

Zeolite-to-zeolite transformations have also been reported from one zeolite into another without having similar structural features. One such example is the transformation of FAU into \*BEA. [46]. In this case an amorphous intermediate was observed and it is likely that an “intermediate A” is transformed into an “intermediate B” much similar to the interpretation of how \*BEA zeolites were observed for the FAU to AFX transformation reported herein. In a sense this observation underlines the unique possibility of using zeolite-to-zeolite transformations to obtain target zeolite phases that are otherwise difficult to achieve, perhaps because of the structural features present in intermediate A are difficult to produce by other approaches.

## 5. Conclusions

The crystallization of AEI and AFX zeolites were studied mainly by zeolite-to-zeolite transformations. Especially the OH/T-atom ratio and the Al-source are critical to obtain the target zeolite. The OSDA is also found to play a crucial role; both by decreasing the dissolution rate of the starting zeolite, but also in the formation and stabilization of the target zeolite.

Use of FAU allowed us to follow the lattice parameter at various points during crystallization and for various synthesis without complete formation of AEI. Since the lattice parameter is proportional to the Al-content in the FAU zeolite it was deduced that at the onset of target zeolite formation, specific values were seen to converge at a range related to that preferred by the target zeolite. This indicates that successful nucleation and/or formation of the target zeolite is dependent on this type of intermediate and dependent on the dissolution of the starting zeolite. In line with this finding, it could also be seen that when the Si/Al ratio in the starting zeolite was chosen close to the target zeolite lower OH/T-atom ratios lead to the successful achievement of the target zeolite and with improved solid yields.

With the choice of optimal OH/T-atom ratio and selection of reactant Si/Al ratio it was also shown that AFX and AEI could, for the first time, be obtained from other starting zeolites than FAU. Successful achievement of AFX and AEI was in this sense obtained from transformation of CHA that



contains similar structural features, but a higher framework density than FAU. Oppositely, we were not able to identify any conditions that allowed us to obtain AEI or AFX from \*BEA that does not contain similar structural features. These observations indicate that zeolite-to-zeolite transformations does not have to proceed from zeolites with low framework densities (i.e. high stabilization energies) to higher framework densities (i.e. lower stabilization energies), but is mainly driven by favorable OSDA-zeolite interactions. Overall results were rationalized in a scheme where especially the dissolution rate of a starting zeolite containing key structural features is essential to obtain a successful zeolite-to-zeolite transformation.

## 6. Acknowledgements

The authors thank Haldor Topsoe A/S and Innovation Fund Denmark for financial support under the Industrial PhD programme (Case no. 1355-0174B).

## 7. References

- [1] Barrer, R. M., *Hydrothermal Chemistry of Zeolites*, Academic Press, London, 1982.
- [2] A. Corma, *Chem. Rev.* 95 (1995) 559-614. <https://doi.org/10.1021/cr00035a006>
- [3] C. D. Chang, *Cat. Rev.* 26 (1984) 323–345. <https://doi.org/10.1080/01614948408064716>
- [4] S. Wilson, P. Barger, *Microporous Mesoporous Mater.* 29 (1999) 117–126. [https://doi.org/10.1016/S1387-1811\(98\)00325-4](https://doi.org/10.1016/S1387-1811(98)00325-4)
- [5] M. A. Djieugoue, A. M. Prakash, L. Kevan, *J. Phys. Chem. B* 104 (2000) 6452–6461. <https://doi.org/10.1021/jp000504j>
- [6] A. Corma, F. Rey, J. Rius, M. J., Sabater, S. Valencia, *Nature* 431 (2004) 287–290. <http://dx.doi.org/10.1038/nature02909>
- [7] U. Olsbye, S. Svelle, M. Bjørgen, P. Beato, T. V. W. Janssens, F. Joensen, S. Bordiga, K. P. Lillerud, *Angew. Chem. Int. Ed.* 51 (2012) 5810–5831. <https://doi.org/10.1002/anie.201103657>
- [8] N. Kosinov, J. Gascon, F. Kapteijn, E. J. M. Hensen, *J. Membr. Sci.* 499 (2016) 65–79. <https://doi.org/10.1016/j.memsci.2015.10.049>
- [9] S. Li, Z. Zong, S. J. Zhou, Y. Huang, Z. Song, X. Feng, R. Zhou, H. S. Meyer, M. Yu, M. A. Carreon, *J. Membr. Sci.* 487 (2015) 141–151. <https://doi.org/10.1016/j.memsci.2015.03.078>
- [10] T. Wu, B. Wang, Z. Lu, R. Zhou, X. Chen, *J. Membr. Sci.* 471 (2014) 338–346. <https://doi.org/10.1016/j.memsci.2014.08.035>
- [11] P. J. Bereciartua, Á. Cantín, A. Corma, J. L. Jordá, M. Palomino, F. Rey, S. Valencia, E. W. Jr. Corcoran, P. Kortunov, P. I. Ravikovitch, A. Burton, C. Yoon, Y. Wang, C. Paur, J. Guzman, A. R. Bishop, G. L. Casty, *Science* 358 (2017) 1068–1071. <http://science.sciencemag.org/content/358/6366/1068>

- [12] Bull, I.; Boorse, R. S.; Jaglowski, W. M.; Koermer, G. S.; Moini, A.; Patchett, J. A.; Xue, W. M.; Burk, P.; Dettling, J. C.; Caudle, M. T. Copper, CHA Zeolite Catalysts. U.S. Patent 0,226,545, 2008.
- [13] J. H. Kwak, R. G. Tonkyn, D. H. Kim, J. Szanyi, C. H. F. Peden, *J. Catal.* 275 (2010) 187–190. <https://doi.org/10.1016/j.jcat.2010.07.031>
- [14] D. W. Fickel, E. D. Addio, J. A. Lauterbach, R. F. Lobo, *Appl. Catal. B Environ.* 102 (2011) 441–448. <https://doi.org/10.1016/j.apcatb.2010.12.022>
- [15] A. M. Beale, F. Gao, I. Lezcano-Gonzalez, C. H. F. Peden, J. Szanyi, *Chem. Soc. Rev.* 44 (2015) 7371–7405. <http://dx.doi.org/10.1039/C5CS00108K>
- [16] F. Gao, J. H. Kwak, J. Szanyi, C. H. F. Peden, *Top. Catal.* 56 (2013) 1441–1459. <https://doi.org/10.1007/s11244-013-0145-8>
- [17] M. Moliner, C. Martínez, A. Corma, *Chem. Mater.* 26 (2014) 246–258. <https://doi.org/10.1021/cm4015095>
- [18] O. Chiyoda, M. E. Davis, *Microporous Mesoporous Mater.* 32 (1999) 257–264. <https://doi.org/10.1021/cm4015095>
- [19] S. I. Zones *J. Chem. Soc. Faraday Trans.* 87 (1991) 3709–3716. <http://dx.doi.org/10.1039/FT9918703709>
- [20] N. Martín, M. Moliner, A. Corma, *Chem. Commun.* 51 (2015) 9965–9968. <http://dx.doi.org/10.1039/C5CC02670A>
- [21] R. Nedyalkova, C. Montreuil, C. Lambert, L. Olsson *Top Catal.* 56 (2013) 550–557. <https://doi.org/10.1007/s11244-013-0015-4>
- [22] T. Sonoda, T. Maruo, Y. Yamasaki, N. Tsunoji, Y. Takamitsu, M. Sadakane, *T. J. Mater. Chem. A* 3 2015 857–865. <http://dx.doi.org/10.1039/C4TA05621C>
- [23] T. Sano, M. Itakura, M. Sadakane, *J. Jpn. Pet. Inst.* 56 (2013) 183–197. <https://doi.org/10.1627/jpi.56.183>
- [24] F. G. Dwyer, P. Chu, *J. Catal.* 59 (1979) 263–271. [https://doi.org/10.1016/S0021-9517\(79\)80030-5](https://doi.org/10.1016/S0021-9517(79)80030-5)
- [25] S. I. Zones, R. A. Van Nordstrand, *Zeolites* 8 (1988) 166–174. [https://doi.org/10.1016/S0144-2449\(88\)80302-6](https://doi.org/10.1016/S0144-2449(88)80302-6)
- [26] T. Moteki, R. F. Lobo, *Chem. Mater.* 28 (2016) 638–649. <https://doi.org/10.1021/acs.chemmater.5b04439>
- [27] K. Itabashi, Y. Kamimura, K. Iyoki, A. Shimojima, T. Okubo, *J. Am. Chem. Soc.* 134 (2012) 11542–11549. <https://doi.org/10.1021/ja3022335>

- [28] K. Honda, M. Itakura, Y. Matsuura, A. Onda, Y. Ide, M. Sadakane, T. J. *Nanosci. and Nanotechnol.* 13 2013 3020-3026(7). <https://doi.org/10.1166/jnn.2013.7356>
- [29] S. I. Zones, Y. Nakagawa, *Micropor. Mater.* 2 (1994) 543–555. [https://doi.org/10.1016/0927-6513\(94\)00025-5](https://doi.org/10.1016/0927-6513(94)00025-5)
- [30] S. Goel, S. I. Zones, E. Iglesia, *Chem. Mater.* 27 (2015) 2056–2066. <https://doi.org/10.1021/cm504510f>
- [31] R. F. Lobo, S. I. Zones, R. C. Medrud, *Chem. Mater.* 8 (1996) 2409 – 2411. <https://doi.org/10.1021/cm960289c>
- [32] P. Hrabanek, A. Zikanova, T. Supinkova, J. Drahokoupil, V. Fila, M. Lhotka, H. Dragounova, F. Laufek, L. Brabec, I. Jirka, B. Bernauer, O. Prokopova, V. Martin-Gil, M. Kocirik, *Microporous Mesoporous Mater.* 228 (2016) 107–115. <https://doi.org/10.1016/j.micromeso.2016.03.033>
- [33] Zones, S. I. Zeolite SSZ-16. U.S. Patent 4,508,837, 1982.
- [34] Zones, S. I.; Nakagawa, Y.; Evans, S. T.; Lee, G. S. Zeolite SSZ-39. U.S. Patent 5,958,370, 1997.
- [35] Zones, S. I. Synthesis of SSZ-16 zeolite catalyst. U.S. Patent 5,194,235, 1992.
- [36] A. W. Burton, G. S. Lee, S. I. Zones, *Microporous Mesoporous Mater.* 90 (2006) 129–144. <https://doi.org/10.1016/j.micromeso.2005.11.022>
- [37] T. Maruo, N. Yamanaka, N. Tsunoji, M. Sadakane, T. Sano, *Chem. Lett.* 43 (2014) 302–304. <https://doi.org/10.1246/cl.130996>
- [38] M. Dusselier, J. E. Schmidt, R. Moulton, B. Haymore, M. Hellums, M. E. Davis, *Chem. Mater.* 27 (2015) 2695–2702. <https://doi.org/10.1021/acs.chemmater.5b00651>
- [39] D. W. Fickel, R. F. Lobo, *J. Phys. Chem. C* 114 (2010) 1633–1640. <https://doi.org/10.1021/jp9105025>
- [40] N. Martin, C. R. Boruntea, M. Moliner, A. Corma, *Chem. Commun.* 51 (2015) 11030–11033. <http://dx.doi.org/10.1039/C5CC03200H>
- [41] P. Wagner, Y. Nakagawa, G. S. Lee, M. E. Davis, S. Elomari, R. C. Medrud, S. I. Zones, *J. Am. Chem. Soc.* 122 (2000) 263–273. <https://doi.org/10.1021/ja990722u>
- [42] M. Moliner, C. Franch, E. Palomares, M. Grill, A. Corma, *Chem. Commun.* 48 (2012) 8264–8266. <http://dx.doi.org/10.1039/C2CC33992G>
- [43] D. Xie, L. B. Mccusker, C. Baerlocher, S. I. Zones, W. Wan, X. Zou, *J. Am. Chem. Soc.* 135 (2013) 10519–10524. <https://doi.org/10.1021/ja4043615>
- [44] S. I. Zones, Y. Nakagawa, G. S. Lee, C. Y. Chen, L. T. Yuen, *Microporous Mesoporous Mater.* 21 (1998) 199–211. [https://doi.org/10.1016/S1387-1811\(98\)00011-0](https://doi.org/10.1016/S1387-1811(98)00011-0)

- [45] H. Fichtner-Schmittler, U. Lohse, G. Engelhardt, V. Patzelov, *Crystal Research and Technology* 19 (1984) K1–K3. <https://doi.org/10.1002/crat.2170190124>
- [46] H. Jon, K. Nakahata, B. Lu, Y. Oumi, T. Sano, *Microporous Mesoporous Mater.* 96 (2006) 72–78. <https://doi.org/10.1016/j.micromeso.2006.06.024>

## Paper 2

The manuscript attached below represents the author's version of the article:

Cristian-R. Boruntea, Lars F. Lundegaard, Peter N. R. Vennestrøm, K-paracelsian ( $\text{KAlSi}_3\text{O}_8 \cdot \text{H}_2\text{O}$ ) and identification of a simple building scheme of dense double-crankshaft zeolite topologies. *International Union of Crystallography Journal* 2019, Volume 6, Part 1, Pages 1 – 6.

This paper is addressing the synthesis and structure refinement of a novel dense zeolite, named K-paracelsian. The discovery of this material is a result of screening the phase space using 1-methyl-DABCO as the OSDA. The chemical composition of this material is closely related to the mineral microcline and structurally closely related to the mineral paracelsian, both of which are feldspars. In opposition to the feldspars, K-paracelsian contains intrazeolitic water corresponding to one molecule per cage. It has been found that K-paracelsian is the endmember of a family of dense double-crankshaft zeolite topologies. A number of known IZA structures and more important a large number of crystallo-chemically healthy hypothetical frameworks can be built by applying the observed building principle.

## K-paracelsian ( $\text{KAlSi}_3\text{O}_8 \cdot \text{H}_2\text{O}$ ) and identification of a simple building scheme of dense double-crankshaft zeolite topologies

Cristian-R. Boruntea<sup>ab</sup>, Peter N. R. Vennestrom<sup>c\*</sup> and Lars F. Lundegaard<sup>a\*</sup>

<sup>a</sup> Haldor Topsøe A/S, Haldor Topsøes Alle 1, Kgs. Lyngby, 2800, Denmark

<sup>b</sup> Instituto de Tecnología Química, Universitat Politècnica de València-Consejo Superior de Investigaciones Científicas, Avenida de los Naranjos s/n, Valencia, 46022, Spain

<sup>c</sup> Umicore Denmark ApS, Nøjsomhedsvej 20, Kgs. Lyngby, 2800, Denmark

Correspondence email: peter.vennestrom@eu.umicore.com; lafl@topsoe.com

**Synopsis** Synthesis and structure refinement of a dense zeolite with a 1-dimensional channel system.

**Abstract** During screening of the phase space using KOH and 1-methyl-4-aza-1-azoniabicyclo[2.2.2]octane hydroxide (1-methyl-DABCO) under hydrothermal zeolite synthesis conditions K-paracelsian was synthesized. SEM EDS and *ex-situ* PXRD analysis revealed a material compositionally closely related to the mineral microcline and structurally closely related to the mineral paracelsian, both of which are feldspars. In contrast to the feldspars, K-paracelsian contains intrazeolitic water corresponding to one molecule per cage. In case of K-paracelsian it might be useful to consider it a link between feldspars and zeolites. It is furthermore shown that K-paracelsian can be described as the simplest endmember of a family of dense double-crankshaft zeolite topologies. By applying the identified building principle, a number of known zeolite topologies can be constructed. It furthermore allows us to construct a range of hypothetical small pore structures that are crystallo-chemically healthy, but which have not yet been realized experimentally.

**Keywords:** K-paracelsian; dense double-crankshaft zeolite topologies; structure refinement;

## 1. Introduction

Zeolites are microporous aluminosilicates belonging to the tectosilicates group, characterized by a well-defined and uniform pore system, free channels and internal voids where water can be located. Their crystalline structure contains tetrahedrally coordinated Si and Al atoms that are connected through oxygen bonds, forming a three-dimensional network with cavities of different size and shapes that can host various cations. These structural features in combination with hosted cation are in direct correlation with their properties that are highly exploited in catalysis, ion exchange and separation applications (Corma, 1995; Davis, 2002)

Synthetic zeolites were initially prepared by mimicking the conditions under which zeolites are formed in nature. Albeit aqueous inorganic alkaline solutions were combined with sources of silica and alumina and treated under high pressure (Barrer, 1982). Due to the need for more siliceous materials most novel zeolites are synthesized today by using organic cations that are soluble in aqueous media, acting as organic structure directing agents (OSDAs), combined with the necessary reaction conditions and a mineralizing agent that allow the nucleation and crystal growth of the desired structure. It is generally accepted that the organic molecule used during the synthesis is incorporated into the zeolite cavities and stabilizing the structure through vdW interactions, among others. However, there are examples where the organic is not occluded, but either participates or modifies the zeolite crystallization and/or growth mechanism. For example, the synthesis of Losod (LOS), a new framework structure at the time (Sieber & Meier, 1974), could be prepared without the OSDA being incorporated into the zeolite cavities. In this case it was speculated that the organic cations might be responsible for keeping the aluminate and silicate species in a reactive state, suggesting that the OSDA is playing a catalytic role rather than having a classic structure directing effect. It was furthermore shown that the synthesis of Losod was highly dependent on the use of sodium cations, which were found to be part of the zeolite product (Sieber & Meier, 1974). This is a good example of how an organic molecule can influence product selectivity, while at the same time the inorganic cation become incorporated in the final material. Both cations seem to play a concerted role in this type of crystallization.

In this contribution we report on the synthesis and structure refinement of a novel dense zeolite material, K-paracelsian with a 1-dimensional channel system. The zeolite was discovered while screening the hydrothermal phase space using potassium hydroxide in combination with 1-methyl-4-aza-1-azoniabicyclo[2.2.2]octane hydroxide (1-methyl-DABCO) and the use of a FAU zeolite as the source of Si and Al. We found that the novel synthesized aluminosilicate is compositionally closely related to the mineral microcline and structurally closely related to the mineral paracelsian. Both are part of the feldspar group. In contrast to the feldspars, the new material, shows intrazeolitic molecular water, which is possible to extract upon heating. We furthermore show that K-paracelsian is the simplest endmember of a family of dense double-crankshaft zeolite topologies.

## 2. Experimental

### 2.1. Synthesis

For a typical synthesis 2.32 g 1-methyl-DABCO (12.5 wt. %) was mixed with 1.97 g KOH (20 wt. %) and 0.743 g H-FAU (Si/Al = 6) to give a molar composition of 1 Si : 0.167 Al : 0.2 OSDA : 0.7 KOH : 20 H<sub>2</sub>O. The resulting gel was mixed for 1 h at room temperature and then transferred into a Teflon lined autoclave. The crystallization was carried out at 150°C for 7 days unless otherwise stated. Solid yields are calculated based on Si/Al ratio in the reactant compared to the product. The raw materials used were: 1-methyl-DABCO prepared in-house (see supporting information for the synthesis procedure), KOH (reagent grade  $\geq 98\%$ , Sigma-Aldrich), in-house prepared co-precipitated amorphous silica-alumina (ASA) and Y-zeolite (CBV-712, from Zeolyst International).

### 2.2. Characterization

The synthesized materials were analyzed by X-ray diffraction using a Phillips PW1800 instrument system in  $\theta$ - $2\theta$  geometry working in Bragg-Brentano mode using CuK $\alpha$  radiation ( $\lambda = 1.541$  Å). An AntonPaar1200 cell equipped with a capillary stage was used for the *in situ* XRD heating experiments. SEM images were recorded using an XL30-SEM instrument operated at 10 kV. The samples were sprinkled over carbon tape and attached on Al-stubs and then coated with a 30 nm layer of carbon to prevent charging. TGA-DSC analysis were performed using a Mettler TGA-DSC instrument with a heating rate of 5 °C / min and the temperature limit at 550 °C. 1D <sup>13</sup>C-NMR was measured using a Bruker 400 MHz instrument in D<sub>2</sub>O as solvent and for the solid state <sup>13</sup>C CP-MAS NMR the spectra have been acquired at 9.4 T using a spinning speed of  $nR = 10.0$  kHz and a CP contact time of 5.0 ms. For the <sup>27</sup>Al and <sup>29</sup>Si MAS NMR spectra a Bruker Avance II HD 400Mhz spectrometer was used. <sup>27</sup>Al MAS NMR spectra were recorded at spinning rate of 20Khz in a Bruker 3.2 mm probe, using a flip angle of  $\pi/12$  and a recycle delay of 1s. <sup>29</sup>Si MAS NMR spectra were recorded at spinning rate of 5 kHz in Bruker 4 mm probe, using a flip angle of 60° and a recycle delay of 60 s.

## 3. Results and discussion

### 3.1. Synthesis

The phase space using 1-methyl-DABCO was explored in alkaline media using NaOH or KOH. Two sources of T-atoms (Si and Al) were selected for this screening study, namely the use of a co-precipitated silica-alumina as well as FAU. When 1-methyl-DABCO is used in combination with NaOH and FAU no crystalline products are observed at low OH<sup>-</sup> concentrations. Increasing the OH<sup>-</sup> concentration leads to a narrow region with LEV in line with previous studies (Xie *et al.*, 2013). Further increase of the basicity yields ANA as the thermodynamic end-point in Na-rich systems (see Table S1 in the supporting information).

In agreement with the example of LOS mentioned in the introduction and many other studies; exchanging the inorganic cation leads to a new set of obtainable phases. At low OH<sup>-</sup> concentrations and high-silica compositions (e.g. Si/Al gel ratios  $\geq 15$ ), when potassium hydroxide is applied together with the 1-methyl-DABCO organic molecule, a phase that we have not yet identified appears together with ERI irrespective of the T-atom source (see Table S2 in the supporting information). At higher OH<sup>-</sup>



concentrations and more Al-rich synthesis gels (Si/Al gel ratio = 6) phase selectivity becomes dependent on the T-atom source (see Table 1). Using an amorphous co-precipitated silica-alumina leads to the well-known LTL phase. However, exchanging the T-atom source to a FAU zeolite leads to another zeolite product (named K-paracelsian herein, see later). This zeolite is furthermore dependent on the concerted effect of both 1-methyl-DABCO and potassium hydroxide. This is evident because the phase is only present as a small impurity when 1-methyl-DABCO is omitted in the gel (see sample 5 in Table 1). We also note that ERI is seen at lower hydroxide concentrations together with an unknown phase.

A phase pure sample of the new zeolite was achieved (sample 4 in Table 1 and Figure 1) by combination of high OH<sup>-</sup>-concentrations, a FAU as T-atoms source and the combination of potassium hydroxide and 1-methyl-DABCO. Occlusion of the OSDA in the zeolite could not easily be measured by <sup>13</sup>C CP-MAS NMR. Only when the number of scans were increased three-fold a small amount of C could be measured in the sample (Figure S1). This is consistent with the interpretation that 1-methyl-DABCO is not occluded in the pore system, as it would have been expected from the classical role of an OSDA, but a small amount can be found on the surface of the crystallites. In the remaining part of the manuscript we will focus on this material specifically.

**Table 1 Summarized product phases for the synthesis system FAU-OSDA-KOH.**

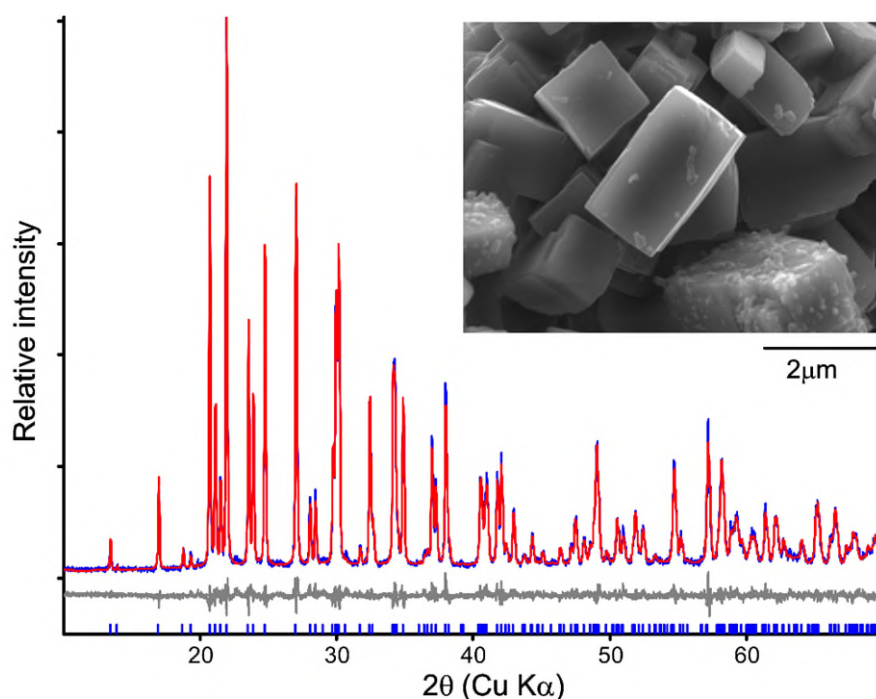
\* indicates that the phase only exist in very small amount.

Sample Number	Si- and Al- sources	OSDA/Si	KOH/Si	Product Phase	M (g)/η (%)
1	FAU (Si/Al = 6)	0.2	0.6	LTL + K-paracelsian	0.44/58
2	FAU (Si/Al = 6)	0.1	0.7	LTL + K-paracelsian	0.3/39
3	FAU (Si/Al = 6)	0.2	0.5	ERI + Unknown	0.3/40
4	FAU (Si/Al = 6)	0.2	0.7	K-paracelsian	0.33/45
5	FAU (Si/Al = 6)	0	0.8	LTL + K-paracelsian *	0.28/36
6	ASA (Si/Al = 6)	0.2	0.6	LTL	0.44/58

### 3.2. Basic characterization and structure refinement

The initial characterization used to reveal the structure of the product (sample 4, Table 1) consisted of SEM imaging and *ex situ* XRD analysis of the as synthesized products. SEM images revealed a homogeneous morphology consisting of large (~2 μm) well faceted crystallites. Point EDS analysis on 5 different crystallites revealed an average composition of 3.3(3) Si/Al and 0.29(3) K/Si. Within the uncertainty of the EDS analysis this is consistent with a stoichiometric compound of the composition  $\text{KAlSi}_3\text{O}_8$ , which is also in agreement with the expected Si/Al ratio from the yield reported in Table 1 and the Si/Al ratio of 2.92 calculated from <sup>27</sup>Si MAS NMR (Figure S2).

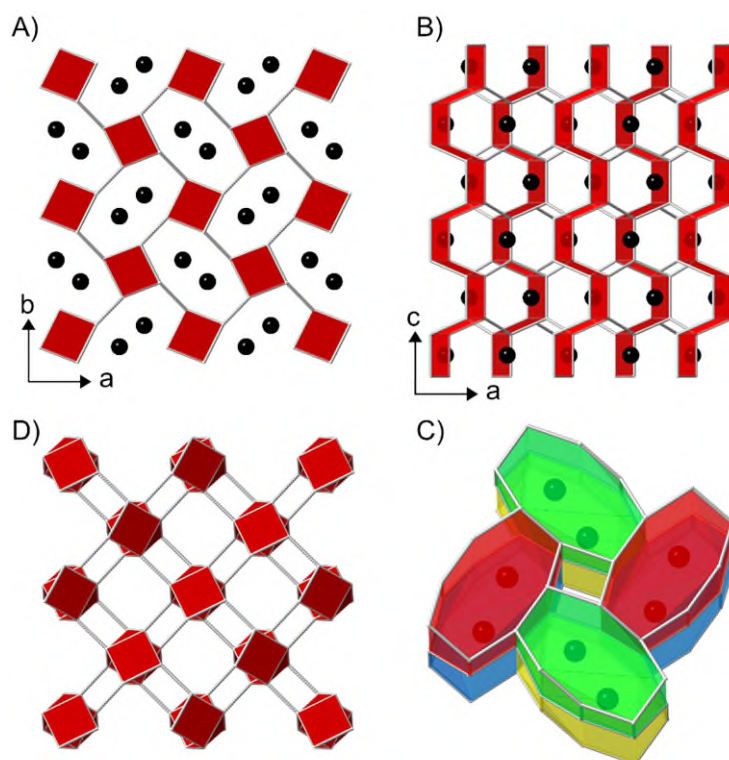
Several attempts using the search-match software HighScorePlus combined with the PDF4+ database (Kabekkodu, 2018) did not result in an identification of the phase. Because the search-match routine failed, an attempt to index the observed powder pattern was performed. Indexing and subsequent LeBail fitting (Coelho, 2018) revealed an orthorhombic unit cell, with the dimensions  $a = 9.198(2) \text{ \AA}$ ,  $b = 9.476(2) \text{ \AA}$  and  $c = 8.593(2) \text{ \AA}$ . The orthorhombic symmetry is also consistent with the morphology observed in the SEM images (see Figure 1). A search of the ICSD database (Hellenbrandt, 2014) using the observed lattice parameters with a 2% tolerance resulted in a match with four different published structures of paracelsian. This is a feldspar mineral with the composition  $\text{BaAl}_2\text{Si}_2\text{O}_8$  and a structure consisting of a three-dimensional framework of corner sharing  $\text{SiO}_4$  and  $\text{AlO}_4$  tetrahedra, and  $\text{Ba}^{2+}$  cations filling interstitial sites. Because of the match in unit cell dimensions and because the crystal chemistry of paracelsian is closely related to what is expected for sample 4, it is reasonable to assume that the new material is structurally closely related to paracelsian. The ionic radius of  $\text{K}^+$  is 133 pm while that of  $\text{Ba}^{2+}$  is 134 pm. It therefore makes perfectly sense that both cations are able to structurally support the same paracelsian topology, but with Si/Al ratios of 3 and 1 respectively to maintain charge neutrality.



**Figure 1** Powder x-ray diffraction pattern and SEM image (insert) of K-paracelsian. The blue curve is the observed data. The red curve is the Rietveld fit of the final structure model, and the grey curve is the difference curve.

A structure model based on the atomic arrangement from orthorhombic (Pnam) paracelsian (Smith, 1953) including the coupled substitution  $\text{Ba}^{2+} + \text{Al}^{3+} \rightarrow \text{K}^+ + \text{Si}^{4+}$  was therefore constructed. A subsequent Rietveld refinement (Coelho, 2018) using fixed atomic positions and fixed occupancies resulted in a good fit, confirming that the new material has the same framework topology as paracelsian. In the final step of Rietveld analysis, the fractional coordinates of all atoms and the occupancy of K were

refined, resulting in an excellent fit (Figure 1), and in chemical meaningful bond distances and angles (See Figure 2A-C and the attached Cif file). The refined occupancy of K is 0.98(1), which is very close to the initially assumed value of 1 for the stoichiometric compound  $\text{KAlSi}_3\text{O}_8$ . The name K-paracelsian is proposed for the new material.



**Figure 2 Framework topology of K-paracelsian and a related feldspar represented by connected T-sites. (A and B) Topology of K-paracelsian. Red planes have been used to emphasis the double-crankshaft chains, and black spheres represent potassium positions. The structure is shown in projection parallel and perpendicular to the double-crankshaft chains respectively. (C) K-paracelsian cages occupied by potassium atoms. All cages are equivalent by space group symmetry ( $Pnam$ ). Colours have been added to emphasis individual cages. (D) Framework topology of the feldspar mineral microcline in projection parallel to the twisted double-crankshaft chains.**

The framework topology of common feldspars like orthoclase, albite and microcline and most other feldspars consist of twisted interconnected double crankshaft chains as shown in figure 2D. In contrast, the paracelsian topology consist entirely of straight interconnected double crankshaft chains, which is also observed in many zeolite topologies like GIS, APC, MER, PHI, SIV and GME (Baerlocher & McCusker, 2018). The question we want to address next is whether K-paracelsian should be considered a feldspar or a zeolite.

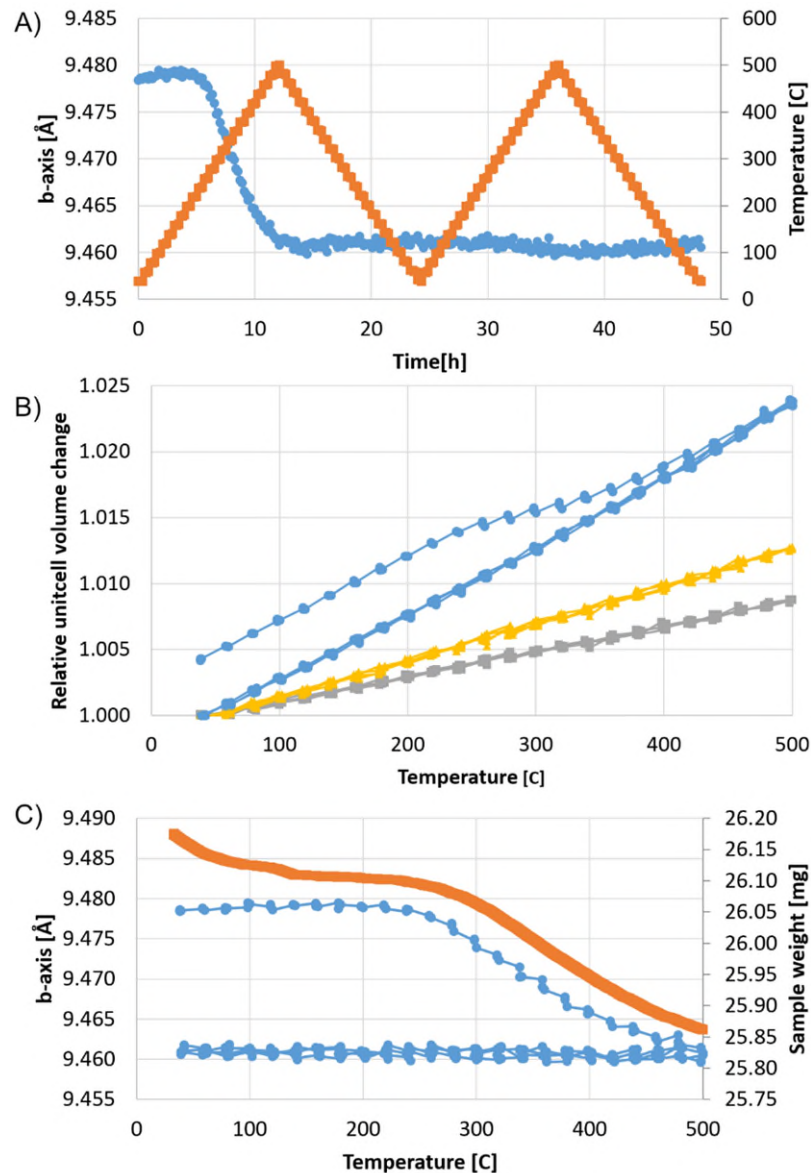
Feldspar and zeolite topologies consist of corner connected  $\text{SiO}_4$  and  $\text{AlO}_4$  tetrahedra, forming a periodic three-dimensional structure. Feldspar topologies are made entirely of 4, 6 and 8-rings of connected tetrahedra. Some small pore zeolites like GIS, APC, MER, PHI, SIV are also constructed entirely from 4, 6 and 8-rings resulting in cages and channels of similar sizes as those observed in

feldspars. In this respect, feldspars could be considered small pore zeolites. Water content is another property used to define the difference between feldspars and zeolites (Barrer, 1982). Feldspars are anhydrous while zeolites are hydrous. From zeolites it is well known that water can escape along the zeolite channels when heated, resulting in a significant change in the observed lattice parameters. For anhydrous feldspars it is only expected to observe changes in lattice parameters that are consistent with the thermal expansion properties of the material. *In situ* XRD heating experiments were therefore performed on K-paracelsian and a reference feldspar material.

### 3.3. Comparison with isocompositional microcline

A fragment of microcline from a graphic granite collected in Setesdalen in Norway was used as a reference for the isocompositional K-paracelsian. Both samples were heated in air from room temperature to 500 °C in steps of 20 °C with a rate of 40 °C/h and cooled to room temperature using a symmetric ramp. XRD data were measured at each step. This heat treatment was repeated twice for each sample (Figure 3A, orange data points). Analysis of the microcline data revealed the sample was composed of 83 wt. % microcline and 17 % albite. Both feldspars show a simple linear relationship with temperature variations and a fully reversible behavior on the four temperature ramps as shown in figure 3B. These observations are fully consistent with simple thermal expansion and contraction.

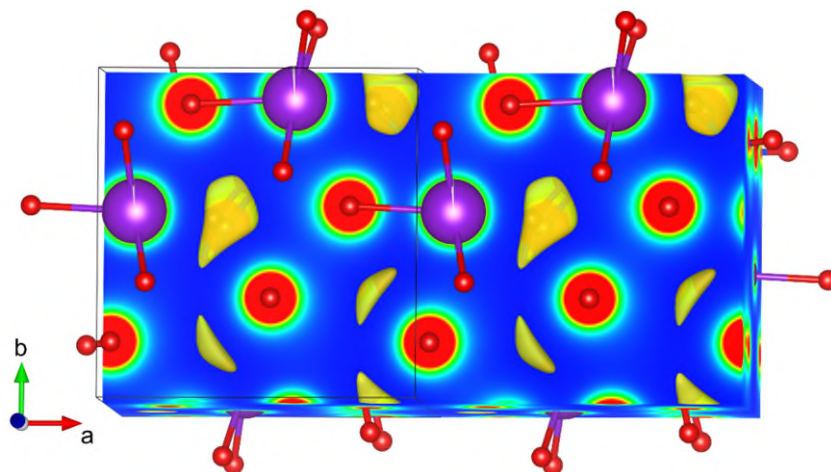
K-paracelsian however, shows a clear non-linear unit cell evolution in the temperature range 250 °C to 450 °C on the first heating ramp (Figure 3A and B). On the following three ramps, K-paracelsian shows a linear and reversible lattice change similar to that observed in the anhydrous feldspars (Figure 3B). The observed thermal expansion is dominated by the strong temperature dependence of the a- and c-parameters, while the b-parameter shows almost no temperature dependence on the last three ramps (Figure 3A). The data from the TGA experiment shows a relative mass loss of 5.7 wt. % in the temperature range 250 °C to 450 °C where the non-linear unit cell evolution was observed (Figure 3C). The heat-treated K-paracelsian sample was reanalyzed at room temperature after 4 weeks of exposure to air. The observed lattice parameters were consistent with those of the dehydrated K-paracelsian, indicating that dehydration is not reversible at ambient conditions.



**Figure 3** Observed changes in K-paracelsian during two cycles of heating. **(A)** Evolution of the b-axis (blue) during the temperature program shown in orange. **(B)** Relative changes in unit cell volume of K-paracelsian (blue) and the reference feldspars (yellow - albite and grey - microcline). **(C)** Observed sample weight during TGA experiment (orange) plotted together with observed b-axis variations (blue) from the *in situ* XRD experiment.

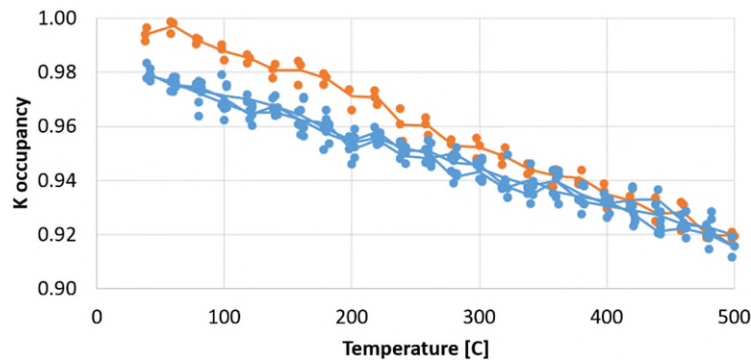
Normal zeolite dehydration behavior, as observed in Chabazite and Faujasite, consist of an initial step gradual weight loss initiated slightly above room temperature and continuing up to 200 °C where at least 90 % of the water have been evaporated. Most of the remaining water will have been evaporated by 400 °C. In contrast to Chabazite and Faujasite the zeolite Natrolite ( $\text{Na}_2\text{Al}_2\text{Si}_3\text{O}_{10} \cdot 2\text{H}_2\text{O}$ ) shows very little weight loss at temperatures up to 250 °C, followed by a steep weight loss of 10 % consistent with a loss of both water molecules (Gottardi & Galli, 1985; van Reeuwijk, 1974). In contrast to most other zeolites all water molecules in Natrolite are located in relatively well-defined positions within the first coordination shell of Na, where they complete a 6-fold coordination shell with a slightly distorted trigonal prism geometry (Meier, 1960).

The dehydration behavior of K-paracelsian is very similar to that of Natrolite, with a weight loss consistent with one water molecule per cage ( $\text{KAlSi}_3\text{O}_8 \cdot \text{H}_2\text{O}$ ). Inspection of the calculated independent atom model (IAM) electron density, as shown in figure 4, reveals a minimum in the density at the position where a water molecule would complete an octahedral coordination of the six oxygen atoms closest to K.



**Figure 4** Calculated independent atom model electron density (Momma & Izumi, 2011) of the K-paracelsian structure. Yellow areas illustrate positions in the cage with minimum electron density.

Inspection of the observed XRD data of the as-synthesized sample did not reveal significant amounts of residual electron density in this position, indicating a more disordered nature of the  $\text{H}_2\text{O}$  positions. The evolution of the K occupancy as a function of temperature is shown in figure 5. The overall apparent temperature dependence of the K occupancy, is an artefact caused by correlation with the thermal parameters. The relative decrease observed on the first heating ramp between 200 °C and 400 °C is reliable and shows that a small fraction of the electron density inside the cages is disappearing at this stage. This observation could be consistent with a water molecule disappearing from the first coordination shell of K, or it could be consistent with an interpretation where a few percent of K ions are missing leaving space available to be occupied by water molecules. The data are not conclusive on this issue.

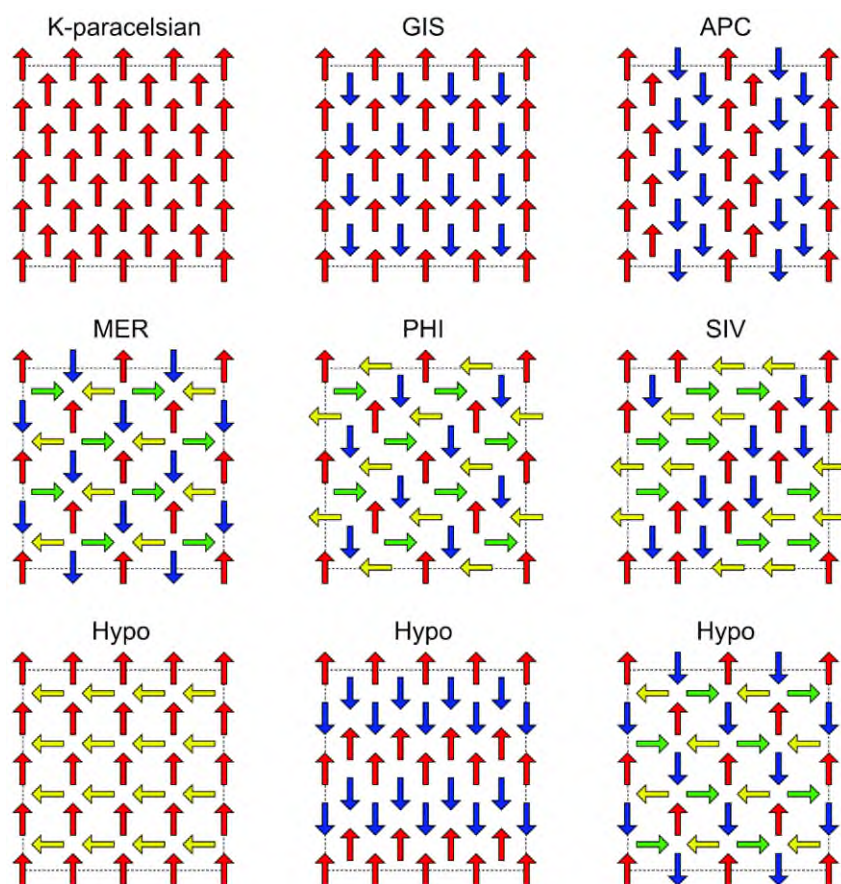


**Figure 5 Refined K-occupancies as a function of temperature. Orange points have been collected on the first heating ramp.**

#### **4. Identification of a simple building scheme of dense double-crankshaft zeolite topologies**

The topology of K-paracelsian is closely related to the known zeolite topologies GIS, APC, MER, PHI and SIV. These topologies can all be constructed by double crankshaft motifs placed in a lattice as shown in Figure 6. The only difference between these topologies is the relative rotational orientation of individual double crankshaft chains. GME is another topology which can be constructed entirely of double crankshaft motifs. But in this case the motifs are arranged in an open hexagonal lattice leading to larger cages and a less dense topology. The building scheme presented in figure 6 defines a family of dense double-crankshaft zeolite topologies, six of which has now been realized. This family consist of topologies with 4-, 6- and 8-rings and have 8-ring channel systems that range from 1-dimensional (K-paracelsian) to 2-dimensional (APC) to 3-dimensional (GIS, MER, PHI, SIV). A large number of hypothetical topologies can be constructed using the building scheme presented in figure 6, where three of them have been shown. There are many approaches to constructing hypothetical zeolite topologies, some of which involve elaborate computational methods (Deem, *et al.*, 2009). Many of these hypothetical topologies may not be possible to realize in practice, because they are thermodynamically unstable. It is worth noticing that by applying the above described building scheme the resulting topologies will be crystallo-chemically healthy, in the sense that they all have very similar stabilization energies including the topologies that have already been realized (GIS, APC, MER, PHI and SIV).





**Figure 6** Schematic drawing of the building scheme used to construct the zeolite topologies in the family of dense double-crankshaft topologies. Each arrow represents a double crankshaft chain as seen in projection along the chain direction, and the direction of the arrow indicate the relative rotational orientation. There is only one physical meaningful solution to the connectivity between double crankshaft chains for each of the schematic drawings, resulting in the final topology. Colors have been applied for visual emphasis of symmetry.

## 5. Conclusions

K-paracelsian was discovered while screening the hydrothermal phase space using potassium hydroxide in combination with 1-methyl-4-aza-1-azoniabicyclo[2.2.2]octane hydroxide (1-methyl-DABCO) and the use of a FAU zeolite as the source of Si and Al. The novel synthesized aluminosilicate is compositionally closely related to the mineral microcline and structurally closely related to the mineral paracelsian. Both are part of the feldspar group. In contrast to the feldspars, the new material, shows intrazeolitic molecular water, which is possible to extract upon heating. This suggests that K-paracelsian could be considered a link between feldspars and zeolites.

We furthermore show that K-paracelsian is the simplest endmember of a family of dense double-crankshaft zeolite topologies. By applying the identified building principle, a number of known zeolite topologies can be constructed. It furthermore allows us to construct a range of hypothetical small pore topologies that are crystallo-chemically healthy and potentially industrially relevant, which could be realized in the future.



**Acknowledgements** The authors thank Haldor Topsoe A/S and Innovation Fund Denmark for financial support under the Industrial PhD program (Case no. 1355-0174B).

## References

- Baerlocher, C. & McCusker, L. B. (2018). *Database of Zeolite Structures* <http://www.iza-structure.org/databases/>.
- Barrer, R. M. (1982). *Hydrothermal Chemistry of Zeolites*. Academic Press.
- Coelho, A. A. (2018). *J. Appl. Cryst.* **51**, 210–218.
- Corma, A. (1995). *Chem. Rev.* **95**, 559–614.
- Davis, M. E. (2002). *Nature*, **417**, 813–821.
- Deem, M. W., Pophale, R., Cheeseman, P. A., Earl, D. J. (2009). *J. Phys. Chem. C*, **113**, 21353–21360.
- Gottardi G. & Galli, E. (1985). *Natural Zeolites*. Springer-Verlag.
- ICDD PDF-4+ International Centre for Diffraction Data* (2018). edited by S. Kabekkodu, Newtown Square, PA, USA.
- Meier, W. M. (1960). *Z. Kristallogr.* **113**, 430–444.
- Momma, K. & Izumi, F. (2011). *J. Appl. Cryst.* **44**, 1272–1276.
- Sieber, W. & Meier, W. M. (1974). *Helv. Chim Acta.* **57**, 1533–1549.
- Smith, J. V. (1953). *Acta Cryst.* **6**, 613–620.
- van Reeuwijk, L. P. (1974). PhD thesis, Agricultural University, Wageningen, The Netherlands.
- Xie, D., McCusker, L. B., Baerlocher, C., Zones, S. I., Wan, W., Zou, X. (2013). *J. Am. Chem. Soc.* **135**, 10519–10524.

## Paper 3

The manuscript attached below represents the author's version of the article:

Cristian-R. Boruntea, German Sastre, Lars F. Lundegaard, Avelino Corma, Peter N. R. Vennestrøm, Synthesis of High-Silica Erionite Driven by Computational Screening of Hypothetical Zeolites. Just accepted for publication in Chemistry of Materials, October 25, 2019.

This paper is exploring the synthesis of a high-Si ERI-type zeolite as the result of an attempt to synthesize a target hypothetical structure for specific applications (e.g. exhaust gas and MTO catalysis). The hypothetical framework, labelled Hypo#1, have been selected based on the structural features of the state-of-the-art small-pore zeolites for DeNO<sub>x</sub> applications as described in Part 1, Chapter 2. A computational energy-based approach was applied that targets large values of OSDA-zeolite stabilization energies, leading to the selection of three new OSDAs as potential candidates for the synthesis of Hypo#1 zeolite. Although the target hypothetical structure Hypo#1 was not able to be prepared, the product diagram is dominated by a novel high-Si ERI-type zeolite. The obtained material has a distinct particle morphology, small crystallites and a tubular to prismatic crystal morphology which is expected to have an important impact on its catalytic applications.

# Synthesis of high-silica ERI driven by computational screening of hypothetical zeolites

Cristian-R. Boruntea<sup>a,b</sup>, German Sastre<sup>b</sup>, Lars F. Lundegaard<sup>a</sup>, Avelino Corma<sup>b \*</sup>, Peter N. R. Vennestrom<sup>c \*</sup>

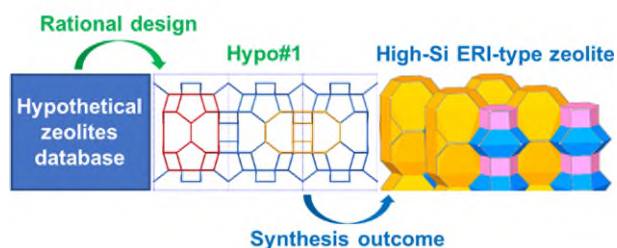
<sup>a</sup> Haldor Topsøe A/S, Haldor Topsøes Alle 1, DK-2800 Kgs. Lyngby, Denmark

<sup>b</sup> Instituto de Tecnología Química, Universitat Politècnica de València-Consejo Superior de Investigaciones Científicas, Avenida de los Naranjos s/n, 46022 Valencia, España

<sup>c</sup> Umicore Denmark ApS, Nøjsomhedsvej 20, DK-2800 Kgs. Lyngby, Denmark

\*Corresponding Author, Email: [acorma@itq.upv.es](mailto:acorma@itq.upv.es); [peter.vennestrom@eu.unicore.com](mailto:peter.vennestrom@eu.unicore.com)

## Abstract



A hypothetical zeolite framework was selected from a database of hypothetical structures and adapted based on structural features relevant for deNO<sub>x</sub> and MTO catalysis. To attempt the realization of this structure a computational energy-based approach was applied to select relevant OSDAs (organic structure directing agents) molecules with large OSDA-zeolite stabilization energies, leading to the selection of three OSDAs (OSDA1, OSDA2, OSDA3) as potential candidates for the synthesis of the hypothetical zeolite (Hypo#1). Instead of Hypo#1, ERI was found to dominate the experimental product outcome when potassium was used as a mineralizing agent. In the case of OSDA3 a novel high-silica ERI was found. The different ERI products were characterized, intergrowth structures ruled out, and special attention was paid to the compositional and morphological features arising from the use of the different OSDAs. In the specific high-Si product obtained using OSDA3 a distinct tubular to prismatic crystal morphology could be seen. Theoretical stabilization energies calculated for potentially competing phases (Hypo#1, ERI, OFF, CHA among others) could be used to rationalize the experimental outcome to a certain extent, but our results show that considering the zeolite-OSDA interaction is probably not sufficient to realize hypothetical frameworks alone, especially for Al-containing zeolites where alkali ions play an important role during crystallization.

## 1. Introduction

Zeolites are crystalline microporous aluminosilicate materials composed of tetrahedrally coordinated T-atoms (typically Si and Al), linked together by oxygen bridges. For each tetrahedron with a trivalent element, such as  $[\text{AlO}_4]^-$ , a negative charge is introduced into the framework that is counterbalanced by a cation. The different ways in which corner connected  $\text{SiO}_4/2$  and  $\text{AlO}_4/2$  tetrahedra are joined together, gives rise to channels, cavities and interconnected voids. The combination of the uniform pore dimensions, ion exchange properties and/or internal acidity combined with thermal stability gives rise to a large number of catalytic applications (1), (2). The development of zeolites as catalyst has historically followed two main tracks namely by: i) exploring known topologies with different compositions, such as Si/Al ratios, heteroatom substitution, and presence of non-framework cations; and ii) discovery of novel topologies with new pore systems, cavity sizes and local coordination environments.

Compositionally, the Si/Al ratio is one of the most important parameters that influence zeolite stability and have a direct impact on the catalytic activity. Typically, Si-rich zeolites show improved stability compared to their Al-rich analogs. Contrarily, the amount of aluminum is typically related to the catalytic activity of the zeolite materials and a tradeoff between activity and structural stability is commonly encountered. For many catalytic applications, intermediate (Si/Al = ca. 4-10) to high-silica (Si/Al > 10) zeolites are preferred. For this reason, the impact of preparing or discovering novel zeolites becomes much higher when the compositional range can be extended into the intermediate and high-silica range.

Most novel zeolite framework types are discovered through a trial-and-error approach using various families of OSDAs (organic structure directing agents) and chemical intuition. Recently, new rational methods have been proposed for enlarging the list of catalytically relevant zeolite frameworks, by either employing computational methods or by using different synthesis procedures (3), (4), (5), (6), (7). An ab initio zeolite synthesis methodology for targeted applications has also recently been proposed where the OSDAs is chosen to mimic the transition state of a specific reaction following a molecular-recognition pattern (8), (9). Although several databases of hypothetical frameworks have been proposed (10), (11), (12), (13) their practical preparation remains an open question due to the poor understanding of nucleation and crystallization mechanisms. Even if considerable advancement has been made in finding novel OSDAs by computer modeling for already made zeolites (14), (15) this approach seems to be less successful when hypothetical frameworks are targeted.

In this study we explore a rational approach for the preparation of novel zeolite materials, and in this case, targeted towards small-pore zeolite applications such as deNO<sub>x</sub> or MTO reactions. First, we search for hypothetical frameworks, by imposing certain framework descriptors on a hypothetical zeolite database, followed by finding suitable OSDAs for the selected framework. By experimentally using the computationally predicted OSDAs under hydrothermal conditions, we noticed that another zeolite emerged, namely a novel high-silica version of the ERI framework that competes favorably with the desired hypothetical structure. Results herein are rationalized by considering theoretical

stabilization energies between different OSDAs, where the synthesis of other possible competing zeolite frameworks are studied for comparison.

## 2. Experimental

### 2.1. Computational models and methods

A framework selection was made from the hypothetical silver database developed by Foster and Treacy (10), (11) containing frameworks with maximum 6 different T-atoms giving a total of 933611 structures, although a large number can be initially discarded by having too high energy ( $>30$  kJ/SiO<sub>2</sub>) leading to 16317 structures from which approximately 50% contain 3-rings and can thus also be discarded. The selection was made using the zeoTsites code (16) imposing various criteria believed to be particularly relevant for small-pore catalytic applications (as described in the Results), this leading to the choice of a hypothetical zeolite that we named Hypo#1 herein. To find suited OSDAs for this hypothetical zeolite, we initially considered OSDAs for cages similar in size and configuration as the *hypo#1* cage. Two overall OSDA families were selected. One family was based on a central flexible alkyl chain and another family was based on a rigid aromatic or aliphatic ring. A number of manual permutations were then considered by introducing substituents and/or functional groups to the primitive structures. The stabilization energy was calculated by applying a molecular docking approach using the COMPASS2 and UFF forcefields available in Materials Studio 8.0 (17). Finally three OSDAs were selected for experimental screening.

A detailed analysis of the stabilization of selected OSDAs together with selected frameworks was later carried out in a similar manner as earlier studies (18), (19). In general, only the zeolite-OSDA van der Waals interaction was taken into account for addressing feasibility. Atomic charges were assigned in the OSDA molecules with the restraint of giving an overall neutral charge. This leads to the simplification of considering only the pure silica framework composition and hence the location of Al and its preferential interaction with the positive charge of the OSDAs is neglected. We reckon this is a simplification given the important role of the Al location, as recently demonstrated in computational studies (20), (21). Our computational approach relates better to systems without Al (pure silica zeolites), but has allowed us to neglect the presence of the counteranion of the OSDA. In fluoride media the counteranion (F<sup>-</sup>) can be modelled accurately, but in OH<sup>-</sup> media defects are often difficult to introduce in a computational model since they are not easy to characterize. In spite of simplifications, models can be very successful if they capture the main interactions at play. This is the case of recent work in cage based zeolites, where the zeolite-OSDA van der Waals interactions play a dominant role and the synthesis is driven towards the zeolite corresponding to larger zeolite-OSDA van der Waals interactions (22), (23). For instance, tetramethylammonium was shown to favor the *gme* cage while bisdiazabicyclooctane derivatives favored *aft* and *t-sfw* cages, present in zeolites with AFX and SFW topologies.

For the calculation of the energies, four force fields were considered, dealing with the zeolite, OSDA, zeolite-OSDA and OSDA-OSDA interactions. As said above, the simplification of not

considering the Al location leads us to simulate neutralised OSDA molecules (with zero total charge but atomic charges different from zero) and, as a consequence the usual cation-cation OSDA-OSDA repulsion is not properly accounted for in our simplified description. Our approach, although including both electrostatic and van der Waals OSDA-OSDA interactions, underestimate the electrostatic OSDA-OSDA repulsion. Because of this, the resulting OSDA-OSDA term is not relevant, and therefore is not included in the discussion. For the zeolite, the recently parameterized rigid-ion force field for silico-alumino-phosphate zeotypes was employed (24), which for the pure silica case is equivalent to a former, less general, parameterization (25). For the zeolite-OSDA, the force field by Catlow *et al.* (26) was employed, for the OSDA-OSDA interaction, the all-atom OPLS force field (27) was used, and for the internal OSDA the forcefield by Oie *et al.* (28) was used. One unit cell of zeolite was considered in each case.

In a first set of calculations (set A in Table 2), one molecule of OSDA was introduced and geometry optimized taking into account all the coordinates and cell parameters, as well as all the energetic terms including the electrostatic part through the Ewald summation. The cutoff chosen for the van der Waals interactions was 12 Å. From the optimized geometry, it was possible to find the micropores where the OSDA molecules remain occluded in their lowest energy configuration (Table S1). Then, with the optimized geometry, a single point energy calculation was performed to extract the contribution of the van der Waals zeolite-OSDA energy corresponding to one cavity (A values in Table 2). 'A' values are important since they reflect the contribution of a single zeolite-OSDA interaction and allow you to compare the fit of a single OSDA molecule between various frameworks and could also be related to the early stages of nucleation.

A second set of calculations (set B in Table 2) was performed by filling all cavities and channels with OSDA molecules until the micropore system is fully packed with OSDA molecules, which is typically the situation experimentally found in the synthesis of zeolites. The full van der Waals zeolite-OSDA energy is then divided by the number of SiO<sub>2</sub> units in the unit cell (B values in Table 2), which allows to extract conclusions about the final system. The B-values are considerable smaller than the A-values by being divided by the number of SiO<sub>2</sub> units in the cell, which allows comparisons between different OSDAs for a given zeolite (vertical comparison in Table 2) and also for a given OSDA with different zeolites (horizontal comparison in Table 2).

In summary, both 'set A' and 'set B' calculations represent zeo-OSDA van der Waals interaction energies. The difference is that 'set A' correspond to only one OSDA molecule per unit cell and the value given is the energy per OSDA molecule, while in the case of 'set B' the unit cell has been saturated with OSDA molecules, and the value given is the zeo-OSDA van der Waals energy of all OSDA molecules divided by the number of SiO<sub>2</sub> in the unit cell. All energy minimizations have been carried out allowing the full relaxation of all the atoms in the system as well as the cell parameters using the BFGS (Broyden-Fletcher-Goldfarb-Shanno) (29), (30), (31), (32) within the GULP software (33), (34).

## 2.2. Hydrothermal synthesis

For the attempt to synthesize the Hypo#1 zeolite, three different approaches were followed. Each OSDA (OSDA1-3) was explored in alkaline conditions with KOH (set 1) and NaOH (set 2) by using either a FAU zeolite or co-precipitated amorphous-silica-alumina (ASA) as the T-atom source. Additionally, fluoride conditions were also applied with TEOS and Aluminum isopropoxide as the source of T-atom (set 3). In a typical synthesis using FAU as the T-atom source and OSDA 3, a mixture of 1.99 g cyclohexane-1,4-bis(trimethylammonium) dihydroxide (12.7 wt. % aqueous solution), 1.81 g KOH (10 wt. % aqueous solution), 0.45 g distilled water and 0.74 g FAU zeolite (Si/Al = 15) was prepared. The gel was mixed 1 h at room temperature and was transferred to a Teflon lined autoclave and heated at 135 °C for 7 days and the solid product separated by filtration and washing with deionized water. Crystallization was carried out at 135 °C for seven days unless otherwise stated.. The raw materials used were: butane-1,4-bis(trimethylammonium) dihydroxide (OSDA1), pentane-1,4-bis(trimethylammonium) dihydroxide (OSDA2), cyclohexane-1,4-bis(trimethylammonium) dihydroxide (OSDA3), KOH (reagent grade  $\geq 98\%$ , Sigma Aldrich), Y-zeolite (CBV712, CBV720, CBV760 obtained from Zeolyst International), ASA (amorphous-silica-alumina) (Si/Al = 6, Si/Al = 15 and Si/Al = 30) prepared in-house. Detailed synthesis procedures for OSDAs can be found in the Supporting Information.

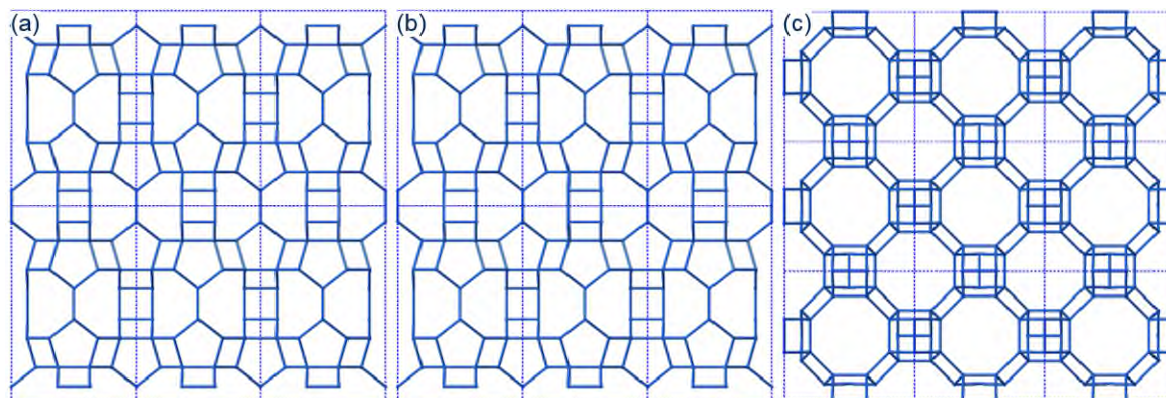
## 2.3. Characterization

The resulting zeolite materials were analyzed in the as-synthesized form by X-ray diffraction using a Phillips PW1800 instrument system in  $\theta$ - $2\theta$  geometry working in reflectance mode using  $\text{CuK}\alpha$  radiation ( $\lambda = 1.541 \text{ \AA}$ ). SEM images were recorded using an XL30-SEM instrument operated at 10 kV. The samples were sprinkled over carbon tape and attached on Al-stubs and then coated with a ca. 30 nm layer of carbon to prevent charging. TGA-DSC analysis were performed using a Mettler TGA-DSC instrument with a heating rate of 5 °C / min and the temperature limit at 550 °C. Product composition was determined using inductively coupled plasma optical emission spectroscopy (ICPOES) on acid digested samples using a Perkin Elmer Optima 7300 DV instrument. The  $^{27}\text{Al}$  MAS NMR spectra were recorded using a Bruker Avance II HD 400 Mhz instrument at spinning rate of 20 kHz in a Bruker 3.2 mm probe, using a flip angle of  $\pi/12$  and a recycle delay of 1 s. The  $^{29}\text{Si}$  MAS NMR spectra were recorded at spinning rate of 5 kHz in Bruker 4 mm probe, using a flip angle of  $60^\circ$  and a recycle delay of 60 s.

## 3. Results and Discussion

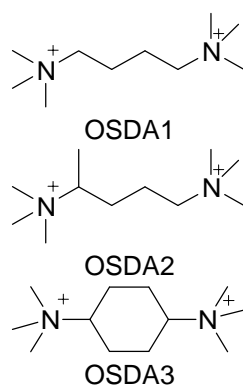
A first selection of small-pore frameworks was carried out by imposing an energy requirement that refines only structures with energies lower than (or equal to) 0.15 eV in combination with an 8-ring window requirement. The selection was further limited to 3-dimensional channel systems, only having 4, 5, 6 and 8-rings present in the structure, as well as minimum 80 % of the 8-rings to be circular. Furthermore, the selected structures were also limited to satisfy feasibility criteria reported elsewhere

(35), (36). One framework was selected (entry 139\_4\_48475) containing 4 T-atoms and 128 SiO<sub>2</sub> per unit cell. The structure was then modified manually to a simpler structure with less cage diversity. The outcome, named Hypo#1 herein, contain two different T-atoms (with a multiplicity of 32 and 16) and a total of 48 T-atoms (SiO<sub>2</sub> units) per unit cell (see file generated by zeoTsites in the SI). Figure 1 shows the framework structure of Hypo#1, seen along the a, b and c directions.



**Figure 1 Framework structure of Hypo#1 zeolite seen along a, b and c direction (blue ribbons represent Si-Si connections. O atoms are omitted for simplicity).**

As a starting point OSDA candidates were selected based on molecules known to stabilize similar sized cages in zeolites where-after an iterative process of manual permutations of substituents was applied. A final selection of three OSDAs (see Figure 2 and Table 2) was afterwards made by taking into account the feasibility of the organic synthesis procedure.



**Figure 2 OSDA candidates selected for exploration in hydrothermal synthesis.**

To evaluate the potential of the selected OSDAs an extensive experimental evaluation under various conditions and using various raw materials was undertaken. Hydrothermal synthesis was explored using OSDA1-3 under alkali conditions using either NaOH or KOH as the mineralizing agent in combination with either amorphous silica-alumina (ASA) or using a FAU zeolite as the T-atom source. The overall synthesis composition was varied through the Si/Al ratios. Furthermore, crystallization in



fluoride media using OSDA1-3 was also investigated as this approach often leads to products strongly dictated by the OSDA-zeolite interaction, especially under Si-rich conditions.

Crystallization in fluoride media revealed amorphous products together with the presence of an unknown phase (not Hypo#1 target framework) for OSDA1, independently of the reaction time. For OSDA2 and 3 a mixture of amorphous, LEV, SOD and pure silica AST was obtained as well as an unknown phase (not Hypo#1 target). The results of the synthesis are reported in the supporting information (Tables S4-S7). The combination of the three OSDAs and NaOH in general leads to products like \*BEA, amorphous or small amounts of an unknown phase (again, not the Hypo#1 target zeolite); indicating a low specificity of the OSDA-zeolite interaction in this system.

Interestingly, when the mineralizing agent is switched to KOH, we observe either amorphous products or ERI for all three OSDAs. This observation points to a strong influence of potassium on the product selectivity in combination with the stabilizing effect of the various OSDA molecules. Table 1 summarizes the products obtained from the synthesis with ASA and FAU as sole Si and Al source for the KOH system.

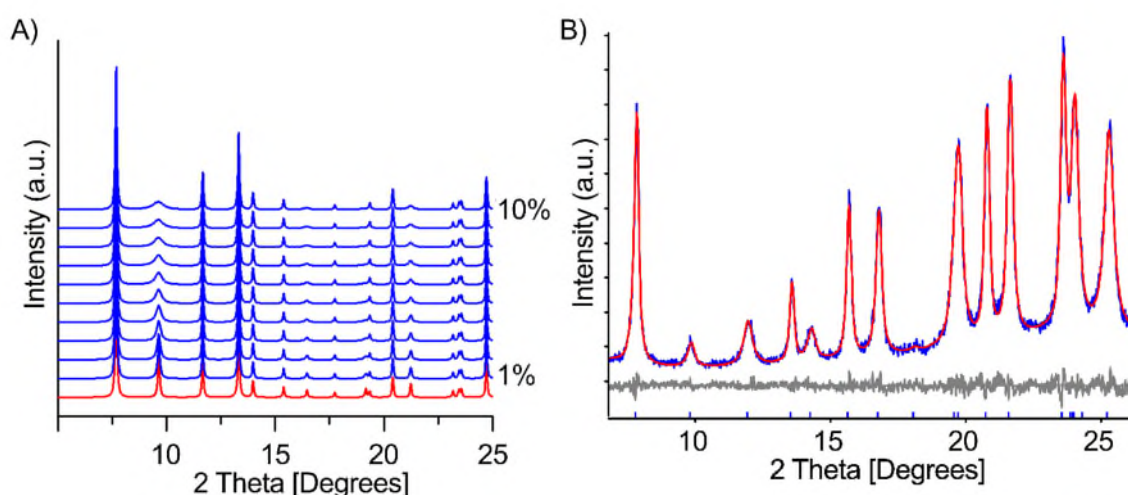
Erionite (ERI) is a well-known small-pore zeolite, that can be found in nature with a Si/Al ratio around 3 (37). It is typically seen as an intergrowth with Offretite (OFF) (38). Pure-phase ERI with higher Si/Al ratios was first reported by Hong et al. by combination of tetraethylammonium, linear diquatery ammonium ions as OSDAs and a charge density mismatch (CDM) approach (39), (40). The UZM-12 material crystallizes mainly in the presence of K<sup>+</sup> or Rb<sup>+</sup> ions and the highest Si/Al ratio achieved has been 6.5. Recently, and yet only reported in the patent literature, is the preparation of SSZ-98, a high-silica ERI molecular sieve with either rod-like or disc-shaped crystal morphologies. Using N,N'-dimethyl-1,4-diazobicyclo[2.2.2]octane as the OSDA (OSDA4, Table 2), Si/Al ratios as high as 13.5 were reported for SSZ-98 (41).

**Table 1 Products and chemical composition of selected synthesis using OSDA1, OSDA2 and OSDA3 from synthesis composition 1.0 SiO<sub>2</sub> : x Al : 0.1 OSDA : 0.3 KOH : 20 H<sub>2</sub>O crystallized for 7 days at 135°C. (x = 0.167, 0.066 and 0.033).**

Sample Number	OSDA	Si and Al-source	Product	Si/Al	K/Si
1	1	ASA (Si/Al=6)	ERI	4.4	0.11
2	1	ASA (Si/Al=15)	amorphous	-	-
3	1	FAU (Si/Al=6)	ERI	4.9	0.11
4	1	FAU (Si/Al=15)	amorphous	-	-
5	2	ASA (Si/Al=6)	ERI	-	-
6	2	ASA (Si/Al=15)	amorphous	-	-
7	2	FAU (Si/Al=6)	ERI	5.1	0.10
8	2	FAU (Si/Al=15)	amorphous	-	-
9	3	ASA (Si/Al=6)	ERI	-	-
10	3	ASA (Si/Al=15)	ERI	-	-
11	3	FAU (Si/Al=6)	ERI <sup>a</sup>	4.9	0.17
12	3	FAU (Si/Al=15)	ERI	11.0	0.11

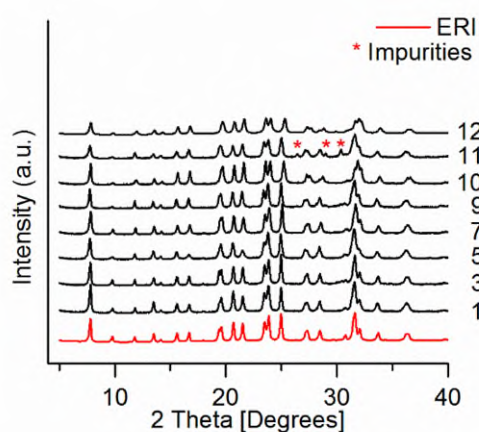
<sup>a</sup>) a minor impurity of a dense phase was detected

For all OSDAs ERI is observed at a Si/Al ratio of 6 in the synthesis gel when KOH is used. However, at higher Si/Al ratios ERI is only obtained using OSDA3. The Si/Al measured in this product is 11, which is the highest Si/Al ratio reported for ERI in the scientific literature so far. The observation that ERI is obtained even at higher Si/Al ratios using OSDA3 indicates that it does indeed provide a suitable structure directing effect for this particular framework topology.



**Figure 3 PXRD patterns of ERI. A) Simulated patterns for ERI (100 % ERI and 0 % OFF, red curve) and for ERI-OFF intergrowth (1 % OFF up to 10 % OFF, blue curves). B) Observed pattern of sample 12 (blue curve) and a model curve (Red) obtained using a LeBail model including peak shape parameters related to particle average size and shape. The grey curve is the difference between the model and the observed data.**

It is well-known that ERI typically crystallizes with intergrowths of OFF. Figure 3A shows simulated PXRD patterns for the 100 % ERI-type zeolite and for the ERI/OFF intergrowths, with various percentages of OFF (1 – 10 %). Already at low amounts of intergrowths anisotropic broadening is seen for some of the peaks with increasing amounts of intergrowth. The observed PXRD pattern of sample 12 does not show additional broadening of the peak at 9 degrees 2 theta, and therefore no indication of stacking disorder in the sample. The difference in relative peak intensities in figure 3A and 3B respectively, is mainly a result of collecting the observed data using variable divergence slits. X-ray diffraction patterns for all obtained ERI products are shown in Figure 4. Only small differences are seen within the synthesized samples, and XRD peak broadening features related to intergrowth with OFF are not observed in any of the presented data.



**Figure 4** PXRD patterns of as-synthesized ERI-type zeolite products using OSDA1 (samples 1 and 3), OSDA2 (sample 5 and 7) and OSDA3 (samples 9, 10, 11, 12). The bottom red pattern shows the calculated pattern for ERI.

ERI is obtained from both amorphous starting materials and the crystalline FAU. Indicating that the reactivity or dissolution rate of the starting material may not be critical for the achievement of ERI as it was observed e.g. for AEI and AFX 0. Synthesis of intermediate-silica (Si/Al = 6.5, UZM-12) ERI using OSDA1 has so far only been reported using the CDM-approach. Whether the use of co-precipitated silica-alumina provides an analogous starting point as the initial precipitation of CDM-gels is unclear, but some similarity in reactivity could exist.

In all cases potassium is seen in the final product. A molar K/Si ratio of 0.11 and Si/Al ratios between 4.4 and 11 corresponds to approximately 3.2-3.6 K per unit cell that contains 2 *can* cages, so it is reasonable to assume that most of the *can* cages are occupied by K<sup>+</sup> ions and perhaps some K<sup>+</sup> is also located in the larger *eri* cages or double-six ring structures also contained in the ERI framework. By comparison of <sup>13</sup>C CP-MAS NMR of the solid product with <sup>13</sup>C-NMR of the OSDA in solution before use (see Figure S2) we find that the OSDAs remain intact throughout the crystallization and are indeed successfully occluded within the cavities of the ERI materials. From TGA analysis of OSDA3

combustion, a weight loss of 21.2% was measured (see Figure S1), which correspond to 3.1 molecules per unit cell or 1.0 OSDA molecules per *eri* cage, whereas this number is lower for OSDA1 and 2. Altogether this points towards the efficient use of the OSDA molecules with approximately one OSDA molecule per *eri* cage and K located both in the *can* and *eri* cages, especially for OSDA3.

The  $^{29}\text{Si}$  MAS NMR measurements for sample 12 (Figure 5a) reveal 3 distinctive peaks that have been assigned to Si(0Al), Si(1Al), Si(2Al) and a broad signal which was assigned to Si(3Al). Deconvolution and calculation of the Si/Al ratio (10) is in good agreement with that measured from ICP (11). The  $^{27}\text{Al}$  MAS NMR spectrum for ERI-type zeolites corresponding to sample 12 (Figure 5b) shows that all the aluminum is located in framework positions with tetrahedral coordination ( $\text{Al}^{\text{IV}}$ ) (peak at approx. 60 ppm).

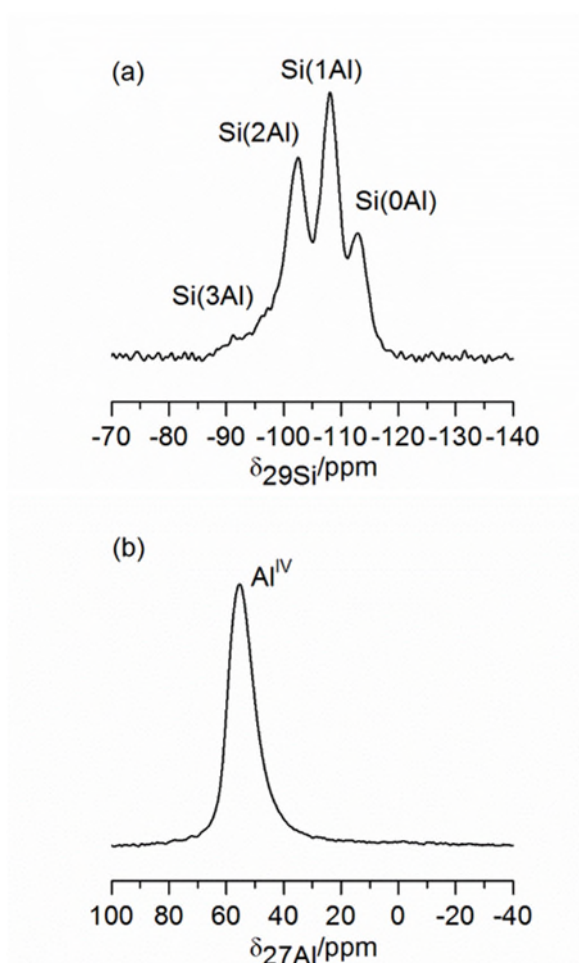
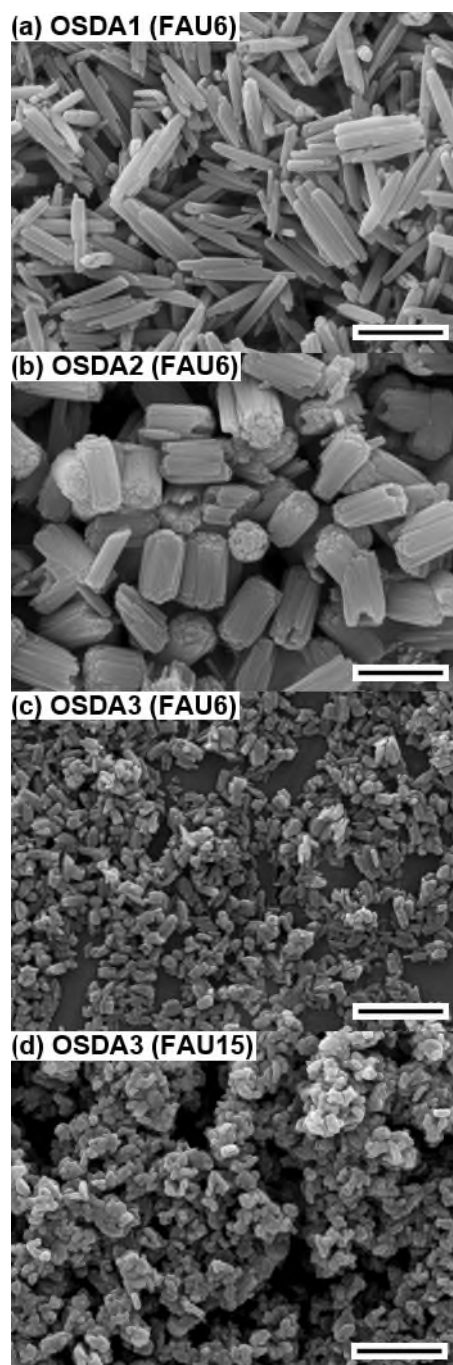


Figure 5  $^{29}\text{Si}$  (a) and  $^{27}\text{Al}$  MAS NMR (b) spectra of ERI-type zeolites corresponding to sample 12.



**Figure 6 SEM images of ERI materials corresponding to samples 3, 7, 11 and 12 respectively, synthesized using FAU as the Si- and Al-source. Scale bars in the images correspond to 1  $\mu\text{m}$ .**

SEM images of the ERI products show various crystal morphologies. For OSDA1 needles or rods are obtained, whereas for OSDA2 shorter and grouped parallel fibers are seen. OSDA3 gives slightly irregular, in this case smaller, crystallites, with tabular to prismatic crystal morphologies.

Recently, the influence of the particle morphologies on the performance of the zeolite catalysts has led to important findings. For example Teketel *et. al.* (43) observed that for the MFS (ZSM-57) particles with a platelet morphology a resistance towards deactivation for the (methanol-to-

hydrocarbons) MTH reaction is seen, compared with the SZR (SUZ-4) needle-like crystals, where a rapid deactivation is noticed. Another example is the study made by Lukaszuk *et. al.* which correlated the product shape selectivity for the MTH reaction with four distinct particle morphologies for OFF-type zeolites (44). As the SEM images in Figure 6 show, control of the morphology can be achieved for ERI by selection of the OSDA, which besides the Si/Al ratio will allow one to modify the catalytic behavior.

### 3.1. General considerations in the preparation of Hypo#1 and ERI zeolites

To rationalize the experimental results obtained, a thorough investigation of the calculated stabilization energies of the OSDAs with the Hypo#1, ERI and various known impurity phases was carried out. The OSDAs considered for the synthesis of Hypo#1 are summarized in Table 2. As described earlier, the main experimental phase observed from the various OSDAs was ERI with no evidence of Hypo#1. CHA and LTL frameworks are also well known impurities during synthesis of ERI zeolites (45) and dense phases such as e.g. PHI, SOD, GIS can also appear. For comparison we have also included the reported OSDA (OSDA4) for SSZ-98, which also experimentally gives the high-Si ERI.

The A values in Table 2 correspond to energies that can be compared across different zeolites for the same OSDA (horizontal comparison in Table 2), but they should not be taken as giving the most stable zeolite system since only one cavity in the unit cell (and not the full micropore system) is considered. B values on the other hand take into account an optimum full loading and thus provides a more realistic prediction of synthesis feasibility. One should be cautious in comparing B-values only as OSDA-OSDA interactions will also be reflected in this number, which is the case when more than one OSDA occupies each cavity. Each set of values is complementary and both should be considered when addressing the stabilization of a framework.

From the theoretical stabilization energies reported in Table 2 (A values) the selected OSDAs *should* favor Hypo#1 and ERI. This indicates that there is a good fit between the OSDAs and the cages in ERI and Hypo#1, respectively. Interestingly, the A value for OSDA4 in ERI is not as high as OSDA1-3 suggesting that a single OSDA4 is not sufficient to stabilize the cage in ERI. When full loadings are considered (Table 2, B values) the picture changes. Now CHA and ERI are favored phases instead of Hypo#1, and this could indeed be one of the reasons why Hypo#1 is not achieved. On the other hand, CHA was never achieved either, again pointing toward a specific behavior of the potassium, which is not captured in the theoretical description.

To elaborate further on the achievement of ERI, and the expansion of the Si/Al ratio especially from OSDA3, it is useful to consider the flexibility of the various OSDAs, as different conformations typically provides less specificity. OSDA1 was previously reported for the synthesis of UZM-12 (ERI framework) and has a high degree of flexibility due to the hydrocarbon chain linking the two trimethylammonium ends. This allows a large number of stabilized conformational configurations. The length of this molecule shows a good fit with the *eri* cage since it adopts an all-trans configuration when located inside the cage, whereas when the molecule is extended e.g. by increasing the hydrocarbon

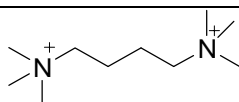
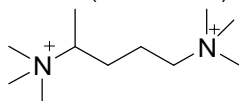
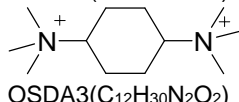
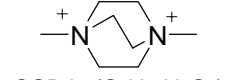
chain length or by substituting end-methyl groups with ethyl groups a gauche conformation is adopted (39).

For OSDA2, the flexibility is lower due to the presence of the methyl group attached to the hydrocarbon chain, which introduces a higher barrier for rotation around the tertiary  $sp^3$  hybridized carbon atom. The number of conformations are therefore limited, and it is less likely to curl together and adopt too many conformations.

In OSDA3, the hydrocarbon backbone is replaced with a cyclohexane ring. The ring-structure introduces more rigidity into the molecule. Nevertheless, conformations such as a boat, chair or a twist form are still possible. Furthermore, the length of OSDA3 is comparable to OSDA1 and OSDA2 (see Table 2). Common for OSDA1-3 is that one molecule occupies each *eri* cage.

In comparison SSZ-98, which also has the ERI structure, and has recently been reported in the patent literature uses N,N'-dimethyl-1,4-diazobicyclo[2.2.2]octane (OSDA4) (41). This molecule shows an even higher degree of rigidity, but does not have the same length.

**Table 2 Characteristics of OSDAs and their stabilization energies (energies are expressed in kJ for A values and kJ/SiO<sub>2</sub> for B values) for Hypo#1, ERI, CHA and OFF. OSDAs 1-3 were prepared in this work, while OSDA4 has recently been used to synthesize SSZ-98 (ERI) reported in the patent literature (41).**

OSDA	N-N distance [Å]	C/N <sup>+</sup>	3CN <sup>a</sup>	4CN <sup>a</sup>	Hypo#1	ERI	CHA	OFF	Energies <sup>b</sup>
 OSDA1(C <sub>10</sub> H <sub>28</sub> N <sub>2</sub> O <sub>2</sub> )	6.4	5	0	2	-153.4 -6.37	-123.5 -6.85	-90.7 -7.53	-104.2 -5.79	A B
 OSDA2(C <sub>11</sub> H <sub>30</sub> N <sub>2</sub> O <sub>2</sub> )	6.5	5.5	1	2	-158.2 -6.56	-138.0 -7.62	-53.1 -4.44	-122.5 -6.75	A B
 OSDA3(C <sub>12</sub> H <sub>30</sub> N <sub>2</sub> O <sub>2</sub> )	6.0	6	2	2	-155.3 -6.46	-130.3 -7.24	-89.7 -7.53	-78.2 -4.34	A B
 OSDA4(C <sub>8</sub> H <sub>20</sub> N <sub>2</sub> O <sub>2</sub> )	3.3	4	0	2	-107.1 -4.44	-89.7 -7.04	-87.8 -7.33	-92.6 -5.11	A B

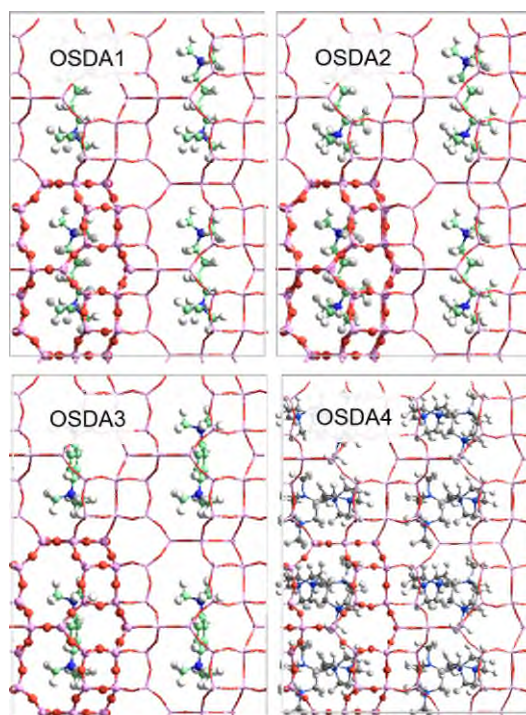
<sup>a</sup> Number of tertiary (3CN) and quaternary (4CN) carbon and nitrogen atoms in the OSDA as defined in (47).

<sup>b</sup> zeolite-OSDA van der Waals energy corresponding to: single occupation (A), full occupation divided by #SiO<sub>2</sub> (B). For each framework the unit cells contain the following number of SiO<sub>2</sub> units: 48 (Hypo#1), 36 (ERI), 36 (CHA), 36 (OFF). Data for set B: in Hypo#1 and OFF, all OSDAs are in a loading of 2 OSDAs per unit cell. In ERI, OSDA1, OSDA2, OSDA3 are in a loading of 2 OSDAs per unit cell, while OSDA4 is in a loading of 4 OSDAs per unit cell. In CHA all OSDAs are in a loading of 3 OSDAs per unit cell.

A quantitative way of expressing the rigidity of an OSDA is by considering the number of tertiary and quaternary carbons and nitrogen (47). These values are reported in Table 2 and are in good agreement with the qualitative description of rigidity given above. The observation of a higher rigidity of OSDA3 and OSDA4 seems to be in good agreement with the fact that these two molecules leads to higher Si/Al products.

Besides rigidity and length, the hydrophobicity of the OSDA is important for the OSDA-framework interaction especially during crystallization. Kubota *et al.* report that the C/N<sup>+</sup> ratio is a good estimate, and that OSDAs with values between 10 and 16 are particularly useful for obtaining high-silica zeolites (47). All the OSDAs used in this work fall outside this range due to the dicationic nature and OSDA3 gives the highest number; perhaps indicating that even more Si-rich materials are achievable with this OSDA.

The theoretical stabilization energy for OSDA4 in ERI is comparable to the numbers we find for OSDA1-3 despite the shorter molecular length. This is in good agreement with the observation that for all other B-values calculated a full loading is achieved with one OSDA per cage, whereas for OSDA4 a full loading in ERI is achieved with two OSDA molecules per cage. Specifically for this OSDA the favorable stabilization energy is achieved with two of the OSDA4 molecules located perpendicular to each other in the *eri* cage. The most stable conformations of the OSDA1-4 inside the *eri* cage are shown in Figure 7.



**Figure 7** Location and configuration of the OSDAs inside the *eri* cage (highlighted). Neighbor (2×1×2) unit cells are shown for the sake of clarity. The view shown is perpendicular to the b axis.



#### 4. Conclusions

In this work we have investigated the peculiar problem of synthesizing hypothetical zeolite frameworks that have been computationally predicted, but never practically prepared. We have followed a rational approach by screening a database of 933611 structures ([www.hypotheticalzeolites.net](http://www.hypotheticalzeolites.net)) and selecting a hypothetical framework. The selected framework was subsequently modified to obtain a more simplified structure, which was designated Hypo#1. Three different OSDAs were selected based on zeolite-OSDA vdW stabilization energies to attempt the experimental realization of Hypo#1. When screening the experimental outcome under fluoride and alkali (NaOH and KOH) hydrothermal conditions the target zeolite was never obtained. Instead we noticed that in the presence of potassium, the synthesis product was ERI, and for OSDA3 a high-Si version could be achieved. In spite of not obtaining a new framework, the morphological features and high Si composition of the obtained ERI-zeolites show promising features for improving various catalytic applications.

Stabilization energies of OSDAs in Hypo#1, ERI, as well as other zeolite frameworks were calculated to rationalize the results. All tested OSDAs (1-3) provides a good fit for the cage in Hypo#1 when one OSDA is considered (A-values, Table 2). However, when an optimum loading is considered ERI and CHA are favored phases (B-values, Table 2). This can partly explain why ERI is achieved instead of Hypo#1, but also highlights the limitations of the approach as CHA is not achieved. ERI is known to crystallize with potassium as the mineralizing agent and thus play a role during crystallization, which is not captured by only considering the zeolite-OSDA vdW stabilization energies. The high Si version of ERI achieved with OSDA3 as well as OSDA4 reported for SSZ-98 is similarly not only explained by the stabilization energies, but seem to relate to the rigidity of the molecule as well.

As this study illustrates, it still remains a challenge to synthesize hypothetical frameworks predicted by *in silico* modeling. One of the barriers is due to the kinetic control that drives zeolite crystallization along with other factors such as the stabilization of the intermediates and the reaction conditions, which are not typically considered in the computational screening. However, the computational modeling of the zeolite-OSDA interaction still provides a viable starting point for the rational design and synthesis of novel zeolites. It especially provides a method for improving and extending the composition of already existing materials, by providing novel OSDAs and by limiting explorative trial-and-error methods.

#### Acknowledgements

The authors thank Haldor Topsoe A/S and Innovation Fund Denmark for financial support under the Industrial PhD programme (Case no. 1355-0174B). We thank MINECO of Spain for funding (SEV-2016-0683 and RTI2018-101033-B-100) and ASIC-UPV for the use of computational facilities. We also thank Prof. M. M. J. Treacy for assistance with the Database of Prospective Zeolite Structures.

## References

- (1) Flanigen, E. M. In *Introduction to Zeolite Science and Practice*; van Bekkum, H., Flanigen, E. M., Jansen, J. C., Eds.; Elsevier Science: Amsterdam, 1991; Chapter 2, pp. 13–34.
- (2) Moscou L. In *Introduction to Zeolite Science and Practice*; van Bekkum, H., Flanigen, E. M., Jansen, J. C., Eds.; Elsevier Science: Amsterdam, 1991; Chapter 1, pp. 1–12.
- (3) Itabashi, K.; Kamimura, Y.; Iyoki, K.; Shimojima, A.; Okubo, T. A working hypothesis for broadening framework types of zeolites in seed-assisted synthesis without organic structure-directing agent. *J. Am. Chem. Soc.* **2012**, *134*, 11542–11549.
- (4) Lu, P.; Villaescusa, L. A.; Cambor, M. A. Driving the Crystallization of Zeolites. *Chem. Rec.* **2018**, *18*, 1–12.
- (5) Guo, P.; Shin, J.; Greenaway, A. G.; Min, J. G.; Su, J.; Choi, H. J.; Liu, L.; Cox P. A.; Hong S. B.; Wright, P. A.; Zou X. A zeolite family with expanding structural complexity and embedded isorecticular structures. *Nature*, **2015**, *524*, 74–78.
- (6) Tsunoji, N.; Yuki, S.; Oumi, Y.; Sekikawa, M.; Sasaki, Y.; Sadakane, M.; Sano, T. Design of Microporous Material HUS-10 with Tunable Hydrophilicity, Molecular Sieving, and CO<sub>2</sub> Adsorption Ability Derived from Interlayer Silylation of Layered Silicate HUS-2. *ACS Appl. Mater. Interfaces*, **2015**, *7*, 24360–24369.
- (7) Verheyen, E.; Joos, L.; Van Havenbergh, K.; Breynaert, E.; Kasian, N.; Gobechiya, E.; Houthoofd, K.; Martineau, C.; Hinterstein, M.; Taulelle, F.; Van Speybroeck, V.; Waroquier, M.; Bals, S.; Van Tendeloo, G.; Kirschhock, C. E. A.; Martens, J. A. Design of zeolite by inverse sigma transformation. *Nature Materials*, **2012**, *11*, 1059–1064.
- (8) Gallego, E. M.; Portilla, M. T.; Paris, C.; León-Escamilla, A.; Boronat, M.; Moliner, M.; Corma, A. "Ab initio" synthesis of zeolites for preestablished catalytic reactions. *Science*, **2017**, *355*, 1051–1054.
- (9) Li, C.; Paris, C.; Martínez-Triguero, J.; Boronat, M.; Moliner, M.; Corma, A. Synthesis of reaction-adapted zeolites as methanol-to-olefins catalysts with mimics of reaction intermediates as organic structure-directing agents. *Nature Catalysis*, **2018**, *1*, 547–554.
- (10) Foster, M. D.; Treacy, M. M. J. A Database of Hypothetical Zeolite Structures. <http://www.hypotheticalzeolites.net> (accessed March 9, 2015).
- (11) Treacy, M. M. J.; Randall, K. H.; Rao, S.; Perry, J. A.; Chadi, D. J. Enumeration of periodic tetrahedral frameworks. *Z. Kristallogr.* **1997**, *212*, 768–791.
- (12) Delgado-Friedrichs, O.; Dress, A. W. M.; Huson, D. H.; Klinowski, J.; Mackay, A. L. Systematic enumeration of crystalline networks. *Nature*, **1999**, *400*, 644–647.
- (13) Earl, D. J.; Deem, M. W. Toward a Database of Hypothetical Zeolite Structures. *Ind. Eng. Chem. Res.* **2006**, *45*, 5449–5454.
- (14) Davis, T. M.; Liu, A. T.; Lew, C. M.; Xie, D.; Benin, A. I.; Elomari, S.; Zones, S. I.; Deem, M. W. Computationally Guided Synthesis of SSZ-52: A Zeolite for Engine Exhaust Clean-up. *Chem. Mater.*, **2016**, *28*, 708–711.

- (15) Schmidt, J. E.; Deem, M. W.; Lew, C.; Davis, T. M. Computationally-Guided Synthesis of the 8-Ring Zeolite AEI. *Top. Catal.* **2015**, *58*, 410–415.
- (16) Sastre, G.; Gale, J. D. ZeoTsites: a code for topological and crystallographic tetrahedral sites analysis in zeolites and zeotypes. *Microporous Mesoporous Mater.* **2001**, *43*, 27–40.
- (17) Dassault Systèmes BIOVIA. <https://www.3dsbiovia.com> (accessed March 16, 2015), Materials Studio, 8.0, San Diego: Dassault Systèmes.
- (18) Sastre, G. A computational chemistry insight into the role of structure directing agents in the synthesis of zeolites. *Phys. Chem. Chem. Phys.* **2007**, *9*, 1052–1058.
- (19) Burton, A. W.; Zones, S. I. Organic molecules in zeolite synthesis: Their preparation and structure-directing effects. *Stud. Surf. Sci. Catal.* **2007**, *168*, 137–179.
- (20) Muraoka, K.; Chaikittisilp, W.; Yanaba, Y.; Yoshikawa, T.; Okubo, T. Directing Aluminum Atoms into Energetically Favorable Tetrahedral Sites in a Zeolite Framework by Using Organic Structure-Directing Agents. *Angew. Chem. Int. Ed.* **2018**, *57*, 3742.
- (21) Muraoka, K.; Chaikittisilp, W.; Okubo, T. Energy Analysis of Aluminosilicate Zeolites with Comprehensive Ranges of Framework Topologies, Chemical Compositions, and Aluminum Distributions. *J. Am. Chem. Soc.* **2016**, *138*, 6184–6193.
- (22) Turrina, A.; Garcia, R.; Cox, P. A.; Casci, J. L.; Wright, P. A. Retrosynthetic Co-Templating Method for the Preparation of Silicoaluminophosphate Molecular Sieves. *Chem. Mater.* **2016**, *28*, 4998–5012.
- (23) Turrina, A.; Garcia, R.; Watts, A. E.; Greer, H. F.; Bradley, J.; Zhou, W.; Cox, P. A.; Shannon, M. D.; Mayoral, A.; Casci, J. L.; Wright, P. A. STA-20: An ABC-6 Zeotype Structure Prepared by Co-Templating and Solved via a Hypothetical Structure Database and STEM-ADF Imaging. *Chem. Mater.* **2017**, *29*, 2180–2190.
- (24) Ghysels, A.; Moors, S. L. C.; Hemelsoet, K.; De Wispelaere, K.; Waroquier, M.; Sastre, G.; Van Speybroeck, V. Shape-Selective Diffusion of Olefins in 8-Ring Solid Acid Microporous Zeolites. *J. Phys. Chem. C* **2015**, *119*, 23721–23734.
- (25) Bushuev, Y. G.; Sastre, G. Atomistic simulations of water and organic templates occluded during the synthesis of zeolites. *Micropor. Mesopor. Mater.* **2010**, *129*, 42–53.
- (26) Catlow, C. R. A.; Freeman, C. M.; Vessal, B.; Tomlinson, S. M.; Leslie, M. Molecular dynamics studies of hydrocarbon diffusion in zeolites. *J. Chem. Soc. Faraday Trans.* **1991**, *87*, 1947–1950.
- (27) Jorgensen, W. L.; Maxwell, D. S.; Tirado-Rives, J. Development and testing of the OPLS all-atom force field on conformational energetics and properties of organic liquids. *J. Am. Chem. Soc.* **1996**, *118*, 11225–11236.
- (28) Oie, T.; Maggiora, G. M.; Christoffersen, R. E.; Duchamp, D. J.; Development of a flexible intra- and intermolecular empirical potential function for large molecular systems. *Int. J. Quantum Chem. Quantum Biol. Symp.* **1981**, *20*, 1–47.
- (29) Broyden, C. G. The convergence of a class of double-rank minimization algorithms. *J. Inst. Math. Appl.* **1970**, *6*, 76–90.
- (30) Fletcher, R. A New Approach to Variable Metric. *Algorithms. Comp. J.* **1970**, *13*, 317–322;

- (31) Goldfarb, D. A Family of Variable Metric Updates Derived by Variational Means. *Math. Comp.* **1970**, *24*, 23–26.
- (32) Shanno, D. F. Conditioning of quasi-Newton methods for function minimization. *Math. Comp.* **1970**, *24*, 647–656.
- (33) Gale, J. D. GULP: A computer program for the symmetry-adapted simulation of solids. *J. Chem. Soc. Faraday Trans.* **1997**, *93*, 629–637.
- (34) Gale, J. D.; Rohl, A. L. The General Utility Lattice Program (GULP). *Mol. Simul.* **2003**, *29*, 291–341.
- (35) Li, Y.; Yu, J.; Xu, R. Criteria for Zeolite Frameworks Realizable for Target Synthesis. *Angew. Chem. Int. Ed.* **2013**, *52*, 1673–1677.
- (36) Liu, X.; Valero, S.; Argente, E.; Botti, V.; Sastre, G. The importance of T···T···T angles in the feasibility of zeolites. *Z. Kristallogr.* **2015**, *230*, 291–299.
- (37) Staples, L.W.; Gard, J.A. The fibrous zeolite erionite; its occurrence, unit cell, and structure. *Mineral. Mag.*, **1959**, *32*, 261–281.
- (38) Schlenker, J. L.; Pluth, J. J.; Smith, J. V. Dehydrated natural erionite with stacking faults of the offretite type. *Acta Crystallogr.*, **1977**, B33, 3265–3268.
- (39) Lee, J. H.; Park, M. B.; Lee, J. K.; Min, H. K.; Song, M. K.; Hong, S. B. Synthesis and Characterization of ERI-Type UZM-12 Zeolites and Their Methanol-to-Olefin Performance. *J. Am. Chem. Soc.* **2010**, *132*, 12971–12982.
- (40) Miller, M. A.; Lewis, G. J.; Gisselquist, J. L.; Moscoso, J. G.; Patton, R. L. UZM-12 and UZM-12HS: crystalline aluminosilicate zeolitic compositions and processes for preparing and using the compositions. U. S. Patent 7,344,694, **2008**.
- (41) Xie, D.; Zones, S. I.; Lew, C. M.; Davis, T. M. Molecular sieve SSZ-98. U. S. Patent 9,409,786, **2016**.
- (42) Boruntea, C.-R.; Lundegaard, L. F.; Corma, A.; Vennestrøm, P. N. R.; Crystallization of AEI and AFX zeolites through zeolite-to-zeolite transformations. *Micropor. Mesopor. Mater.* **2019**, *278*, 105–114.
- (43) Teketel, S.; Lundegaard, L. F.; Skistad, W.; Chavan, S. M.; Olsbye, U.; Lillerud, K. P.; Beato, P.; Svelle, S. Morphology-induced shape selectivity in zeolite catalysis. *J. Catal.* **2015**, *327*, 22–32.
- (44) Łukaszuk, K. A.; Rojo-Gama, D.; Øien-Ødegaard, S.; Lazzarini, A.; Berlier, G.; Bordiga, S.; Lillerud, K. P.; Olsbye, U.; Beato, P.; Lundegaard, L. F.; Svelle, S. Zeolite morphology and catalyst performance: conversion of methanol to hydrocarbons over offretite. *Catal. Sci. Technol.* **2017**, *7*, 5435–5447.
- (45) Xie, D.; Chen, C. Y. Synthesis of aluminosilicate zeolite SSZ-98. U. S. Patent 20,160,375,428, **2016**
- (46) Lillerud, K. P.; Raeder, J. H. On the synthesis of erionite—offretite intergrowth zeolites. *Zeolites*, **1986**, *6*, 474–483.
- (47) Kubota, Y.; Helmkamp, M. M.; Zones, S. I.; Davis, M. E. Properties of organic cations that lead to the structure-direction of high-silica molecular sieves. *Microporous Mater.* **1996**, *6*, 213–229.

# General overview and conclusions

The synthesis of two small-pore zeolites: SSZ-39 (framework code: AEI) and SSZ-16 (framework code: AFX) have been extensively studied for a detailed understanding of the zeolite-to-zeolite transformations (ZTZ). This was done with the aim of preparing a tool box, to provide a helpful insight for the design and synthesis of novel zeolite structures. For this study, the original synthesis of AEI and AFX zeolites has been first considered. In the original synthesis the Al-source is a FAU zeolite and the Si-source is sodium silicate ( $\text{Na}_2\text{SiO}_3$ ); (the amount of Si introduced with the FAU zeolite is usually neglected, but it was considered for the study presented herein and especially for a high accuracy of the experiments).

The behavior of the FAU zeolite has been followed. When broad synthesis conditions are applied for reaction mixtures that contains FAU ( $\text{Si}/\text{Al} = 15$ ) and  $\text{Na}_2\text{SiO}_3$ , the product phase diagram is highly dependent on the total amount of  $\text{OH}^-$  and the amount of organic structure directing agent (OSDA). A clear delimitation in the product phase is observed, which consist either from pure AEI, a mixture in various proportions of AEI and unconverted FAU, or only FAU zeolite. Phase-pure AEI it is observed only in specific ranges of  $\text{OH}^-/\text{T}$ -atoms and is describing a narrow region between 0.63 – 0.70 being in the same time independent of the amount of OSDA used, for the conditions investigating herein. Moreover, the AEI product is taking the form of a diagonal area, with a mixture of AEI and FAU outside the preferred region (described by the  $\text{OH}^-/\text{T}$ -atoms ratio) and only unconverted FAU it is seen further away. The only competing phase to be seen it is FAU zeolite for both low and high  $\text{OH}^-$  amount.

The special role of a zeolite used as raw material in synthesis of SSZ-39 is clearly pointed out by the difficulty of obtaining the desired product from other Si- and Al-sources. It was shown that when either highly reactive Si and Al-sources are used, such as e.g.  $\text{Si}(\text{OEt})_4$  and fumed  $\text{SiO}_2$  combined with  $\text{Al}(\text{iPrO})_3$ , or species with a relative low reactivity such as e.g. co-precipitated amorphous silica-alumina, SSZ-39 is no longer obtained. This means that the OSDA is not able to play a templating role, which translates to the fact that OSDA-zeolite (Al) interactions are not stable for a time long enough for a stable nucleus to form. This points to the fact that the Al-species introduced in the reaction, must have special characteristics (e.g. geometry

and spatial configuration), for the OSDA-zeolite interaction to take place. When a pure zeolite-to-zeolite transformation is applied and the same overall Si/Al ratio is used with respect to the original synthesis a similar preferred region for the product is observed, described by almost identical window in terms of OH<sup>-</sup>/T-atoms ratios.

Comparison of the SSZ-39 prepared by original synthesis and zeolite-to-zeolite transformation revealed a small, but still clear improved inclusion of the OSDA for the ZTZ transformation. This translates for relative higher Si/Al ratios and lower sodium content, (revealed by Na/Al and Na/aei cage), for similar amounts of OSDA and OH<sup>-</sup>/T-atoms used in the synthesis gel for zeolite-to-zeolite transformation approach compared to original synthesis. The analysis of the <sup>13</sup>C CP-MAS NMR of the solid product and the <sup>13</sup>C-NMR of the OSDA, showed that the OSDA is intact for both synthesis approaches, which indicates that the different behavior of the zeolite-to-zeolite transformation is not attributed to the degradation of the OSDA. Another important difference between the OS and the ZTZ is the high yield that is obtained when a FAU (Si/Al = 15) is used as raw material. Analysis of the <sup>29</sup>Si and <sup>27</sup>Al MAS NMR spectra, revealed that the majority of the aluminum is tetrahedrally coordinated, proved by the peak at approx. 60 ppm. The materials prepared by the original synthesis and zeolite-to-zeolite transformation revealed two well-defined peaks at -111 ppm which was correlated with the Si without neighboring Al-atoms and at -105 ppm corresponding to Si with one neighboring Al-atom. The peak between -100 and -103 ppm was associated with Si linked to two Al-atoms. The signal for the sample prepared with sodium silicate is less well-defined, pointing to a material with more structural defects for the original synthesis. When it comes to the materials prepared by ZTZ, the lack of structural defects suggest a possible better inclusion of the OSDA in the zeolite cages as well.

One of the most interesting information about the behavior of zeolites as an Al-source has been extracted from the discovery that the lattice parameter of the unconverted FAU is increasing as the OH<sup>-</sup> amount is increasing. This is based on the selective dissolution of the Si from the FAU raw material and is a direct consequence of the (total amount of) OH<sup>-</sup> attack on the framework Si-O-Si bonds. It must be mentioned here that the total amount of OH<sup>-</sup> is described by the OH<sup>-</sup> introduced with the NaOH, with the sodium silicate and with the OSDA. The selective dissolution of the Si points to the fact that the initial extracted species have a higher content of

silicon, compared with the starting FAU zeolite. Moreover, the experiments have shown that only after a certain amount of silicon is extracted and FAU is reaching a higher aluminum content, the AEI is observed in the phase space. It was also observed that at higher OH<sup>-</sup>/T-atoms ratios, the AEI product is not any longer obtained. At this stage the FAU-material can be described by an even higher amount of Si extracted. When the lattice parameter of the unconverted FAU is above 24.52 Å, the AEI product is not anymore seen in the phase space.

The correlation of the lattice parameter and the Si/Al ratio of the FAU zeolite revealed that the AEI is no longer obtained when relative high amounts of OH<sup>-</sup> are used in the synthesis gel. This corresponds with a Si/Al ratio approximately < 6. In a similar manner, for a lower OH<sup>-</sup> amount, just before the AEI appears, the Si/Al ratio of the unconverted FAU is approximately > 8. This means that for a successful synthesis of AEI an intermediate zeolite with the Si/Al ratio in the above range it is necessary. When a FAU zeolite with a Si/Al ratio similar to the preferred Si/Al ratio in the product, the crystallization of the target zeolite is taking place at even lower OH<sup>-</sup>/T-atoms, suggesting that the silicon extraction is probably not necessary. This important finding is also responsible of obtaining the target zeolite with considerable higher yields. Following the zeolite-to-zeolite transformation, by PXRD during each day of the crystallization time revealed that the process takes place without any other crystalline or amorphous phases, detectable by X-ray diffraction. Full transformation from FAU to AEI was achieved during 5 days of crystallization. The analysis of the SEM images taken at different crystallization stages, revealed the presence of agglomerates of FAU octahedral crystals for the first days and the presence of orthorhombic box shaped ({100}, {010} and {001} pinacoids) crystallites of AEI. The SEM images have also shown the AEI particles growing on surface of the FAU which suggest that the nucleation could take place on the FAU surface.

AEI zeolite material has also been successfully synthesized for the first time from CHA – type zeolites, which has similar structural features and framework density as the target zeolite. However, when a zeolite with different structural units is used, e.g. BEA\*, the preferred product is no longer obtained.

For the study of AFX – type zeolites, a complete zeolite-to-zeolite transformation was applied and a similar synthesis approach as for AEI was also

followed. When a FAU zeolite with a Si/Al ratio of 15 is used as raw material, the desired product appear in a narrow range of 0.8 to 0.9  $N_{OH^-}/N_{Tatoms}$  alongside with modest synthesis yields (approx. 35 %). BEA\* zeolite is a powerful competing phase, stimulated by both the high synthesis gel SAR and the OSDA that it is also favoring the synthesis of this type of zeolite product. The product diagram is considerably changing when a FAU zeolite with Si/Al ratio 6 is used. The yields obtained are much higher, above 90 %, which points to the fact that when the Si/Al ratio of the parent zeolite is synchronized with the Si/Al ratio preferred by the product, the required  $OH^-$  amount is decreasing. AFX – type zeolite appear to be synthesized on a much broader interval between 0.4 – 0.9  $OH^-/T$ -atoms, together with BEA\* and ANA zeolites as competing phases. Following the intermediate stages of the AFX synthesis, by PXRD combined with SEM images revealed no amorphous or other crystalline solids and specific morphology for AFX crystallites after 2 days. The SSZ-16 (AFX zeolite) have also been synthesized from other zeolites with similar structural feature e.g. CHA – type zeolites, but we were unable to identify the right conditions when \*BEA zeolite, with different structural features is used as raw material.

Based on the experimental results a scheme was introduced, where an unknown type of intermediate is formed based on the selective slow dissolution of the parent zeolite. This intermediate species are then fast forming the desired product. If the rates of the dissolution of the zeolite raw materials and the crystallization of the zeolite target are not matched, the intermediate species can equilibrate and a competing zeolite becomes the preferred product. Dissolution of the parent zeolite, does not necessary mean complete dissolution.

All these observations indicate that the zeolite-to-zeolite transformation don't have necessary to proceed from low framework densities to higher, but the overall synthesis conditions, such as the total amount of  $OH^-$  and favorable OSDA – zeolite interaction highly influence the success of the synthesis.

Exploration of the hydrothermal phase space by using a combination of potassium hydroxide (KOH) and 1-methyl-4-aza-1-azoniabicyclo[2.2.2]octane hydroxide (1-methyl-DABCO), lead to the synthesis of a novel dense zeolite, described herein under the name K-paracelsian. The synthesis of this type of material is highly dependent on the use of KOH in the synthesis gel, together with 1-methyl-DABCO.



The OSDA it is found to play more an inhibiting role for the nucleation of other zeolite phases such as LTL framework, rather than having a classic structure directing role. This is supported by the  $^{13}\text{C}$  CP-MAS NMR of the as-prepared zeolite compared with the  $^{13}\text{C}$  NMR of the OSDA in solution, which revealed that the OSDA is not occluded inside the zeolite pores. Small amounts of residual C are detected on the surface of the zeolite only when the number of scans is threefold increased.

Depending on the amount of  $\text{OH}^-$  introduced in the synthesis gel ERI – type zeolites are favorite at low amounts and K-paracelsian together with LTL are the products of high basic synthesis gels. Pure K-paracelsian is achieved only when 1-methyl-DABCO is used in the reaction mixture. Using FAU as raw material also leads to the new zeolite, in difference from amorphous co-precipitated silica-alumina that is favoring LTL – type zeolites. When the synthesis composition is switched to Na – rich system, LEV and ANA materials are seen to be the product outcome.

The first attempts of structure refining based on *ex situ* XRD analysis, revealed that the unit-cell dimensions of the as-prepared zeolite is similar to that of the feldspar mineral paracelsian with the formula  $\text{BaAl}_2\text{Si}_2\text{O}_8$ . This structure is similar to that of a zeolite and consist of a three-dimensional network with  $\text{Ba}^{2+}$  cations filling interstitial sites and corner sharing  $\text{SiO}_4$  and  $\text{AlO}_4$  tetrahedra. The Rietveld refinement of the structure model build with the atomic arrangements from orthorhombic (*Pnam*) paracelsian, including also the substitution  $\text{Ba}^{2+} + \text{Al}^{3+} \rightarrow \text{K}^+ + \text{Si}^{4+}$ , using fixed atomic positions and fixed occupancies, followed by subsequent refining the fractional coordinates of all atoms and the K occupancy resulted in excellent fit with the experimental data and meaningful chemical bonds and angles. It was concluded that the new material has the same framework structure as the paracelsian mineral.

The initial characterization of the prepared zeolite, including SEM analysis and *ex situ* PXRD revealed that K-paracelsian is compositionally closely related to the mineral microcline and structurally closely related to the paracelsian mineral. Both minerals are part of the feldspar group. A reference feldspar (microcline sample with a content of 83 wt. % microcline and 17 wt. % albite) was used for comparison. *In situ* PXRD of the microcline and albite showed a linear relationship with the temperature variation and a fully reversible behavior during the thermal treatment correlated with a simple expansion and contraction of the unit-cell. The analysis of TGA experiments of

the as-prepared zeolite, combined with *in situ* PXRD, showed a non-linear unit-cell evolution in the temperature range of 250 – 450 °C. This also corresponds to a relative mass loss of 5.7 wt. %, showed by the TGA experiment. A temperature dependence of the a and c parameters was observed to be responsible for the thermal expansion, while the b parameter show almost no temperature dependence on the last part of the thermal treatment.

The heat-treated sample was reanalyzed after 4 weeks of being exposed to air. A similar behavior in the lattice parameter was observed with that of dehydrated K-paracelsian. This indicates that the rehydration is not reversible at room temperature. The dehydration process of K-paracelsian was found to resemble that of natrolite, where the observed weight loss consist of one molecule of water per cage ( $\text{KAlSi}_3\text{O}_8 \cdot \text{H}_2\text{O}$ ).

Further inspection of the calculated independent atom model electron density showed a minimum of the density in the positions where a water molecule will complete the octahedral coordination of the oxygen atoms that are in the first sphere of coordination of potassium. From the fact that no significant amount of residual electron density could be observed from the inspection of the observed XRD data, could be concluded that the  $\text{H}_2\text{O}$  positions have a disordered nature. This is also proving that the substitution of  $\text{Ba}^{2+}$  with of the ionic radius of 134 ppm, by the  $\text{K}^+$ , with the radius of 133 ppm is possible to support the same structure and also to make place for a water molecule.

Based on the observation that K-paracelsian is closely related to other small pore zeolites, that are all constructed from double-crankshaft motifs, such as: GME, GIS, APC, MER, PHI, SIV a new building scheme was proposed. The structural difference between all of these known IZA framework topologies is the relative orientation of the double-crankshaft chains. When these building structural motifs are arranged in an open hexagonal lattice, this leads to larger cages and lower density structures, where the GME framework is an example of such. The building scheme purposed defined a new family of dense double-crankshaft zeolite topologies, with structures build entirely from four, six and eight rings; ranging from one-dimensional (K-paracelsian), to two-dimensional (APC) and three-dimensional (GIS, MER, PHI, SIV). It was shown that a large number of hypothetical zeolite structures can be

constructed, by applying the purposed building scheme. The hypothetical frameworks build in this way are crystallo-chemically healthy and are characterized by very similar stabilization energies. This represents an easy and reliable method of finding new frameworks as hypothetical zeolite structures usually requires elaborate computational methods.

The novel zeolite material, named herein K-paracelsian, can be considered as an intermediate structure between feldspars and zeolites. Moreover, K-paracelsian is the simplest end-member of a family of dense double-crankshaft zeolite frameworks. By applying the building scheme described herein a large number of new structures can be build. Three of this hypothetical structures have been constructed as an example.

A rational approach has been applied with the aim of synthesizing novel small-pore zeolites for DeNO<sub>x</sub> applications. This included the selection of an hypothetical structure, that was used as a synthesis target. Three frameworks have been selected from a database of 933611 structures ([www.hypotheticalzeolites.com](http://www.hypotheticalzeolites.com)) and 15 organic structure directing agents (OSDAs) have been found by molecular docking. This was done either by correlation with similar cages of known IZA zeolites and subsequent modification of the OSDAs or by chemical intuition. The manuscript: "Synthesis of high-silica ERI driven by computational screening of hypothetical zeolites" presented in this thesis, refers solely at Hypo#1. The structure is described in chapter 2 as Hypo#3, but the name form the manuscript Hypo#1 will be used in this conclusive remarks. The framework have been selected by applying descriptors that have been established based on the state-of-the-art small pore zeolites for exhaust gas catalysis. After that the selected framework have been manually modified with the aim of obtaining a more simple molecular sieve. The new obtained framework has passed the feasibility criteria for zeolite structures and was designated Hypo#1. Three OSDAs have been selected, based on the synthesis feasibility, followed by their usage in synthesis gels.

The results of the synthesis prepared under alkali conditions using either NaOH or KOH as mineralizing agents in combination with amorphous-silica-alumina (ASA) or FAU zeolite lead to the a low specificity of OSDA-zeolite interaction. This conclusion is dictated by the product outcome such as BEA\*, amorphous or traces of

an unknown phase (not Hypo#1). The fluoride media experiments have shown only amorphous and unknown phase for OSDA1, whereas for the OSDA2 and OSDA3 amorphous, LEV, SOD and pure silica AST was obtained alongside with unknown phase which was not Hypo#1.

When the mineralizing agent is switched to KOH, ERI – type zeolite is seen to dominate the product diagram. This finding showed a clear improvement in the selectivity when  $K^+$  cations are introduced in the synthesis gel, in combination with the templating effect of the various OSDAs applied. Although the target zeolite hypothetical framework Hypo#1 was not obtained, a novel high-Si ERI type zeolite has been successfully synthesized. It deserves mentioning that ERI framework is resembling much of the state-of-the-art small-pore zeolite features that have been showed to play an extremely important role for DeNO<sub>x</sub> applications. However, even more important is the variety of particle morphologies that is shown by this material. Needle like particles have been synthesized with OSDA1, packed short needles with OSDA2; on the other hand for OSDA3, small crystallites with tubular to prismatic morphology are achieved. This diversity of the particle morphology is predicted to have an important influence on the catalytic applications of this material.

When the stabilization energies of the predicted OSDAs for the target framework Hypo#1 are compared and the ERI is the synthesis product, useful information about the OSDA-zeolite interaction could be extracted. This was also the case for other zeolite frameworks reported to be present as impurities in the synthesis of ERI – type zeolites such as: CHA, OFF and LTL. Based on the theoretical findings, all the tested OSDAs (1-4) are well suited to direct the synthesis towards Hypo#1 (e.g. 1 OSDA / u.c., see A values reported in Table 2, part of the article “Synthesis of high-silica ERI driven by computational screening of hypothetical zeolites”). This suggest that the target zeolite Hypo#1 may be favorite by a low concentration of the OSDA in the synthesis gel. However, in the more realistic case of full loading, Hypo#1 is not the most stable and ERI and CHA becomes the most favored structures. The lowest zeolite-OSDA energy for OSDA1 corresponds to CHA zeolite. And similarly, for the other OSDAs considered, the most stable structures are: ERI (OSDA2), CHA and ERI (OSDA3), and CHA (OSDA4), suggesting that OSDA2 is particularly suited for the synthesis of high-Si ERI zeolite. From these results we cannot explain why CHA was not obtained with none of the OSDAs, but we can explain that ERI was obtained with

OSDA2 and OSDA3. The introduction of Al in the calculations would potentially allow to obtain more accurate results.

This study shows that considering pure silica frameworks, neglecting the electrostatic interactions and taking into account neutral the overall charge of the OSDA is not sufficient for the synthesis of hypothetical zeolites. Moreover is showing the complexity of the zeolite preparation chemistry, where many parameters, (not considered by computational screening) are known to influence each other, such as the kinetic control, stabilization of the intermediates and the reaction conditions, or the role of the metal cations. The successful synthesis of high-Si ERI with three distinct particle morphologies, proves however that targeting hypothetical frameworks by a simplified computational modeling approach of the zeolite-OSDA interaction is beneficial for improving existing materials and expanding the synthesis possibilities supported by a rational design.

# A future perspective

## Is the zeolite's hydrothermal method a type of formal-Gödelian system? (a speculative insight)

Cristian-R. Boruntea

### Affiliations:

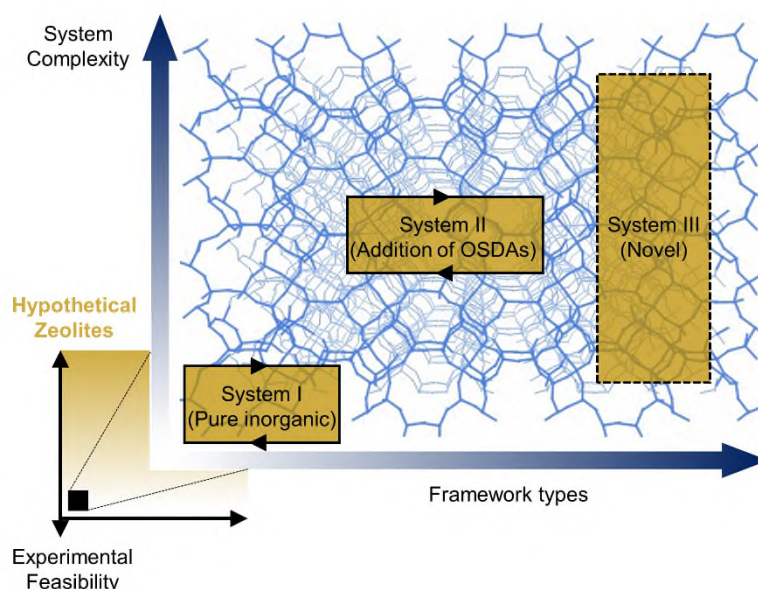
Instituto de Tecnología Química, Universitat Politècnica de València - Consejo Superior de Investigaciones Científicas, Avenida de los Naranjos s/n, 46022 Valencia, Spain

**Abstract:** The limitations on the zeolite's hydrothermal method, seen through the lens of a type of formal-Gödelian system are briefly discussed. The original pure inorganic system and the superior rank system created by the introduction of organic templates are examples in this regard. Based on the current trends, the future modification of any reaction condition and/or intrinsic parameter of the hydrothermal method will minimally affect the product outcome. The system is expected to adopt a closed-loop behavior and an input-output circularity. The use of OSDAs to satisfy the zeolite thermodynamic metastability is still seen to be necessary but not anymore sufficient for increasing the number of novel frameworks. The introduction of a higher rank system is proposed and its implications are summarized. It is envisioned that this will led to a novel approach for the zeolite and catalyst community.

**One Sentence Summary:** Formulating the limitations on novel zeolites preparation may increase the number of framework types.

Zeolites are fascinating materials, covering highly important catalytic processes and are of paramount importance for a sustainable future (1), (2), (3). Their preparation however, falls into a nebulous area, marked by uncertainty, inconsistency and inscrutability. The hydrothermal method is the most common synthesis procedure for zeolites, characterized by a particular complexity and poor understanding of mechanistic insights (4), (5). Although interesting novel synthetic routes have been proposed continuously in the last decades, their success is still challenging to be applied for a higher number of frameworks (6), (7), (8). There is a clear limit in the preparation of novel zeolite frameworks, which otherwise would increase their industrial applicability and boost their performance. This is reflected in the enormous difference between the number of theoretically predicted frameworks

(hypothetical zeolites are found to be in the order of millions) (9) and the real number of distinct zeolite structures (which is only going above 200) (10). This is known as the zeolite conundrum (11); and while various studies addressed the feasibility of such hypothetical frameworks (12), (13), the said difference remains an *unsolvable* challenge. Although consistent high-throughput methodologies for screening through reaction conditions and intrinsic parameters have been employed for zeolite synthesis, the product output is still poor and unattractive in its diversity.



Today, novel zeolite structures are still rarely obtained, by using more and more complicated OSDAs (organic structure directing agents) (14) that dramatically affect the material's industrial feasibility. Moreover, the hydrothermal method in itself is responsible for the small number of distinct zeolite frameworks and for the slowing-down of new discovery entries (15). The authors expects that, in the near-time future the modification of any parameter of the hydrothermal system, will led the system to enter in a closed-loop and it will always yield similar products. This may be a consequence of the fact that only the same parameters are modified over and over. It also suggests that the system in its current form will never be able to yield a higher number of novel zeolite frameworks. The hydrothermal system as it is used today is limited and incomplete. Insight in the scientific past of zeolite synthesis shows that this is actually its second limitation. The first limitation of the hydrothermal system was solved by R. Barrer (16), by "breaking" the closed-loop of the pure inorganic system with the introduction of OSDAs. It is clear now that the loop was not broken with the introduction of organic moieties, but just enlarged enough for allowing scientists to obtain structures that would have been impossible to be made, by using the original pure inorganic system. This is in some way similar to adding a new axiom to a formal system, irrefutably demonstrated by Kurt Gödel in 1931 to be incomplete and inconsistent (17); which eventually will have the same fate. Nevertheless, this may have some benefits for the hydrothermal system, and until the system is looping again the number of novel zeolite frameworks may be increased. The further continuous use of novel OSDAs is expected to have a significantly lower impact on the discovery of novel zeolite frameworks compared to the beginning, which indicates that the use of

OSDAs is necessary, but not anymore sufficient. Only when the addition of OSDAs was found to perfectly answer an *essential property* of zeolites (e.g. thermodynamic metastability), the creation of system II was possible.

The usage of organic molecules didn't complete in any way, nor modify the first inorganic system. It created the premises for a novel system, superior in rank which ultimately will follow the same pattern as the original system I by entering in an unattractive circularity in terms of product diversity. This circularity comes as a property of a system that burned-out its predilection for novelty. The creation of superior systems to answer the *unsolvability* of a problem, was already seen in science. For a rigorous definition of the *photon*, *quantum mechanics* was created. For the calculation of the square root of a negative number, the creation of imaginary and complex numbers was necessary. This was followed by a succession of discoveries in the field of physics and mathematics and led to an unprecedented inflation of the scientific advancement.

The challenge for broadening the type of the zeolite frameworks, may be the creation of a new system superior to the previous one (system III). Finding a new "element" to answer a similar or another *essential property* of zeolites may be key in such endeavor. Such superior system is not necessarily more complex, however a highly complicated system may result. The subsequent challenge than is trying to solve the complexity limitation of working inside of a such higher-rank system. This was seen with the introduction of OSDAs which was responsible for making the understanding of zeolite crystallization knotty and unwieldy, although it had clear benefits. As Richard Feynman stated "when a law is right it can be used to find another one, (...) this process has developed in an avalanche of discoveries, each new discovery permits the tools of much more discovery."

**Acknowledgements:** I would like to thank my partner Brigitte Devocht for helpful discussions and for revising this manuscript.

## References and Notes:

1. Mark. E. Davis, Ordered porous materials for emerging applications. *Nature* **417**, 813–821 (2002).
2. A. Corma, Inorganic Solid Acids and Their Use in Acid-Catalyzed Hydrocarbon Reactions. *Chem. Rev.* **95**, 559-614 (1995).
3. A. Corma, *From microporous to mesoporous molecular sieve materials and their use in catalysis*. *Chem. Rev.* **97**, 2373–2419 (1997).
4. Mark E. Davis, Raul. F. Lobo, *Zeolite and molecular sieve synthesis*. *Chem. Mater.* **4**, 756–768 (1992).
5. A. Corma, Mark E. Davis, Issues in the Synthesis of Crystalline Molecular Sieves: Towards the Crystallization of Low Framework-Density Structures. *ChemPhysChem* **5**, 304–313 (2004).
6. Peng Bai, *et al.* Discovery of optimal zeolites for challenging separations and chemical transformations using predictive materials modeling. *Nat. Commun.* **6**, 5912 (2015).
7. Mark E. Davis, Organizing for better synthesis. *Nature* **364**, 391–393 (1993).



8. E. M. Gallego, *et al.* "Ab initio" synthesis of zeolites for preestablished catalytic reactions. *Science* **355**, 1051–1054 (2017).
9. M. D. Foster, M. M. J. Treacy, A Database of Hypothetical Zeolite Structures: <http://www.hypotheticalzeolites.net> (2018).
10. C. Baerlocher, L. McCusker, Database of Zeolite Structures. <http://www.iza-structure.org/databases/> (2018).
11. V. A. Blatov, G. D. Ilyushin, D. M. Proserpio, *The zeolite conundrum: why are there so many hypothetical zeolites and so few observed? A possible answer from the zeolite-type frameworks perceived as packings of tiles.* *Chem. Mater.* **25**, 412–424 (2013).
12. M. D. Foster, *et al.* *Chemically feasible hypothetical crystalline networks.* *Nature Mater.* **3**, 234–238 (2004).
13. Yi Li, Jihong Yu, Ruren Xu, Criteria for Zeolite Frameworks Realizable for Target Synthesis, *Angew. Chem. Int. Ed.* **52**, 1673–1677 (2013).
14. Xie, D., *et al.*, SSZ-52, a Zeolite with an 18-Layer Aluminosilicate Framework Structure Related to That of the DeNO<sub>x</sub> Catalyst Cu-SSZ-13. *J. Am. Chem. Soc.* **135**, 10519–10524 (2013).
15. M. Mazur, *et al.*, Synthesis of 'unfeasible' zeolites. *Nature Chemistry* **8**, 58–62 (2016).
16. Barrer, R. M, *Hydrothermal Chemistry of Zeolites* (Academic Press, London, 1982).
17. K. Gödel, Über formal unentscheidbare Sätze der Principia Mathematica und verwandter Systeme, I. *Monatshefte für Mathematik und Physik* **38**, 173–198 (1931).

# Annexes

## Supporting Information

### Crystallization of AEI and AFX zeolites through zeolite-to-zeolite transformations

Cristian-R. Boruntea<sup>a,b</sup>, Lars F. Lundegaard<sup>a</sup>, Avelino Corma<sup>b \*</sup>, Peter N. R. Vennestrøm<sup>c \*</sup>

<sup>a</sup> Haldor Topsøe A/S, Haldor Topsøes Alle 1, DK-2800 Kgs. Lyngby, Denmark

<sup>b</sup> Instituto de Tecnología Química, Universitat Politècnica de València-Consejo Superior de Investigaciones Científicas, Avenida de los Naranjos s/n, 46022 Valencia, España

<sup>c</sup> Umicore Denmark ApS, Nøjsomhedsvej 20, DK-2800 Kgs. Lyngby, Denmark

\*Corresponding Author, Email: [acorma@itq.upv.es](mailto:acorma@itq.upv.es); [peter.vennestrom@eu.umicore.com](mailto:peter.vennestrom@eu.umicore.com)

#### Content

Synthesis of OSDAs used for the synthesis of AEI and AFX aluminosilicates.

Table S1. Chemical composition of selected AEI samples from synthesis in the 1 Si : 0.033 Al : x NaOH : y OSDA : 40 H<sub>2</sub>O system using a combination of sodium silicate and FAU (Si/Al=15) or FAU (Si/Al=30) only.

Figure S2. PXRD of AEI-type zeolite synthesized from CHA (Si/Al = 15) as the sole Si- and Al- source.

Figure S3. PXRD of AFX-type zeolite synthesized from CHA (Si/Al = 7) as the sole Si- and Al- source.

Figure S4. SEM images of selected products after one and two days in the synthesis of AFX with FAU as the sole Si- and Al-source. Scale bars in the images corresponds to 2 μm.

Figure S5 a) <sup>13</sup>C CP-MAS NMR of the as-prepared AEI zeolite synthesized using FAU as the Si- and Al- source b) 1D <sup>13</sup>C-NMR of the OSDA.

Figure S6 a) <sup>13</sup>C CP-MAS NMR of the as-prepared AFX zeolite synthesized using FAU as the Si- and Al- source b) 1D <sup>13</sup>C-NMR of the OSDA.

Figure S7. <sup>29</sup>Si (a) and <sup>27</sup>Al MAS NMR (b) spectra of AFX-type zeolites prepared by zeolite-to-zeolite transformation (IZC).

Figure S8. TGA and DSC thermograms for SSZ-39 (AEI) zeolite prepared by original synthesis (a) and by zeolite-to-zeolite transformation (b) and for SSZ-16 (AFX) synthesized by zeolite-to-zeolite transformation (c).

### **1,1,3,5-tetramethylpiperidinium hydroxide**

In a 1L flask 250 ml methanol (Sigma-Aldrich,  $c \geq 99\%$ ) was mixed with 29.5 g (0.26 mole), 30.7 g solution 3,5-dimethylpiperidine (Sigma-Aldrich,  $c \geq 96\%$ ) and 37.5 (0.272 mole)  $K_2CO_3$  (Riedel-de Haën,  $c = 99\%$ ). Then, under stirring and placing the flask on an ice bath, 107.5 g (0.757 mole), methyl iodide (Sigma-Aldrich,  $c = 99\%$ ,  $\rho = 2.28$  g/ml) was added dropwise. The reaction mixture became yellowish after approximately half of the  $CH_3-I$  was added. After all the methyl iodide was introduced, the ice bath was removed and the flask was covered with Al foil. There is no distinguishable thermal effect during the alkylation process. After 7 days the reaction mixture (white) was filtrated to remove the insoluble inorganic salts. The filtered solution (brawny) was vacuum concentrated to dryness. The resulting solid contains both the product and inorganic salts. In order to remove the inorganic impurities, 250 ml chloroform was added to dissolve the organic product and the insoluble salts were removed by filtration. The resulting filtered solution (brown-yellowish) was vacuum concentrated to dryness. The solid was recrystallized from a mixture of isopropanol ( $\approx 700$  ml) and absolute ethanol ( $\approx 150$  ml) where a small amount of activated charcoal was added. The obtained solution was filtrated on a fluted filter and cooled down at room temperature. The organic salt recrystallized as white needles. The product was recuperated by filtration and was washed with 30 ml isopropanol. The final amount of product after a second recrystallization was 34.3 g (0.1275 mole), which correspond to an yield of  $\eta = 49\%$ . The organic salt was characterized by  $^{13}C$ -NMR,  $^1H$ -NMR, melting point (274-275 °C) and PXRD.

The transformation of the iodide salt to the hydroxide form, was done by using the ion exchange Amberlite IRN78 Resin by mixing overnight (24 h). The filtrated solution had a concentration of 7.95 % and the ion exchange yield was  $\eta = 86.4\%$ .

### **1,4-bis(1,4-diazabicyclo[2.2.2]octane)butyl dihydroxide**

In a 500 mL flask 34 g (0.3 mole) DABCO (Sigma-Aldrich,  $c = 99\%$ ) was dissolved in 150 mL methanol (Sigma-Aldrich,  $c = 99\%$ ) and the mixture was stirred for half an hour. The flask was placed on an ice bath and 14 mL (0.1 mole), 1,4-dibromobutane (Sigma-Aldrich,  $c = 99\%$ ,  $\rho = 1.808$  g/mL) was added dropwise. The ice bath was removed and the reaction mixture was vigorously mixed for 5 days at room temperature. Then, 250 mL diethylether (Sigma-Aldrich,  $c = 99\%$ ) was added and the solid was filtrated and washed with 200 mL diethylether. The obtained yield was approx. 91 %. The organic salt was characterized by  $^{13}C$ -NMR,  $^1H$ -NMR.

The transformation of the iodide salt to the hydroxide form, was done by using the ion exchange Amberlite IRN78 Resin by mixing overnight (24 h). The obtained solution had a concentration of 11.35 % and the ion exchange yield was  $\eta = 80\%$ .

Table S1. Chemical composition of selected AEI samples from synthesis in the 1 Si : 0.033 Al : x NaOH : y OSDA : 40 H<sub>2</sub>O system using a combination of sodium silicate and FAU (Si/Al=15) or FAU (Si/Al=30) only.

Sample number	OSDA/Si	NaOH/Si	N <sub>OH</sub> /N <sub>Tatoms</sub>	Si/Al	Na/Al	Na/u.c.
Synthesis with sodium silicate and FAU (Si/Al=15)						
6	0.07	0.21	0.65	8.55	0.295	1.48
10	0.12	0.17	0.66	9.16	0.263	1.24
14	0.17	0.13	0.67	9.37	0.243	1.12
11	0.12	0.19	0.68	8.36	0.293	1.50
12	0.12	0.21	0.7	7.98	0.367	1.96
Zeolite-to-zeolite transformation with FAU (Si/Al=30)						
31	0.17	0.5	0.65	10.36	0.175	0.74
28	0.12	0.56	0.66	9.43	0.218	1.00
32	0.17	0.52	0.67	9.75	0.217	0.97
29	0.12	0.58	0.68	8.70	0.277	1.37
30	0.12	0.6	0.7	8.17	0.311	1.63

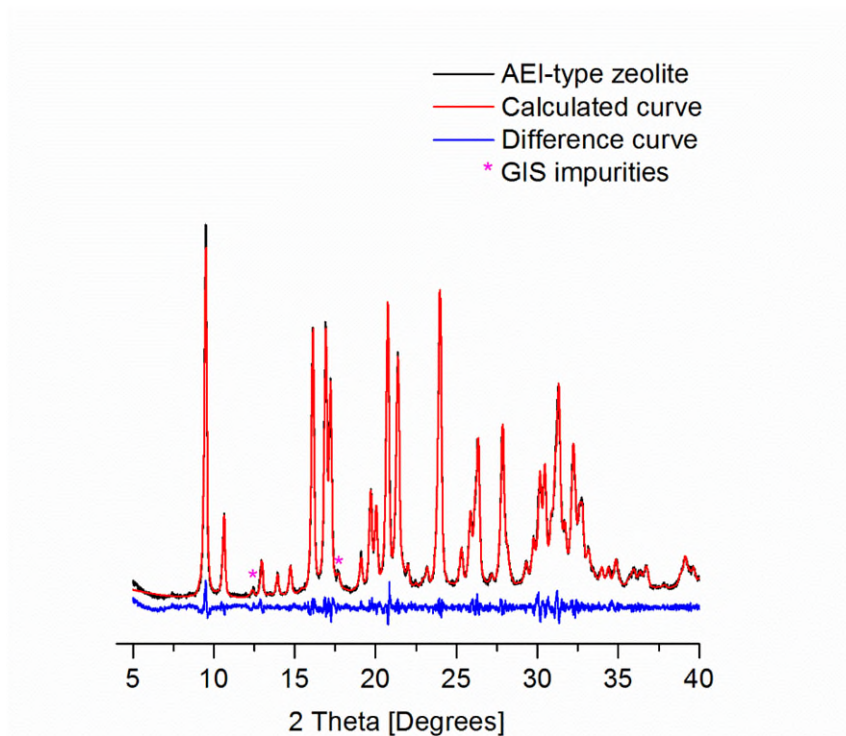


Figure S2. PXRD pattern of AEI-type zeolite synthesized from CHA (Si/Al = 15) as the sole Si- and Al-source.

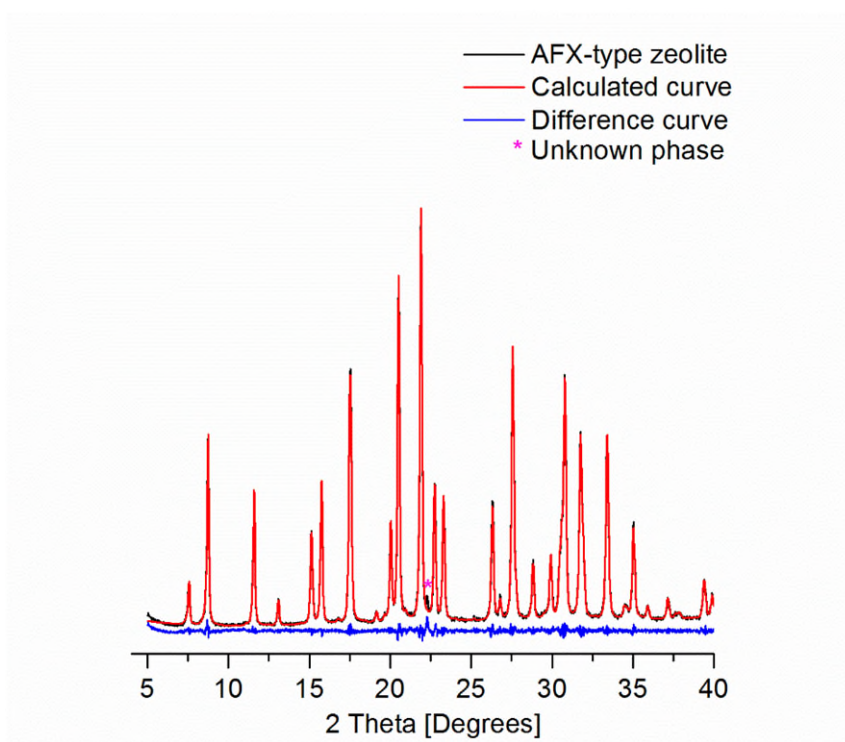


Figure S3. PXRD pattern of AFX-type zeolite synthesized from CHA (Si/Al = 7) as the sole Si- and Al-source.

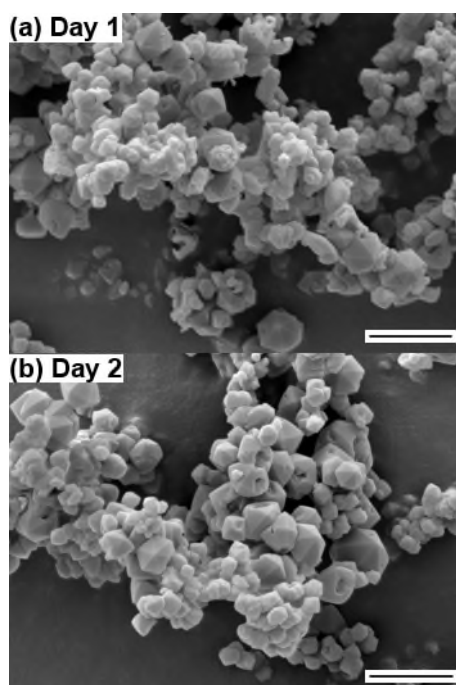


Figure S4. SEM images of selected products after one and two days in the synthesis of AFX with FAU as the sole Si- and Al-source. Scale bars in the images corresponds to 2  $\mu\text{m}$ .

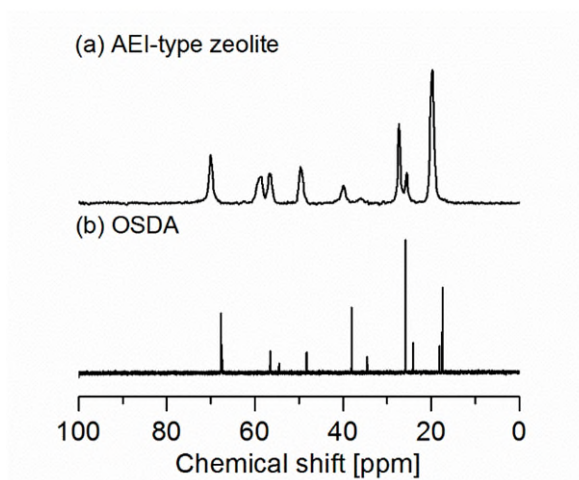


Figure S5 a)  $^{13}\text{C}$  CP-MAS NMR of the as-prepared AEI zeolite synthesized using FAU as the Si- and Al- source b) 1D  $^{13}\text{C}$ -NMR of the OSDA.

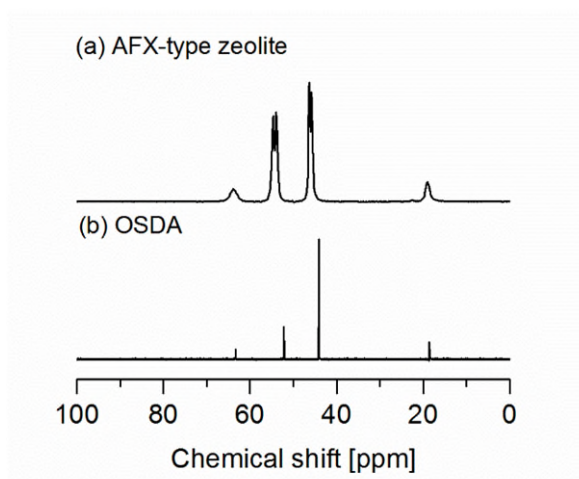


Figure S6 a)  $^{13}\text{C}$  CP-MAS NMR of the as-prepared AFX zeolite synthesized using FAU as the Si- and Al- source b) 1D  $^{13}\text{C}$ -NMR of the OSDA.

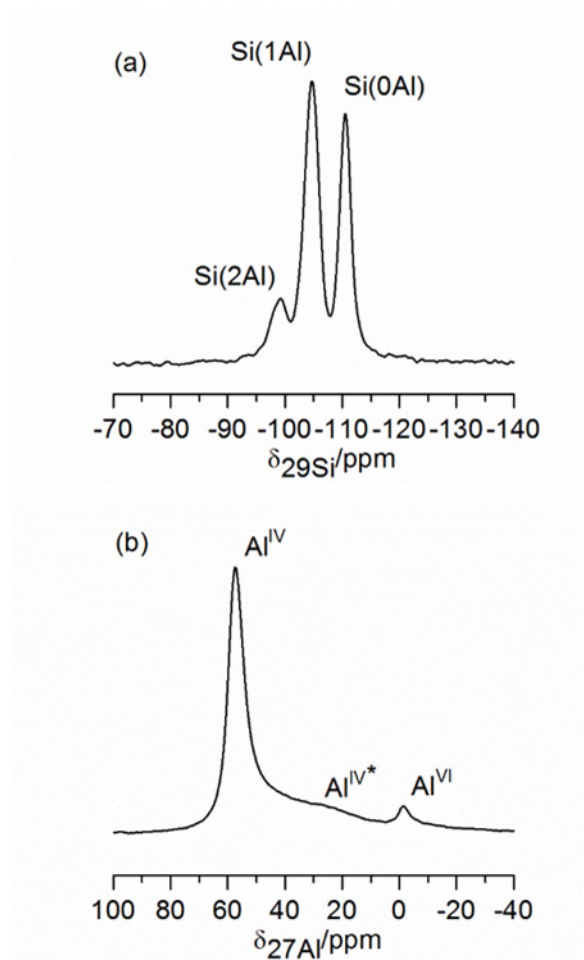


Figure S7.  $^{29}\text{Si}$  (a) and  $^{27}\text{Al}$  MAS NMR (b) spectra of AFX-type zeolites prepared by zeolite-to-zeolite transformation (IZC).

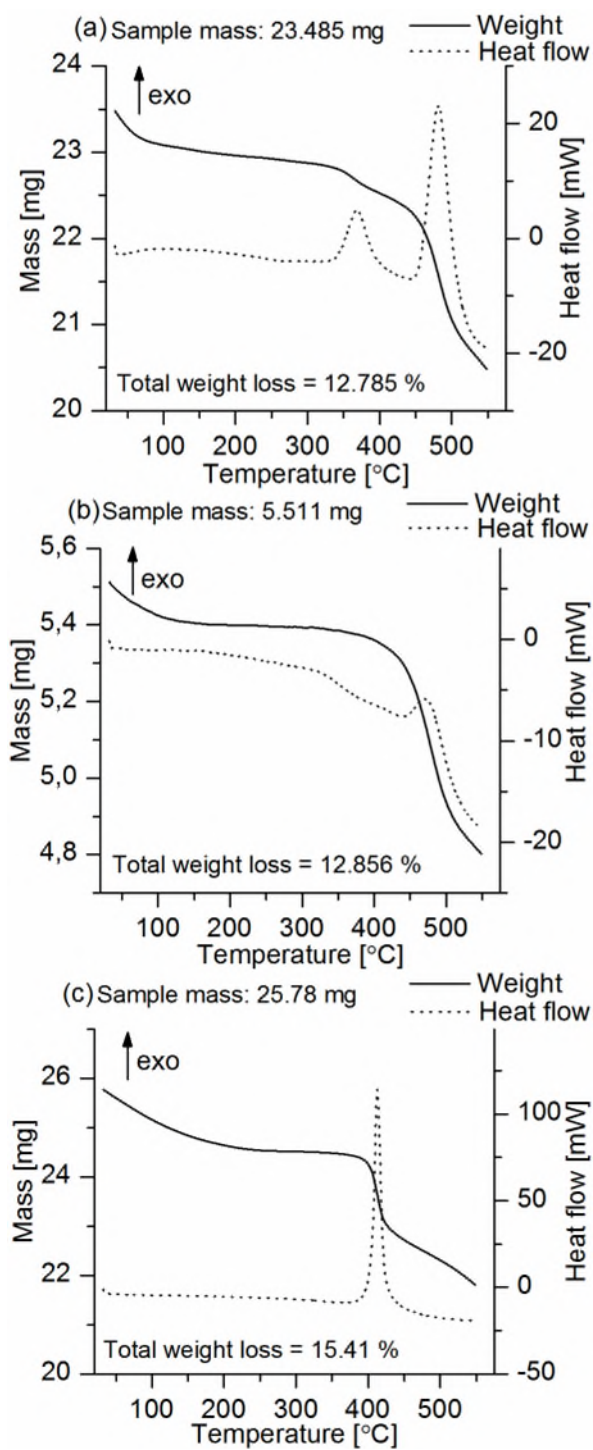


Figure S8. TGA and DSC thermograms for SSZ-39 (AEI) zeolite prepared by original synthesis (a) and by zeolite-to-zeolite transformation (b) and for SSZ-16 (AFX) synthesized by zeolite-to-zeolite transformation (c).



## Supporting information

### **K-paracelsian ( $\text{KAlSi}_3\text{O}_8 \cdot \text{H}_2\text{O}$ ) and identification of a simple building scheme of dense double-crankshaft zeolite topologies**

Cristian-R. Boruntea<sup>ab</sup>, Peter N. R. Vennestrøm<sup>c\*</sup> and Lars F. Lundegaard<sup>a\*</sup>

<sup>a</sup> Haldor Topsøe A/S, Haldor Topsøes Alle 1, Kgs. Lyngby, 2800, Denmark

<sup>b</sup> Instituto de Tecnología Química, Universitat Politècnica de València-Consejo Superior de Investigaciones Científicas, Avenida de los Naranjos s/n, Valencia, 46022, Spain

<sup>c</sup> Umicore Denmark ApS, Nøjsomhedsvej 20, Kgs. Lyngby, 2800, Denmark

Correspondence email: peter.vennestrom@eu.umicore.com; lafl@topsoe.com

#### **Content:**

Synthesis of 1-methyl-4-aza-1-azoniabicyclo[2.2.2]octane hydroxide (1-methyl-DABCO) used for the preparation of K-Paracelsian.

Table S1 Products and chemical composition of selected synthesis using 1-methyl-DABCO from synthesis composition 1.0  $\text{SiO}_2$  : xx Al : aa OSDA : bb NaOH : 20  $\text{H}_2\text{O}$  crystallized for 7 days at 150 °C.

Table S2 Products and chemical composition of selected synthesis using 1-methyl-DABCO from synthesis composition 1.0  $\text{SiO}_2$  : xx Al : aa OSDA : bb KOH : 20  $\text{H}_2\text{O}$  crystallized for 7 days at 150 °C, U = Unkown.

Figure S1 a)  $^{13}\text{C}$  CP-MAS NMR of the as-prepared K-Paracelsian zeolite; b) 1D  $^{13}\text{C}$ -NMR of the OSDA.

Figure S2.  $^{29}\text{Si}$  (a) and  $^{27}\text{Al}$  MAS NMR (b) spectra of K-Paracelsian zeolite.

CIF file

Synthesis of 1-methyl-4-aza-1-azoniabicyclo[2.2.2]octane hydroxide (1-methyl-DABCO) used for the preparation of K-Paracelsian.

In a 250 mL flask 20.4 g (0.12 mole) DABCO (Sigma-Aldrich, c = 99 %) was dissolved in 60 mL methanol (Sigma-Aldrich, c = 99 %) and the mixture was stirred for half an hour. The flask was placed on an ice bath and 7.6 mL (0.12 mole) methyl iodide (Sigma-Aldrich, c = 99 %,  $\rho = 2.28 \text{ g/mL}$ ) was added dropwise. The ice bath was removed and the reaction mixture was vigorously mixed for 5 days at room temperature. Then, 100 mL diethyl ether (Sigma-Aldrich, c = 99 %) was added and the solid was filtrated and washed with 200 mL diethyl ether. The organic salt was characterized by  $^{13}\text{C}$ -NMR,

<sup>1</sup>H-NMR. The transformation of the iodide salt to the hydroxide form, was done by using the ion exchange Amberlite IRN78 Resin by mixing overnight (24 h). The filtrated solution had a concentration of 12.5 wt. %.

Table S1 Products and chemical composition of selected synthesis using 1-methyl-DABCO from synthesis composition 1.0 SiO<sub>2</sub> : xx Al : aa OSDA : bb NaOH : 20 H<sub>2</sub>O crystallized for 7 days at 150 °C.

FAU (Si/Al=12.5)		NaOH	
OSDA	0.45	0.55	0.65
0.1	145/Amorphous	146/Amorphous	147/LEV
0.2	148/Amorphous+ANA	149/LEV+ANA	150/LEV+ANA
0.3	151/LEV+ANA	152/LEV+ANA	153/LEV+ANA
FAU (Si/Al=6)		NaOH	
OSDA	0.5	0.6	0.7
0.1	154/LEV	155/LEV+ANA	156/LEV+ANA
0.2	157/LEV+ANA	158/LEV+ANA	159/LEV+ANA
0.3	160/LEV+ANA	161/LEV+ANA	162/ANA

Table S2 Products and chemical composition of selected synthesis using 1-methyl-DABCO from synthesis composition 1.0 SiO<sub>2</sub> : xx Al : aa OSDA : bb KOH : 20 H<sub>2</sub>O crystallized for 7 days at 150 °C, U = Unkown.

Si/Al (FAU/ASA)	OSDA	KOH	SN/PXRD	M (g)/η(%)
15	0.2	0.4	390/Amorphous+U	0.30/41
30	0.2	0.25	391/Amorphous+U	0.35/47
6 (ASA)	0.2	0.6	392/LTL	0.36/40
15 (ASA)	0.2	0.4	393/ERI+Amorphous	0.31/40
30 (ASA)	0.2	0.25	394/Amorphous+U	0.21/28

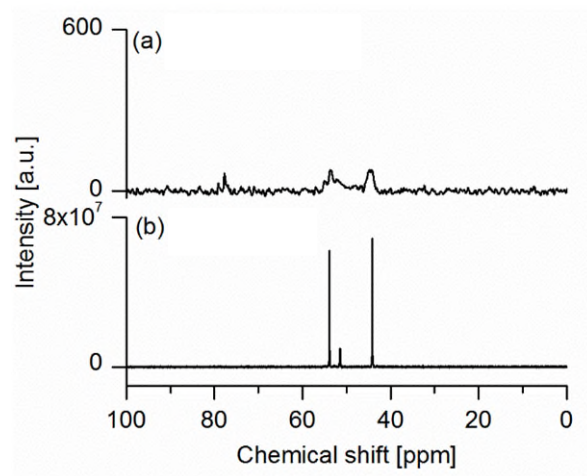


Figure S1 a)  $^{13}\text{C}$  CP-MAS NMR of the as-prepared K-Paracelsian zeolite; b) 1D  $^{13}\text{C}$ -NMR of the OSDA.

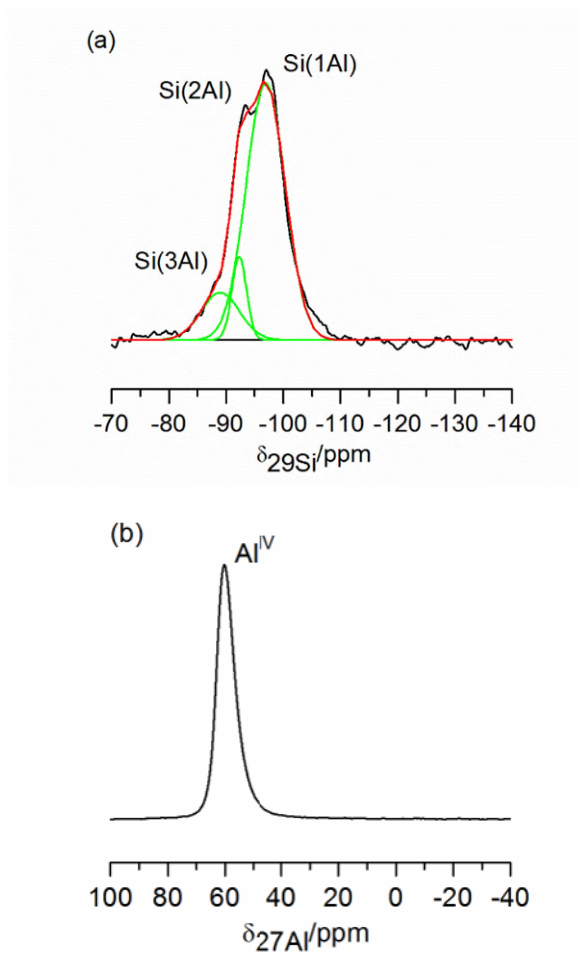


Figure S2.  $^{29}\text{Si}$  (a) and  $^{27}\text{Al}$  MAS NMR (b) spectra of K-Paracelsian zeolite.

## CIF file

```
_chemical_name_mineral ?K-paracelsian?
_diffrn_radiation_type 'Cu K\alpha'
_cell_length_a 9.203877
_cell_length_b 9.478482
_cell_length_c 8.598872
_cell_angle_alpha 90
_cell_angle_beta 90
_cell_angle_gamma 90
_cell_volume 750.1551
_symmetry_cell_setting orthorhombic
_symmetry_space_group_name_H-M Pnam
loop_
_symmetry_equiv_pos_as_xyz
'x, y, z '
'-x, -y, z+1/2 '
'-x+1/2, y+1/2, -z '
'-x+1/2, y+1/2, z+1/2 '
'x, y, -z+1/2 '
'-x, -y, -z '
'x+1/2, -y+1/2, -z+1/2 '
'x+1/2, -y+1/2, z '
loop_
_atom_site_label
_atom_site_type_symbol
_atom_site_symmetry_multiplicity
_atom_site_fract_x
_atom_site_fract_y
_atom_site_fract_z
_atom_site_occupancy
_atom_site_B_iso_or_equiv
```

K1 K 4 0.9051775 0.4208219 0.25 0.9882289 1  
Si1 Si 8 0.06910811 0.1996188 0.9329407 0.75 0.7990633  
Al1 Al 8 0.06910811 0.1996188 0.9329407 0.25 0.7990633  
Si2 Si 8 0.2203551 0.9106303 0.9326256 0.75 0.7990633  
Al2 Al 8 0.2203551 0.9106303 0.9326256 0.25 0.7990633  
O1 O 8 0.1831324 0.07407488 0.9802215 1 0.3179766  
O2 O 8 0.1465411 0.35327 0.9583315 1 0.3179766  
O3 O 8 0.9238067 0.188464 0.04226799 1 0.3179766  
O4 O 4 0.02246383 0.1828873 0.75 1 0.3179766  
O5 O 4 0.2701965 0.9041192 0.75 1 0.3179766

## Supporting Information

### Synthesis of high-silica ERI driven by computational screening of hypothetical zeolites

Cristian-R. Boruntea<sup>a,b</sup>, German Sastre<sup>b</sup>, Lars F. Lundegaard<sup>a</sup>, Avelino Corma<sup>b \*</sup>, Peter N. R. Vennestrom<sup>c \*</sup>

<sup>a</sup> Haldor Topsøe A/S, Haldor Topsøes Alle 1, DK-2800 Kgs. Lyngby, Denmark

<sup>b</sup> Instituto de Tecnología Química, Universitat Politècnica de València-Consejo Superior de Investigaciones Científicas, Avenida de los Naranjos s/n, 46022 Valencia, España

<sup>c</sup> Umicore Denmark ApS, Nøjsomhedsvej 20, DK-2800 Kgs. Lyngby, Denmark

\*Corresponding Author, Email: [acorma@itq.upv.es](mailto:acorma@itq.upv.es); [peter.vennestrom@eu.umicore.com](mailto:peter.vennestrom@eu.umicore.com);

#### Content

Synthesis of OSDAs used in the preparation of ERI-type zeolites.

Table S1. Products and chemical composition of selected synthesis using OSDA1, OSDA2 from synthesis composition 1.0 SiO<sub>2</sub> : xx Al : 0.1 OSDA : a NaOH : 20 H<sub>2</sub>O crystallized for 7 days at 135°C, U = Unknown.

Table S2. Products and chemical composition of selected synthesis using OSDA1, OSDA2 from synthesis composition 1.0 SiO<sub>2</sub> : xx Al : 0.1 OSDA : 0.3 KOH : 20 H<sub>2</sub>O crystallized for 7 days at 135°C, U = Unknown.

Table S3. Products and chemical composition of selected synthesis using OSDA3 from synthesis composition 1.0 SiO<sub>2</sub> : xx Al : 0.1 OSDA : a KOH : b NaOH : 20 H<sub>2</sub>O crystallized for 7 days at 135°C, U = Unknown.

Table S4. Products and chemical composition of selected synthesis using OSDA1, OSDA2, OSDA3 from synthesis composition 1.0 SiO<sub>2</sub> : x Al : 0.5 OSDA : 1.0 HF : 5 H<sub>2</sub>O crystallized for several days at 135°C, U = Unknown.

Table S5. Location of 1 molecule of SDA in zeolites with different environments. 'x' means that the molecule locates in the corresponding cavity/channel; '+' means that the molecule occupies more than one cavity/channel simultaneously.

Table S6. Number of cavities and SiO<sub>2</sub> per unit cell in each zeolite.

Table S7. Amounts of OSDA occluded in the ERI materials determined by weight loss after combustion at 550°C measured by TGA.

Figure S1. TGA-DSC thermograms of ERI-type zeolites corresponding to samples 1, 5 and 12.

Figure S2. (b), (d), (f) 1D  $^{13}\text{C}$ -NMR of the OSDAs and (a), (c), (e)  $^{13}\text{C}$  CP-MAS NMR of the corresponding ERI materials, for samples 3, 7 and 12 respectively, synthesized using FAU as the Si- and Al- source.

ZeoTsites generated file for Hypo#1.

Synthesis of OSDAs used in the preparation of ERI-type zeolites.

Synthesis of butane-1,4-bis(trimethylammonium) dihydroxide (OSDA1).

OSDA1 was synthesized by adding 29 mL (0.24 mol) 1,4-dibromobutane (99 wt. %, Sigma-Aldrich) to a solution made by mixing 145 mL (0.6 mol) of trimethylamine (4.2 mol/L ethanolic solution, Sigma Aldrich) and 150 mL methanol (99 wt. %, Sigma-Aldrich). The resulted mixture was stirred at room temperature for 7 days. The obtained solid was filtered and washed with absolute ethanol and the product was further purified by recrystallization from absolute ethanol. The product was obtained with approx. 80 % yield and it was characterized by m.p.,  $^{13}\text{C}$ -NMR and  $^1\text{H}$ -NMR.

Synthesis of pentane-1,4-bis(trimethylammonium) dihydroxide (OSDA2).

OSDA2 was prepared by mixing 12 mL (0,086 mol) dibromopentane (97 wt. %, Sigma-Aldrich) to a solution made from 62 mL (0,258 mol) of trimethylamine (4.2 mol/L ethanolic solution, Sigma Aldrich) and 50 mL methanol (99 wt. %, Sigma-Aldrich). The reaction mixture was refluxed for 30 h and then it was cooled down to room temperature and the solvent was removed by reduced pressure. The obtained solid was mixed with 50 mL absolute ethanol and the alcohol was vacuum distilled; this procedure was repeated for 3 times. The product was characterized by  $^{13}\text{C}$ -NMR and  $^1\text{H}$ -NMR. The identification work on this type of spectra proved to be complicated due to the presence of an asymmetric carbon in the molecule and also because of some substitution or/and transposition by-products favored by the substrate structure and high basicity of the reaction mixture.

Synthesis of cyclohexane-1,4-bis(trimethylammonium) dihydroxide (OSDA3).

A mixture of 30 mL formic acid (89.5 wt. % aqueous solution, Sigma-Aldrich), 6.1 g  $\text{NaHCO}_3$ , 5 g trans-1,4-diaminocyclohexane (98% purity powder, Sigma Aldrich) and 14 mL formaldehyde (37 wt. % aqueous solution, Sigma-Aldrich) was refluxed until no visible evolution of  $\text{CO}_2$  was noticed. The reaction mixture was vacuum distilled after 50 mL HCl (2 mol/L aqueous solution) was added, followed by the addition of an excess of NaOH and extraction 3 times with chloroform. The chloroform portions were combined and 8 mL of methyl iodide (99 wt. %, Sigma-Aldrich) was added followed by mixing

overnight. The obtained solid was dissolved in water and ion exchange to hydroxide form, using an ion exchange resin. The product was characterized by  $^{13}\text{C}$ -NMR and  $^1\text{H}$ -NMR.

Table S1. Products and chemical composition of selected synthesis using OSDA1, OSDA2 from synthesis composition 1.0  $\text{SiO}_2$  : xx Al : 0.1 OSDA : a NaOH : 20  $\text{H}_2\text{O}$  crystallized for 7 days at  $135^\circ\text{C}$ , U = Unknown.

Si/Al	OSDA1/Si	$\text{H}_2\text{O}/\text{Si}$	NaOH/Si	SN/PXRD	NOH <sup>-</sup> / NTatoms
FAU6	0.1	20	0.2	234/amorphous+FAU	0.343
FAU6	0.1	20	0.4	235/FAU+ANA	0.514
FAU6	0.1	20	0.6	236/ANA	0.686
FAU15	0.1	20	0.2	239/amorphous	0.375
FAU15	0.1	20	0.4	240/amorphous+ANA	0.56
FAU15	0.1	20	0.6	241/FAU+ANA	0.75
FAU30	0.1	20	0.2	244/amorphous	0.387
FAU30	0.1	20	0.4	245/amorphous+U	0.581
FAU30	0.1	20	0.6	246/ANA	0.744
ASA6	0.1	20	0.2	289/FAU+ANA	0.343
ASA6	0.1	20	0.4	290/FAU+ANA+SOD	0.514
ASA6	0.1	20	0.6	291/ ANA+GIS+SOD+U	0.686
ASA15	0.1	20	0.2	294/amorphous	0.375
ASA15	0.1	20	0.4	295/amorphous+ANA	0.56
ASA15	0.1	20	0.6	296/FAU+ANA	0.75
ASA30	0.1	20	0.2	299/amorphous	0.387
ASA30	0.1	20	0.4	300/amorphous	0.581
ASA30	0.1	20	0.6	301/FAU+ANA	0.744
Si/Al	OSDA2/Si	$\text{H}_2\text{O}/\text{Si}$	NaOH/Si	SN/PXRD	NOH <sup>-</sup> / NTatoms
FAU6	0.1	20	0.2	304/ FAU	0.343
FAU6	0.1	20	0.4	305/ANA+U	0.514
FAU6	0.1	20	0.6	306/ANA	0.686
FAU15	0.1	20	0.2	309/amorphous	0.375
FAU15	0.1	20	0.4	310/amorphous+ANA	0.56
FAU15	0.1	20	0.6	311/FAU+ANA+MOR +U	0.75
FAU30	0.1	20	0.2	314/amorphous	0.387
FAU30	0.1	20	0.4	315/amorphous	0.581
FAU30	0.1	20	0.6	316/FAU+ANA	0.744
ASA6	0.1	20	0.2	319/amorphous	0.343
ASA6	0.1	20	0.4	320/amorphous (?)	0.514
ASA6	0.1	20	0.6	321/amorphous (?)	0.686
ASA15	0.1	20	0.2	324/amorphous	0.375
ASA15	0.1	20	0.4	325/amorphous+ANA	0.56
ASA15	0.1	20	0.6	326/amorphous (?)	0.75
ASA30	0.1	20	0.2	329/ ANA	0.387
ASA30	0.1	20	0.4	330/amorphous	0.581
ASA30	0.1	20	0.6	331/amorphous	0.744



Table S2. Products and chemical composition of selected synthesis using OSDA1, OSDA2 from synthesis composition 1.0 SiO<sub>2</sub> : xx Al : 0.1 OSDA : 0.3 KOH : 20 H<sub>2</sub>O crystallized for 7 days at 135°C, U = Unknown.

Si/Al	OSDA1/Si	H <sub>2</sub> O/Si	KOH/Si	SN/PXRD	NOH/NTatoms	M (g)
FAU6	0.1	20	0.3	358/ERI	0.429	0.74
FAU15	0.1	20	0.3	359/amorphous	0.469	0.48
FAU30	0.1	20	0.3	360/amorphous+U	0.484	0.51
ASA6	0.1	20	0.3	361/ERI	0.429	0.74
ASA15	0.1	20	0.3	362/amorphous	0.469	0.45
ASA30	0.1	20	0.3	363/amorphous	0.484	0.20
Si/Al	OSDA2/Si	H <sub>2</sub> O/Si	KOH/Si	SN/PXRD	NOH/NTatoms	M (g)
FAU6	0.1	20	0.3	364/ERI	0.429	0.71
FAU15	0.1	20	0.3	365/amorphous	0.469	0.41
FAU30	0.1	20	0.3	366/amorphous	0.484	0.52
ASA6	0.1	20	0.3	367/ERI	0.429	0.71
ASA15	0.1	20	0.3	368/amorphous	0.469	0.54
ASA30	0.1	20	0.3	369/amorphous	0.484	0.48

Table S3. Products and chemical composition of selected synthesis using OSDA3 from synthesis composition 1.0 SiO<sub>2</sub> : xx Al : 0.1 OSDA : a KOH : b NaOH : 20 H<sub>2</sub>O crystallized for 7 days at 135°C, U = Unknown.

Si/Al (FAU)	OSDA3/Si	NaOH/Si	KOH/Si	SN/PXRD	NOH/NTatoms	M (g)
6	0.1	0.3	0	352/FAU	0.429	0.58
15	0.1	0.3	0	353/BEA	0.469	0.58
30	0.1	0.3	0	354/Amorphous	0.484	0.78
6	0.1	0	0.3	355/ERI	0.429	0.6
15	0.1	0	0.3	356/ERI	0.469	0.7
30	0.1	0	0.3	357/Amorphous+U	0.484	0.92
Si/Al (ASA)	OSDA3/Si	NaOH/Si	KOH/Si	SN/PXRD	NOH/NTatoms	M (g)
6	0.1	0.3	0	370/U	0.429	0.53
15	0.1	0.3	0	371/BEA	0.469	0.4
30	0.1	0.3	0	372/BEA	0.484	0.21
6	0.1	0	0.3	373/ERI	0.429	0.58
15	0.1	0	0.3	374/ERI	0.469	0.45
30	0.1	0	0.3	375/amorphous	0.484	0.22

Table S4. Products and chemical composition of selected synthesis using OSDA1, OSDA2, OSDA3 from synthesis composition 1.0 SiO<sub>2</sub> : x Al : 0.5 OSDA : 1.0 HF : 5 H<sub>2</sub>O crystallized for several days at 135°C, U = Unkown.

Si/Al	OSDA1	H2O	HF	SN/PXRD	Time (days)	M (g)
15	0.5	5	1	381/Amorphous + U	14	2.35
Infini	0.5	5	1	382/Amorphous + U		2.49
15	0.5	5	1	383/Amorphous + U	28	2.78
Infini	0.5	5	1	384/Amorphous + U		2.59
15	0.5	5	1	385/Amorphous + U	7	2.24
Infini	0.5	5	1	386/Amorphous + U		1.8
Si/Al	OSDA2	H2O	HF	XRD	Time (days)	M (g)
15	0.5	5	1	395/LEV + U	28	2.20
Infini	0.5	5	1	396/AST		0.81
15	0.5	5	1	397/Amorphous + U	14	2.72
Infini	0.5	5	1	398/AST		0.79
15	0.5	5	1	406/Amorphous + U	7	3.83
Infini	0.5	5	1	407/Amorphous + U		2.50
Si/Al	OSDA3	H2O	HF	XRD	Time (days)	M (g)
15	0.5	5	1	399/LEV+SOD+AST	28	1.24
Infini	0.5	5	1	400/AST		1.127
15	0.5	5	1	401/Amorphous + U	14	1.57

Table S5. Location of 1 molecule of SDA in zeolites with different environments. 'x' means that the molecule locates in the corresponding cavity/channel; '+' means that the molecule occupies more than one cavity/channel simultaneously.

	CHA	ERI	Hypo#1		OFF	
	<i>cha</i>	<i>eri</i>	[4 <sup>8</sup> 5 <sup>8</sup> 8 <sup>6</sup> ]	<i>pau</i>	<i>gme</i>	channel
<b>OSDA1</b>	x	x	x			x
<b>OSDA2</b>	x	x	x			x
<b>OSDA3</b>	x	x	x		+	+
<b>OSDA4</b>	x	x		x	x	

Table S6. Number of cavities and SiO<sub>2</sub> per unit cell in each zeolite.

	<b>CHA</b>	<b>ERI</b>	<b>Hypo#1</b>		<b>OFF</b>	
	<i>cha</i>	<i>eri</i>	[4 <sup>8</sup> 5 <sup>8</sup> 8 <sup>6</sup> ]	<i>pau</i>	<i>gme</i>	channel
<b>Num/u.c.</b>	3	2	2	2	1	1
<b>SiO<sub>2</sub>/u.c.</b>	36	36	48		18	

Table S7. Amounts of OSDA occluded in the ERI materials determined by weight loss after combustion at 550°C measured by TGA.

<b>Sample Number</b>	<b>OSDA</b>	<b>Si and Al-source</b>	<b>Temperature (°C)</b>	<b>Total weight loss (wt.%)</b>	<b>OSDA / u.c.</b>	<b>OSDA / eri-cage</b>
1	1	ASA (Si/Al=6)	325-475	<b>16.1</b>	<b>2.38</b>	<b>0.8</b>
5	2	ASA (Si/Al=6)	350-475	<b>13.3</b>	<b>1.90</b>	<b>0.63</b>
12	3	FAU (Si/Al=6)	275-475	<b>21.20</b>	<b>3.09</b>	<b>1.03</b>

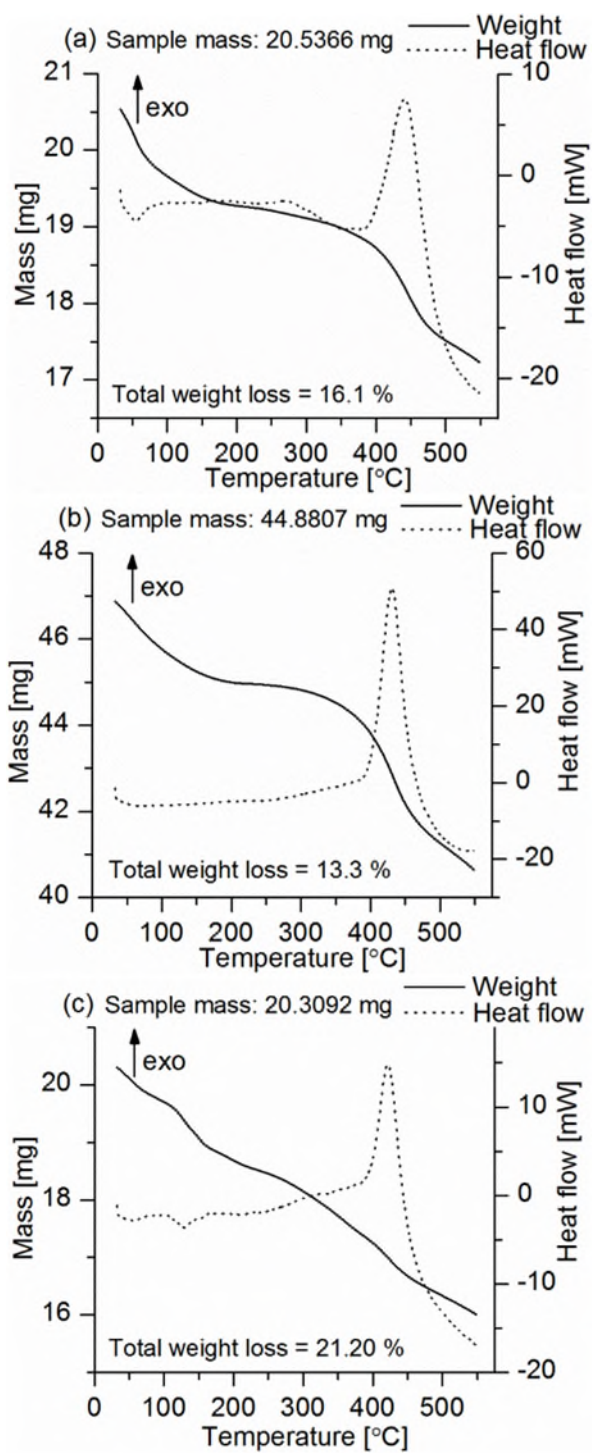


Figure S1. TGA-DSC thermograms of ERI-type zeolites corresponding to samples 1, 5 and 12.

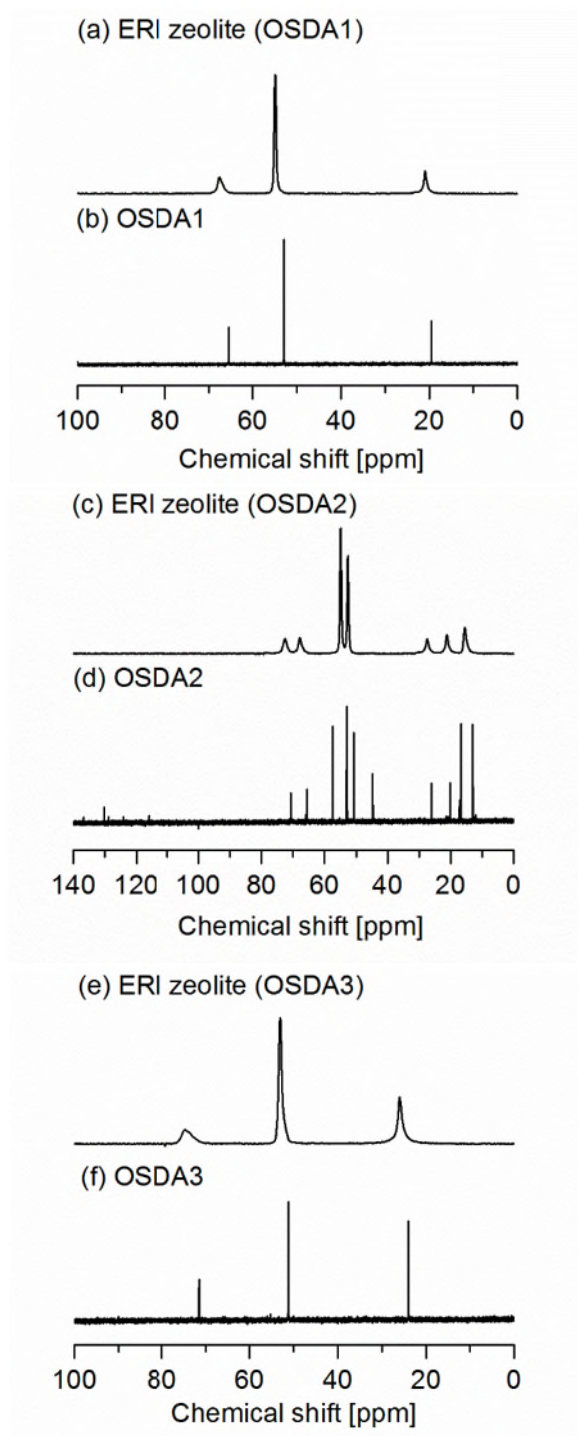


Figure S2. (b), (d), (f) 1D  $^{13}\text{C}$ -NMR of the OSDAs and (a), (c), (e)  $^{13}\text{C}$  CP-MAS NMR of the corresponding ERI materials, for samples 3, 7 and 12 respectively, synthesized using FAU as the Si- and Al- source.

ZeoTsites generated file for Hypo#1 (presented as Hypo#3 in this thesis).

zeoTsites (version 1.2.7.4) generated this output file

Connectivity and geometry of 139\_4\_48475\_mo\_slc.x

TITLE 139\_4\_48475\_modif\_slc

Cell parameters:

12.206269 12.206269 19.179717 90.000000 90.000000 90.000000

		T	O
Number of atoms in the asymmetric unit =	2	2	6
Number of atoms in the full unit cell =	48	48	96

atom number	atom label	coordination sequence	T-type
1	Si1	4 10 19 32 52 76 103 136 172 213 258 303 355	1
2	Si2	4 9 18 32 52 75 99 133 171 207 250 302 361	2

Number of topologically different T-types: 2

Multiplicity of each T-type: 32 16

atom number	atom label	vertex symbol (multiplicity below)	Number
1	Si1	4 4 5 8 5 8 1 1 1 1 1 1	32
2	Si2	4 5 4 8 4 8 1 1 1 1 1 1	16

Average topological geometry analysis:

T1type	T2type	T-O-T	T1-O	O-T2	T1-T2	Number
( 1)	( 1)	151.205	1.600	1.600	3.098	48
( 1)	( 2)	138.366	1.613	1.609	3.012	30
( 2)	( 1)	138.366	1.609	1.613	3.012	2
( 2)	( 2)	158.581	1.600	1.600	3.094	16

T1type	T-O-T	T-O	T1-T2	Number
( 1)	147.996	1.603	3.076	128
( 2)	148.474	1.605	3.053	64

T1type	O-T-O	Number
( 1)	109.482	192
( 2)	109.475	96

Average total geometry analysis:

	T-O	O-O	T-T	
	1.604	2.618	3.064	
	0.0056	0.0057	0.0138	(Standard deviation)
	1.590	2.569	3.007	(Minimum value)
	1.613	2.662	3.181	(Maximum value)

Criteria for zeotype feasibility: (DOI: 10.1002/anie.201206340)  
 (Criteria only for minimised structures)

Criteria:	Value:	Pass:
(1) $OO-1.6284 \times TO-0.0071 < 0.0009$	-0.0004	+
(2) $TT+4.8929 \times TO-10.9128 < 0.0046$	-0.0016	+
(3a) $\sigma(TO) < 0.0196$	0.0056	+
(3b) $\sigma(OO) < 0.0588$	0.0057	+
(3c) $\sigma(TT) < 0.0889$	0.0138	+
(4a) $\text{Max}(TO)-\text{Min}(TO) < 0.0634$	0.0227	+
(4b) $\text{Max}(OO)-\text{Min}(OO) < 0.2746$	0.0933	+
(4c) $\text{Max}(TT)-\text{Min}(TT) < 0.3332$	0.1741	+
(5*) $1.5967 < TO < 1.6076$	1.6037	+

(\* ) Only for alumino-silicate

T-T-T Criteria for zeotype feasibility: (DOI: 10.1515/zkri-2014-1801)  
 (Criteria only for minimised structures)

Criteria:	Pass:
All rings	+

Feasible structure according to TTT-criteria

The geometry and connectivity parameters for Hypo#11 are presented below:

zeoTsites (version 1.2.7.4) generated this output file

Connectivity and geometry of 139\_4\_82028\_slc.xtl

Cell parameters:

14.196477 14.196477 35.035162 90.000000 90.000000 90.000000

		T	O
Number of atoms in the asymmetric unit =	4	12	
Number of atoms in the full unit cell =	112	224	

atom number	atom label	coordination sequence												T-type	
1	Si	4	9	18	31	46	66	91	118	149	184	221	262	308	1
2	Si	4	9	17	29	45	65	89	115	142	173	210	254	303	2
3	Si	4	9	17	29	45	65	87	110	139	175	213	252	293	3
4	Si	4	10	19	30	45	63	84	112	143	175	212	251	292	4

Number of topologically different T-types: 4

Multiplicity of each T-type: 32 32 32 16

atom number	atom label	vertex symbol (multiplicity below)							Number
1	Si	4	4	4	8	8	8	109	
		1	1	1	2	1	1		
2	Si	4	4	4	6	8	8	109	
		1	1	1	1	1	1		
3	Si	4	4	4	6	6	8	109	
		1	1	1	1	1	1		
4	Si	4	6	4	6	6	8	109	
		1	1	1	1	1	1		

Average total geometry analysis:

	T-O	O-O	T-T	
	1.604	2.619	3.069	
	0.0023	0.0039	0.0054	(Standard deviation)
	1.587	2.515	3.030	(Minimum value)
	1.621	2.672	3.156	(Maximum value)

Criteria for zeotype feasibility: (DOI: 10.1002/anie.201206340)  
(Criteria only for minimised structures)

Criteria:	Value:	Pass:
(1) OO-1.6284xTO-	0.0071<0.0009	-0.0005 +
(2) TT+4.8929xTO-	10.9128<0.0046	0.0070 -
(3a)	sigma(TO)<0.0196	0.0023 +
(3b)	sigma(OO)<0.0588	0.0039 +



(3c)	$\sigma(\text{TT}) < 0.0889$	0.0054	+
(4a)	$\text{Max}(\text{TO}) - \text{Min}(\text{TO}) < 0.0634$	0.0343	+
(4b)	$\text{Max}(\text{OO}) - \text{Min}(\text{OO}) < 0.2746$	0.1567	+
(4c)	$\text{Max}(\text{TT}) - \text{Min}(\text{TT}) < 0.3332$	0.1264	+
(5*)	$1.5967 < \text{TO} < 1.6076$	1.6044	+

(\* ) Only for alumino-silicate

T-T-T Criteria for zeotype feasibility: (DOI: 10.1515/zkri-2014-1801)  
 (Criteria only for minimised structures)

Criteria: Pass:

All rings +

Feasible structure according to TTT-criteria

The geometry and connectivity parameters for Hypo#1 (thesis) are presented below:

zeoTsites (version 1.2.7.4) generated this output file

Connectivity and geometry of 139\_4\_82028\_modif\_slc.xtl

TITLE 139\_4\_82028\_modif\_slc

Cell parameters:

14.287092 14.287092 12.391785 90.000000 90.000000 90.000000

		T	O
Number of atoms in the asymmetric unit =		3	8
Number of atoms in the full unit cell =		40	80

atom number	atom label	coordination sequence												T-type	
1	Si1	4	9	18	31	46	66	90	115	146	182	219	261	306	1
2	Si2	4	9	17	29	45	64	86	112	141	174	212	252	295	2
3	Si3	4	9	17	28	42	62	87	113	142	174	208	249	293	3

Number of topologically different T-types: 3

Multiplicity of each T-type: 16 16 8

atom number	atom label	vertex symbol (multiplicity below)						Number
1	Si1	4	4	4	8	8	8	16
		1	1	1	2	1	1	
2	Si2	4	4	4	6	8	8	16
		1	1	1	1	1	1	
3	Si3	4	4	4	6	8	8	8
		1	1	1	1	1	1	

Average total geometry analysis:

T-O	O-O	T-T	
1.605	2.621	3.057	
0.0066	0.0114	0.0095	(Standard deviation)
1.589	2.520	3.014	(Minimum value)
1.624	2.666	3.117	(Maximum value)

Criteria for zeotype feasibility: (DOI: 10.1002/anie.201206340)  
(Criteria only for minimised structures)

Criteria:	Value:	Pass:
(1) OO-1.6284xTO-	0.0071<0.0009 0.0010	-
(2) TT+4.8929xTO-	10.9128<0.0046 -0.0032	+
(3a) sigma(TO)<0.0196	0.0066	+
(3b) sigma(OO)<0.0588	0.0114	+

(3c)	sigma(TT)<0.0889	0.0095	+
(4a)	Max(TO)-Min(TO)<0.0634	0.0347	+
(4b)	Max(OO)-Min(OO)<0.2746	0.1468	+
(4c)	Max(TT)-Min(TT)<0.3332	0.1033	+
(5*)	1.5967 < TO < 1.6076	1.6048	+

(\* ) Only for alumino-silicate

T-T-T Criteria for zeotype feasibility: (DOI: 10.1515/zkri-2014-1801)  
 (Criteria only for minimised structures)

Criteria: Pass:

All rings +

Feasible structure according to TTT-criteria

The geometry and connectivity parameters for Hypo#22 are presented below:

zeoTsites (version 1.2.7.4) generated this output file

Connectivity and geometry of 139\_5\_3770809\_slc.xt

Cell parameters:

14.071459 14.071459 44.143715 90.000000 90.000000 90.000000

		T	O
Number of atoms in the asymmetric unit =	5	15	
Number of atoms in the full unit cell =	144	288	

atom number	atom label	coordination sequence	T-type
1	Si	4 9 18 32 49 69 93 120 150 186 227 270 317	1
2	Si	4 9 18 32 49 69 92 118 150 189 231 272 314	2
3	Si	4 9 18 31 46 66 92 121 153 188 226 270 320	3
4	Si	4 9 17 29 45 65 89 116 146 181 220 263 311	4
5	Si	4 9 17 28 41 59 85 115 145 177 213 254 301	5

Number of topologically different T-types: 5

Multiplicity of each T-type: 32 32 32 32 16

atom number	atom label	vertex symbol (multiplicity below)	Number
1	Si	4 4 4 8 8 8 1 1 1 2 1 1	140
2	Si	4 4 4 8 8 8 1 1 1 2 1 1	140
3	Si	4 4 4 8 8 8 1 1 1 2 1 1	140
4	Si	4 4 4 6 8 8 1 1 1 1 1 1	140
5	Si	4 6 4 8 4 8 1 1 1 1 1 1	140

Average total geometry analysis:

T-O	O-O	T-T	
1.606	2.622	3.056	
0.0020	0.0029	0.0083	(Standard deviation)
1.591	2.531	2.948	(Minimum value)
1.614	2.675	3.174	(Maximum value)

Criteria for zeotype feasibility: (DOI: 10.1002/anie.201206340)  
(Criteria only for minimised structures)

Criteria:	Value:	Pass:
-----------	--------	-------

(1)	$OO-1.6284 \times TO - 0.0071 < 0.0009$	-0.0001	+
(2)	$TT+4.8929 \times TO - 10.9128 < 0.0046$	-0.0010	+
(3a)	$\sigma(TO) < 0.0196$	0.0020	+
(3b)	$\sigma(OO) < 0.0588$	0.0029	+
(3c)	$\sigma(TT) < 0.0889$	0.0083	+
(4a)	$\text{Max}(TO) - \text{Min}(TO) < 0.0634$	0.0235	+
(4b)	$\text{Max}(OO) - \text{Min}(OO) < 0.2746$	0.1444	+
(4c)	$\text{Max}(TT) - \text{Min}(TT) < 0.3332$	0.2257	+
(5*)	$1.5967 < TO < 1.6076$	1.6056	+

(\* ) Only for alumino-silicate

T-T-T Criteria for zeotype feasibility: (DOI: 10.1515/zkri-2014-1801)  
(Criteria only for minimised structures)

Criteria: Pass:

All rings +

Feasible structure according to TTT-criteria

The geometry and connectivity parameters for Hypo#21 are presented below:

zeoTsites (version 1.2.7.4) generated this output file

Connectivity and geometry of 139\_5\_3770809\_modif\_slc.xtl

TITLE 139\_5\_3770809\_modif\_slc

Cell parameters:

14.095892 14.095892 17.264263 90.000000 90.000000 90.000000

		T	O
Number of atoms in the asymmetric unit =	4	12	
Number of atoms in the full unit cell =	56	112	

atom number	atom label	coordination sequence												T-type	
1	Si1	4	9	18	32	49	69	92	117	147	186	231	276	320	1
2	Si2	4	9	18	31	46	66	92	121	153	188	225	267	317	2
3	Si3	4	9	17	29	45	65	89	116	146	181	220	262	308	3
4	Si4	4	9	17	28	41	59	85	115	145	177	213	254	301	4

Number of topologically different T-types: 4

Multiplicity of each T-type: 16 16 16 8

atom number	atom label	vertex symbol (multiplicity below)							Number
1	Si1	4	4	4	8	8	8	16	
		1	1	1	2	1	1		
2	Si2	4	4	4	8	8	8	16	
		1	1	1	2	1	1		
3	Si3	4	4	4	6	8	8	16	
		1	1	1	1	1	1		
4	Si4	4	6	4	8	4	8	8	
		1	1	1	1	1	1		

Average total geometry analysis:

T-O	O-O	T-T	
1.606	2.622	3.053	
0.0049	0.0053	0.0142	(Standard deviation)
1.590	2.533	2.949	(Minimum value)
1.615	2.674	3.173	(Maximum value)

Criteria for zeotype feasibility: (DOI: 10.1002/anie.201206340)  
 (Criteria only for minimised structures)

Criteria:	Value:	Pass:
(1) OO-1.6284xTO-	0.0071<0.0009 -0.0000	+

(2)	$TT+4.8929 \times TO - 10.9128 < 0.0046$	-0.0015	+
(3a)	$\sigma(TO) < 0.0196$	0.0049	+
(3b)	$\sigma(OO) < 0.0588$	0.0053	+
(3c)	$\sigma(TT) < 0.0889$	0.0142	+
(4a)	$\text{Max}(TO) - \text{Min}(TO) < 0.0634$	0.0246	+
(4b)	$\text{Max}(OO) - \text{Min}(OO) < 0.2746$	0.1410	+
(4c)	$\text{Max}(TT) - \text{Min}(TT) < 0.3332$	0.2238	+
(5*)	$1.5967 < TO < 1.6076$	1.6060	+

(\* ) Only for alumino-silicate

T-T-T Criteria for zeotype feasibility: (DOI: 10.1515/zkri-2014-1801)  
(Criteria only for minimised structures)

Criteria: Pass:

All rings +

Feasible structure according to TTT-criteria

The geometry and connectivity parameters for Hypo#2 are presented below:

zeoTsites (version 1.2.7.4) generated this output file

Connectivity and geometry of aa.xtl

TITLE 139\_5\_3770809\_modif2\_slc

Cell parameters:

14.141977 14.141977 24.938100 90.000000 90.000000 90.000000

		T	O
Number of atoms in the asymmetric unit =		3	9
Number of atoms in the full unit cell =		80	160

atom number	atom label	coordination sequence												T-type	
1	Si1	4	9	17	29	45	65	89	115	143	178	220	266	314	1
2	Si2	4	9	18	31	46	66	91	118	150	188	229	273	320	2
3	Si3	4	9	17	28	41	59	85	115	145	175	207	248	301	3

Number of topologically different T-types: 3

Multiplicity of each T-type: 32 32 16

atom number	atom label	vertex symbol (multiplicity below)						Number
1	Si1	4	4	4	6	8	8	32
		1	1	1	1	1	1	
2	Si2	4	4	4	8	8	8	32
		1	1	1	2	1	1	
3	Si3	4	6	4	8	4	8	16
		1	1	1	1	1	1	

Average total geometry analysis:

T-O	O-O	T-T	
1.607	2.623	3.050	
0.0035	0.0039	0.0113	(Standard deviation)
1.590	2.536	2.951	(Minimum value)
1.617	2.671	3.171	(Maximum value)

Criteria for zeotype feasibility: (DOI: 10.1002/anie.201206340)

(Criteria only for minimised structures)

Criteria:	Value:	Pass:
(1) OO-1.6284xTO-	0.0071<0.0009 -0.0000	+
(2) TT+4.8929xTO-	10.9128<0.0046 -0.0021	+
(3a)	sigma(TO)<0.0196 0.0035	+
(3b)	sigma(OO)<0.0588 0.0039	+



(3c)	sigma(TT)<0.0889	0.0113	+
(4a)	Max(TO)-Min(TO)<0.0634	0.0275	+
(4b)	Max(OO)-Min(OO)<0.2746	0.1349	+
(4c)	Max(TT)-Min(TT)<0.3332	0.2203	+
(5*)	1.5967 < TO < 1.6076	1.6066	+

(\* ) Only for alumino-silicate

T-T-T Criteria for zeotype feasibility: (DOI: 10.1515/zkri-2014-1801)  
 (Criteria only for minimised structures)

Criteria: Pass:

All rings +

Feasible structure according to TTT-criteria

The geometry and connectivity parameters for Hypo#31 are presented below:

zeoTsites (version 1.2.7.4) generated this output file

Connectivity and geometry of 139\_4\_48475\_slc.xtl

Cell parameters:

17.517051 17.517051 24.090054 90.000000 90.000000 90.000000

		T	O
Number of atoms in the asymmetric unit =	4	12	
Number of atoms in the full unit cell =	128	256	

atom number type	atom label	coordination sequence	T-
1	Si	4 10 19 32 52 78 106 137 172 211 256 306 359	1
2	Si	4 10 20 33 52 78 106 137 171 209 255 306 360	2
3	Si	4 10 20 33 52 78 106 137 171 209 255 306 360	2
4	Si	4 9 18 33 53 74 97 131 176 219 252 291 351	3

Number of topologically different T-types: 3

Multiplicity of each T-type: 32 64 32

atom number	atom label	vertex symbol (multiplicity below)	Number
1	Si	4 5 4 5 6 8 1 1 1 1 1 1	125
2	Si	4 4 5 8 6 8 1 1 1 1 1 1	125
3	Si	4 4 5 8 6 8 1 1 1 1 1 1	125
4	Si	4 5 4 8 4 8 1 1 1 1 1 1	125

Average total geometry analysis:

T-O	O-O	T-T	
1.602	2.618	3.071	
0.0022	0.0026	0.0075	(Standard deviation)
1.588	2.553	3.016	(Minimum value)
1.614	2.666	3.181	(Maximum value)

Criteria for zeotype feasibility: (DOI: 10.1002/anie.201206340)  
(Criteria only for minimised structures)

Criteria:	Value:	Pass:
(1) OO-1.6284xTO- 0.0071<0.0009	0.0012	-
(2) TT+4.8929xTO-10.9128<0.0046	-0.0016	+

(3a)	$\sigma(\text{TO}) < 0.0196$	0.0022	+
(3b)	$\sigma(\text{OO}) < 0.0588$	0.0026	+
(3c)	$\sigma(\text{TT}) < 0.0889$	0.0075	+
(4a)	$\text{Max}(\text{TO}) - \text{Min}(\text{TO}) < 0.0634$	0.0256	+
(4b)	$\text{Max}(\text{OO}) - \text{Min}(\text{OO}) < 0.2746$	0.1127	+
(4c)	$\text{Max}(\text{TT}) - \text{Min}(\text{TT}) < 0.3332$	0.1657	+
(5*)	$1.5967 < \text{TO} < 1.6076$	1.6025	+

(\* ) Only for alumino-silicate

T-T-T Criteria for zeotype feasibility: (DOI: 10.1515/zkri-2014-1801)  
 (Criteria only for minimised structures)

Criteria: Pass:

All rings +

Feasible structure according to TTT-criteria

Results obtained from the selections performed on the hypothetical zeolites database (the numbers represent hypothetical zeolite names).

Selection 1	Selection 2	63_4_38039829	139_5_8181929
131_5_26525156	166_4_638849	63_4_38042411	139_5_8181945
139_3_1151	166_4_1107233	63_4_38675850	139_5_8235452
139_5_3278844	194_5_6507766	63_4_41395511	139_5_8255019
139_5_3778516	194_5_6508580	65_3_403	140_2_2107
139_5_5416729	5_2_22346	65_3_4213	141_3_9213
139_5_5417097	5_2_23255	65_3_4280	141_3_9230
148_2_26839	9_2_325	65_3_4283	141_3_9232
160_2_35	10_2_283	65_3_6887	141_3_10666
162_2_10714	10_2_286	65_3_7144	141_3_25015
163_2_251282	10_2_469	65_3_8183	141_3_25107
164_2_612	10_2_521	65_3_8290	141_3_25271
164_3_155147	10_2_540	65_3_8348	141_4_632648
164_3_160927	10_2_1041	65_3_8350	141_4_848726
164_3_222207	11_2_14373	65_3_9887	141_4_848737
164_3_222653	11_2_14881	65_4_20919	141_4_850351
166_2_113	11_2_14882	65_4_21744	141_4_850352
166_2_118	11_2_14937	65_4_21842	141_4_850353
166_2_257	11_2_14960	65_4_36452	141_4_850419
166_2_298	11_2_15884	65_4_58699	141_4_899082
166_3_6095	11_2_15889	65_4_98726	141_4_899099
166_3_6096	11_2_15946	65_4_158368	141_4_993041
166_3_6133	12_2_4811	65_4_209594	141_4_993042
166_3_6333	12_2_11589	65_4_209595	141_4_993053
166_3_6363	12_2_22336	65_4_264920	141_4_993091
166_3_8906	12_2_22343	65_4_264937	141_4_993110
166_3_8908	12_2_22663	65_4_267434	141_4_993121
166_3_10192	12_2_23093	65_4_267988	141_4_1037666
166_3_15913	12_2_23390	65_4_268005	141_4_2423102
166_3_16009	12_2_24382	65_4_268075	141_4_2423957
166_3_17406	12_2_24446	65_4_268077	141_4_2423975
166_3_17498	12_2_24447	65_4_268078	141_4_2429747
166_3_17782	12_2_26172	65_4_309730	141_4_2443329
166_3_19035	12_2_26249	65_4_316521	141_4_2443341
166_4_245260	12_2_26283	65_4_316523	141_4_2443633
166_4_402576	13_2_187687	65_4_404257	
166_4_402577	13_2_187922	65_4_404260	Selection 3
166_4_402606	13_2_257065	65_4_418271	63_4_12718531
166_4_402614	14_2_36023	65_4_423987	59_4_279598
166_4_403259	14_2_36026	65_4_438394	59_4_279597
166_4_403287	14_2_45154	65_4_445433	59_4_279455
166_4_405612	15_2_138507	65_4_445531	58_2_371
166_4_405620	15_2_138554	65_4_445552	15_2_192398
166_4_405642	15_2_138613	65_4_515450	12_2_22829
			141_4_2430861

166_4_405643	15_2_138866	65_4_540139	141_3_25004
166_4_419220	15_2_139528	65_4_569515	139_4_59431
166_4_419228	16_2_101530	65_4_613457	139_4_103
166_4_419258	17_2_28799	65_4_644300	139_3_939
166_4_419892	20_2_14469	65_4_673683	126_2_162450
166_4_419930	20_2_21613	70_2_232107	74_3_990842
166_4_422226	22_2_138153	74_2_1097	66_2_3799
166_4_422256	24_2_9793	74_2_1871	65_4_65219
166_4_509590	26_2_9	74_2_2173	63_4_18912483
166_4_627560	36_2_13	74_2_3752	63_4_12718534
166_4_1093085	42_2_43	74_3_756985	Selection 4
166_4_1093089	47_2_4	74_3_757128	59_4_239382
166_4_1093313	48_2_187543	74_3_765702	59_4_223361
166_4_1093317	51_2_214	74_3_773054	59_4_209077
166_4_1096886	51_3_18542	74_3_789172	55_3_38549
166_4_1096979	51_3_18614	74_3_790047	53_3_343227
166_4_1099262	51_3_21998	74_3_878369	51_3_75299
166_4_1099359	51_3_34753	74_3_1003004	51_3_38215
176_3_2746847	51_3_34766	74_3_1014165	12_2_18203
189_2_40	51_3_37133	74_3_1486099	194_5_5784608
189_3_1609	51_3_37749	74_3_1489516	194_5_4704629
189_3_1615	51_3_71401	74_3_1628980	194_5_4611447
189_4_201811	51_3_106926	74_3_1693140	194_5_4607679
194_2_25	51_3_108071	74_3_1711805	194_5_4605751
194_2_26	51_3_110924	74_3_2237536	194_5_4605483
194_2_31	51_4_6824406	74_3_2544269	194_4_131121
194_3_853	52_2_40468	74_3_2858481	194_4_129505
194_3_854	53_2_349	74_3_2858484	194_4_128329
194_3_858	53_2_476	74_3_2859377	194_4_126941
194_3_860	53_2_764	74_3_2968838	194_4_103923
194_3_867	53_3_201601	74_3_2969104	194_4_102891
194_3_868	53_3_201602	74_3_2969112	194_4_102747
194_3_1139	53_3_269113	87_3_1504534	194_4_101468
194_3_1140	53_3_343459	87_3_1559272	189_5_15491270
194_3_1653	53_3_343852	87_3_1581879	141_4_4050056
194_3_1684	53_3_343922	119_2_33	141_4_2314333
194_3_1945	53_3_343935	119_3_2839	141_4_2310019
194_3_1946	53_3_343940	119_3_3556	141_4_2287188
194_3_2074	53_3_773939	119_3_4625	141_3_42207
194_3_2075	54_2_33797	119_3_5602	141_3_41362
194_4_34512	54_2_129672	119_3_9471	141_3_6818
194_4_34514	55_2_2	119_4_283193	140_2_5619
194_4_34521	55_2_153	119_4_341583	139_5_7572131
194_4_34522	55_2_175	119_4_342318	139_5_7526324
194_4_34693	55_2_203	119_4_349635	139_5_7304013
194_4_34708	55_3_10209	119_4_380750	139_5_6829522
194_4_35190	55_3_18899	119_4_515206	139_5_6303431
194_4_35191	55_3_37181	119_4_526531	139_5_6271791

194_4_35195	55_3_37248	119_4_552748	139_5_4072182
194_4_35197	55_3_39518	119_4_557835	139_4_137707
194_4_35204	55_3_49695	119_4_690056	139_4_130884
194_4_35205	55_3_49766	119_4_690063	139_4_97705
194_4_46868	55_3_51263	119_4_706579	139_4_48475
194_4_47045	55_3_51673	119_4_706585	139_3_3464
194_4_47050	55_3_76560	119_4_707628	139_3_3018
194_4_47052	55_4_1870089	119_4_723094	139_3_2399
194_4_47059	55_4_1962620	121_2_4345	136_2_63
194_4_55789	55_4_1962622	123_2_11	131_5_45597034
194_4_70265	55_4_1962668	123_3_162	131_5_45574395
194_4_70267	55_4_1962670	123_3_168	131_5_42877970
194_4_70315	55_4_1962676	123_3_361	131_5_42758173
194_4_70317	55_4_1986977	123_3_363	131_4_580901
194_4_71135	56_2_43712	123_3_618	131_4_511122
194_4_71137	57_2_8329	123_3_651	131_4_284235
194_4_80505	57_2_8345	123_4_2907	131_3_11233
194_4_80510	57_2_8571	123_4_2908	131_2_182
194_4_80611	57_2_11209	123_4_2912	123_4_12692
194_4_80613	58_2_15	123_4_6274	123_4_8092
194_4_80816	58_2_245	123_4_6287	123_3_442
194_4_80817	58_2_369	123_4_14742	122_2_28236
194_4_85331	59_3_3095	131_3_3535	119_4_891007
194_4_85332	59_3_4706	131_3_4329	119_4_888525
194_4_85336	59_4_159833	131_3_4482	119_4_887536
194_4_85338	59_4_159874	131_3_4499	119_4_880039
194_4_85342	59_4_208940	131_3_7740	87_3_2565287
194_4_85343	59_4_253719	131_3_7764	74_3_2866339
194_4_107047	59_4_253890	131_3_11384	74_2_1652
194_4_107048	59_4_270354	131_4_103823	74_2_1346
194_4_148946	59_4_280029	131_4_115898	65_4_680500
194_5_1577452	59_4_280041	131_4_117244	65_4_678190
194_5_1577457	59_4_281576	131_4_200590	65_4_649231
194_5_1577466	59_4_281587	131_4_201546	65_4_649220
194_5_1577467	59_4_281589	131_4_237786	65_4_646946
194_5_1577951	59_4_445957	131_4_243624	65_4_646944
194_5_1577952	60_2_45	131_4_243634	65_4_625475
194_5_1577958	60_2_45864	131_4_243636	65_4_521527
194_5_1577966	60_2_45946	131_4_244353	65_4_518048
194_5_1585135	60_2_46161	131_4_244362	65_4_512363
194_5_1585144	62_2_4150	131_4_431648	65_4_509603
194_5_1585145	62_3_1590786	131_4_431692	65_4_493172
194_5_1585316	62_3_1591890	131_4_431740	65_4_485434
194_5_1585317	62_3_2048990	131_4_692608	65_4_465873
194_5_1585330	62_3_3836149	131_5_9336896	65_4_465867
194_5_1585331	62_3_4759097	131_5_26524857	65_4_462558
194_5_1585816	62_3_4842097	131_5_26524858	65_4_411181
194_5_1585822	62_3_5015112	131_5_26524916	65_4_299690

194_5_1608022	62_3_5122425	131_5_26525120	65_4_298986
194_5_1608024	62_3_5167092	131_5_26525220	65_4_253408
194_5_1608031	62_3_5374756	131_5_26525221	65_4_236971
194_5_1608032	62_3_5922561	131_5_45666006	65_4_157100
194_5_1608203	62_3_5982376	136_2_175	65_4_67120
194_5_1608204	63_2_205	136_2_602	65_3_7536
194_5_1608217	63_3_26862	136_2_622	65_3_7490
194_5_1608218	63_3_34968	139_3_947	65_3_7459
194_5_1608690	63_3_46913	139_3_1121	65_3_3002
194_5_1608691	63_3_52098	139_3_1353	63_4_38001412
194_5_1608695	63_3_56433	139_3_1997	63_4_35783321
194_5_1608697	63_3_71633	139_3_2003	63_4_34447083
194_5_1778057	63_3_81145	139_3_2008	63_4_24194019
194_5_2175791	63_3_82007	139_3_2010	63_4_24190537
194_5_2175798	63_3_84908	139_3_3002	63_4_22224217
194_5_2175938	63_3_91194	139_3_3003	63_4_22002710
194_5_2175943	63_3_94926	139_3_3132	63_4_21949004
194_5_2175945	63_3_95296	139_4_7120	63_4_19718557
194_5_2175952	63_3_151265	139_4_7291	63_4_19416412
194_5_2175953	63_3_154984	139_4_38029	
194_5_2176355	63_4_1874283	139_4_38494	Selection 5
194_5_2176361	63_4_1878404	139_4_38502	53_3_696789
194_5_2176369	63_4_3034191	139_4_70531	59_4_272503
194_5_3268707	63_4_12709491	139_4_70603	60_2_67122
194_5_3270284	63_4_13112754	139_4_81926	62_3_1775461
194_5_3270286	63_4_13117992	139_4_81931	62_3_1779578
194_5_3270312	63_4_13118041	139_4_81933	62_3_1782871
194_5_3270314	63_4_13123254	139_4_82028	62_3_5592921
194_5_3297449	63_4_13123279	139_4_82041	169_2_6011
194_5_3297486	63_4_13914512	139_4_82221	169_2_10573
194_5_3297488	63_4_13914535	139_4_82225	178_2_15704012
194_5_3710809	63_4_15497895	139_4_82226	194_4_142836
194_5_3710813	63_4_17546320	139_4_82233	20_2_26370
194_5_3710815	63_4_17567550	139_4_83413	20_2_28216
194_5_3710819	63_4_17586284	139_4_119602	36_2_61
194_5_3710820	63_4_18894203	139_4_119647	
194_5_3711014	63_4_18909397	139_4_119649	Selection 6
194_5_3711021	63_4_19364011	139_4_141595	20_2_26522
194_5_3713580	63_4_19373250	139_4_175837	152_2_107944
194_5_3713581	63_4_19383326	139_4_177003	
194_5_3713688	63_4_19464428	139_4_180851	
194_5_3713689	63_4_19468300	139_5_3280776	
194_5_3713699	63_4_19632855	139_5_3767827	
194_5_3713700	63_4_19632859	139_5_3767829	
194_5_3713901	63_4_19636621	139_5_3768008	
194_5_3722022	63_4_19718568	139_5_3768009	
194_5_3722023	63_4_19761159	139_5_3768013	
194_5_3722135	63_4_19775134	139_5_3768014	

194_5_3722319	63_4_21249292	139_5_3770803	
194_5_3722320	63_4_21883006	139_5_3770809	
194_5_3722324	63_4_21938109	139_5_3770811	
194_5_3722326	63_4_24204079	139_5_3778517	
194_5_3920204	63_4_24205146	139_5_3778619	
194_5_3920209	63_4_24232384	139_5_3778620	
194_5_3920211	63_4_24232413	139_5_3778625	
194_5_3920215	63_4_24233871	139_5_3778630	
194_5_3920216	63_4_24233902	139_5_3778632	
194_5_3920375	63_4_24234199	139_5_3778811	
194_5_3920376	63_4_24265629	139_5_3823203	
194_5_3920380	63_4_24899495	139_5_3823484	
194_5_3920382	63_4_24899921	139_5_5416727	
194_5_3920386	63_4_24907381	139_5_5417091	
194_5_3920387	63_4_24918852	139_5_5418298	
63_3_46951	63_4_24921652	139_5_5418300	
63_4_22004019	63_4_29446852	139_5_5679714	
63_4_22598125	63_4_29456003	139_5_5679719	
63_4_22629417	63_4_32131909	139_5_5682971	
65_4_264919	63_4_32131911	139_5_7806583	
123_3_88	63_4_32162533	139_5_7848990	
123_4_6275	63_4_35650235	139_5_7849006	
131_4_237785	63_4_35650238	139_5_7852012	
131_4_431866	63_4_35759037		



